

LUGI VANVITELLI UNIVERSITY OF
CAMPANIA

DOCTORAL THESIS

**Manifestation of cluster structure
of weakly bound light nuclei in
direct nuclear reactions**

Author:

Bakytzhan URAZBEKOV

Supervisor:

Prof. Nunzio ITACO

Co-Supervisor:

Prof. Andrey DENIKIN

Department of Mathematics and Physics



Declaration of Authorship

I, Bakytzhan URAZBEKOV, declare that this thesis titled, “Manifestation of cluster structure of weakly bound light nuclei in direct nuclear reactions” and the work presented in it are my own. I confirm that:

- This work was done wholly while in candidature for a research degree at Luigi Vanvitelli university of Campania.
- Where I have consulted the published work of others, this is always clearly attributed.
- Where I have quoted from the work of others, the source is always given. With the exception of such quotations, this thesis is entirely my own work.
- I have acknowledged all main sources of help.

Signed:

Date:

*“By the love of God, the nations are created,
And you love them like yourself.
Love people as brothers, like freedom,
Then truth and life are for you. ”*

Abay Qunanbayev
Kazakh poet and philosopher

Abstract

Manifestation of cluster structure of weakly bound light nuclei in direct nuclear reactions

by Bakytzhan URAZBEKOV

In this work, the following light weakly bound atomic nuclei are studied: ${}^6\text{He}$, ${}^6\text{Li}$, and ${}^9\text{Be}$. A three-body model $\alpha + 2\text{N}$ for ${}^6\text{He}$ and ${}^6\text{Li}$, and $2\alpha + \text{N}$ model for ${}^9\text{Be}$ are applied. The wave function of the three-body system is obtained within the framework of the Stochastic Variational Model based on the Gaussian basis. The interaction potentials for three-body systems have a Pauli projector, which excludes forbidden states. An analytical expression is obtained for the density distribution function of nuclear matter using the three-body wave function. The root-mean-square matter radii of ${}^6\text{He}$, ${}^6\text{Li}$, ${}^9\text{Be}$ nuclei are calculated and given comparisons with other sources.

The interactions of ${}^6\text{He}$, ${}^6\text{Li}$, and ${}^9\text{Be}$ with the simplest particles, such as α , d are studied in detail. On the basis of the calculated density distribution functions, the folding interaction potentials are obtained. The resulting folding interaction potential is applied to calculate the differential cross sections of elastic scattering in the framework of the optical model. Using the Coupled Channels approach for the ${}^9\text{Be}$ induced reactions the role of different reaction channels is studied, and deformation parameters are derived. The comparisons of theoretical cross sections with experimental data in inelastic channels for nuclear reaction $d + {}^9\text{Be} \rightarrow d + {}^9\text{Be}^*$ are given.

Within the framework of the Coupled Reaction Channels method, the cross sections for nuclear reactions of single-nucleon and cluster transfers are calculated taking into account the internal structure of ${}^6\text{He}$, ${}^6\text{Li}$, and ${}^9\text{Be}$ nuclei. The contributions of the α -cluster and nucleon involved transfer channels for ${}^6\text{He}$, ${}^6\text{Li}$, and ${}^9\text{Be}$ are demonstrated. The obtained results based on the proposed theoretical approach reflect the cluster structure of the exploring nuclei.

Acknowledgements

I believe that if it were not for these people, then the thesis in the form, in which you are reading it, would not have taken place.

I am very grateful to my scientific supervisors Prof. Nunzio Itaco and Prof. Andrey Denikin, who gave a great chance to implement my scientific ideas. Their suggestions, ideas and comments always enabled me to see my goals much clearer, encouraging me to deepen my knowledge in nuclear physics.

Undoubtedly, I think it is worthwhile to thank the staff of the Department of Physics and Astronomy and the CIRCE laboratory: Prof. D'Onofrio, Prof. Galianella, G. Porzio, L. Morales, and all other members.

In addition, I would like to address my gratitude to Prof. Vladimir Kukulin (Moscow State University), with whom I had an honor and pleasure to discuss my future career and who had an immense influence on me as a scientist, Prof. Sayabek Sakhiyev (Abay State University), taught not only physics to me, but has always been an example of a decent man I want to become.

I also want to thank my dear friends Riccardo Mancino and Felice Pignatelli, without whom I could not just cope with simple life questions in Caserta.

Thanks to Prof. Ian Thompson (Lawrence Livermore National Laboratory) for explaining the input file for the FRESCO code, Prof. Alexandr Volya (Florida State University), for providing the values of the spectroscopic amplitudes of alpha particles for p-shell nuclei.

With this work, I would like to express my sincere love to my wife Meruyert, who has always supported me at all stages of my scientific career, and my newborn daughter Dina, who has been a source of my strength and positiveness.

Contents

Declaration of Authorship	i
Abstract	iii
Acknowledgements	iv
Contents	v
Introduction	1
1 The three body model	9
1.1 Three body wave function	10
1.2 Transformation of the basis function	12
1.3 Overlap matrix elements	14
1.4 Normalization and correlation density function	17
1.5 Density distribution functions	18
1.6 Root mean square radii	21
2 Theoretical models describing nuclear reactions	24
2.1 Description of elastic scattering	24
2.2 The coupled channels method for inelastic scattering	27
2.3 The coupled-reaction-channels method for the transfer reactions	30
2.4 Distorted Wave Born Approximation	32
2.5 Spectroscopic Amplitudes within the Shell Model	36
2.6 Double folding potential	39
3 The three-body wave functions and their properties	44
3.1 The three-body wave functions	44
3.2 Density Function of Nuclear Matter	47
4 $\alpha + {}^6\text{He}$ nuclear reactions	53
4.1 Elastic scattering	53
4.2 Elastic transfer	56

5	$\alpha + {}^6\text{Li}$ nuclear reactions	59
5.1	Elastic scattering	59
5.2	Elastic transfer	60
6	$d + {}^9\text{Be}$ nuclear reactions	64
6.1	Elastic channel	64
6.2	Inelastic scattering	66
6.3	One-nucleon transfer reactions	68
6.4	Cluster-transfer reaction	73
	Summary and Conclusions	80
	A Definitions from the quantum theory of angular momenta	83
	B Parameters of the three body wave function for ${}^6\text{He}$	88
	Bibliography	95

List of Figures

1	Schematic representation of the cluster structure of some nuclei, and their half-life, if unstable. Alpha particle, proton and neutron are marked in yellow, red and orange, respectively. The allocation of ${}^6\text{He}$, ${}^6\text{Li}$ and ${}^9\text{Be}$ nuclei means the selected as objects of study. Read the text for more details..	4
1.1	The schemes of Jacobi coordinate sets for the three body system.	11
2.1	An incoming plane wave scattering off a body making a distorted wave	25
2.2	The arrangement of radial vectors in the DWBA on example of the $A + b \rightarrow a + B$ nuclear reaction. Here $A = a + \nu$ and $B = b + \nu$.	34
2.3	Radius vectors for the double folding model.	41
3.1	The correlation function $W(x, y)$ for the ground state of ${}^6\text{He}$	46
3.2	The same caption as in the Fig.3.1, but for ${}^6\text{Li}$	47
3.3	The same caption as in the Fig.3.1, but for ${}^9\text{Be}$	48
3.4	The nuclear matter density distribution of ${}^6\text{He}$ with the cluster component contributions;	49
3.5	The same caption as in Fig. 3.4, but for ${}^6\text{Li}$	49
3.6	The same caption as in Fig. 3.4, but for ${}^9\text{Be}$	50
3.7	Comparison of the total nuclear matter density distribution function of ${}^6\text{He}$ with the LSSM calculations [67].	50
4.1	The folding potential V^{DF} calculated with the density functions of nuclear matter of ${}^6\text{He}$. The $\alpha + \alpha$ designation is for the $V_{\alpha+\alpha}^{DF}$ potential, while $2N + \alpha$ is for the $V_{2N+\alpha}^{DF}$ potential.	54
4.2	The differential cross section of the elastic scattering of ${}^6\text{He}$ by α -particles at $E_{lab} = 151\text{MeV}$ calculated with the different potentials: the double folding potential (blue solid), the WS1- ${}^6\text{He}$ (gray dashed) [41] and WS2- ${}^6\text{He}$ (gray dotted) [41]. Experimental data were taken from [41].	55

4.3	The cross sections of the elastic channel taking into account few possible reaction mechanisms: elastic scattering (solid gray), simultaneous transfer of di-neutron (gray dashed), sequential transfer of di-neutron (dotted) and their coherent sum (solid blue). Experimental data were taken from [41].	55
4.4	Schematic representation of the elastic transfer nuclear reaction, on the left - the simultaneous transfer of two nucleons, on the right - the sequential transfer of two nucleons.	57
5.1	The folding potential $V^{DF}(r)$ calculated with the density functions of nuclear matter of ${}^6\text{Li}$. The $\alpha + \alpha$ designation is for the $V_{\alpha+\alpha}^{DF}$ potential, while $2N + \alpha$ is for the $V_{2N+\alpha}^{DF}$ potential.	60
5.2	The differential cross section of the elastic scattering of ${}^6\text{Li}$ by α -particles at $E_{lab} = 166\text{MeV}$ with the different potentials: the double folding potential DF- ${}^6\text{Li}$ (blue solid), the WS1- ${}^6\text{Li}$ (gray dashed) [41]. Experimanetal data taken from [41].	61
5.3	The cross sections of the elastic transfer reaction are represented in terms of the transfer mechanisms: elastic scattering (solid gray), simultanious transfer of d (gray dashed), sequential transfer of $2N$ (dotted) and their coherent sum (solid blue). Experi manetal data taken from [41].	62
5.4	Schematic representation of the elastic transfer nuclear reaction, on the left - the simultaneous transfer of two nucleons, on the right - the sequential transfer of two nucleons.	63
6.1	The folding potential $V^{DF}(r)$ calculated with the density functions of nuclear matter of ${}^9\text{Be}$. The $d + 2\alpha$ designation is for the $V_{d+2\alpha}^{DF}$ potential, while $d + N$ is for the V_{d+N}^{DF} potential, see Eq. (4.1).	65
6.2	The angular distribution of elastic scattering data of d from ${}^9\text{Be}$ at laboratory energy 19.5 MeV in comparison with theoretical calculations within the OM (solid curve).	65
6.3	The cross sections of inelastic scattering ${}^9\text{Be}(d, d){}^9\text{Be}^*$ ($E_{exc}=2.43$ MeV) at laboratory energies 19.5 MeV (full circle) and 35 MeV (full triangle). Theoretical curves are described in the text. . . .	66
6.4	The target coupling schemes in the ${}^9\text{Be}(d, p){}^{10}\text{Be}$ (upper) and the ${}^9\text{Be}(d, t){}^8\text{Be}$ (lower) nuclear reactions. The bold two-headed arrows indicate $E\lambda$ transitions. The spin re-orientation effects are indicated as back-pointing arrows.	70

6.5	Differential cross sections for the ${}^9\text{Be}(d, p){}^{10}\text{Be}^*$ reactions at 19.5 MeV leading to different final states (labelled in the figure) in ${}^{10}\text{Be}$. The experimental data are shown in comparison with theoretical results obtained within the CRC method.	70
6.6	Differential cross sections for the ${}^9\text{Be}(d, t){}^8\text{Be}^*$ reactions at 19.5 and 35 MeV leading to different final states (labelled in the figure) in ${}^8\text{Be}$. The experimental data are shown in comparison with theoretical results obtained within the CRC method.	72
6.7	The scheme illustrates the reaction mechanisms taken into account in CRC calculations of the cross sections for ${}^9\text{Be}(d, \alpha){}^7\text{Li}$ reaction.	74
6.8	Differential cross sections for the ${}^9\text{Be}(d, \alpha){}^7\text{Li}$ reactions measured at 19.5 MeV and 35 MeV energy with the ${}^7\text{Li}$ observed in the ground or low-lying excited states in the exit channels.	75
6.9	The scheme illustrates the energy balance of the different intermediate stages for the two-step mechanisms of ${}^9\text{Be}(d, \alpha){}^7\text{Li}$ transfer reaction. The Q -values for the different intermediate channels are shown near the corresponding lines. The numbers near the arrows correspond to the spectroscopic amplitudes of the heaviest reaction participants. For example, spectroscopic amplitude for the ${}^9\text{Be} = {}^8\text{Li} + p$ configuration is equal $\mathcal{A} = -0.947$	77
6.10	Contributions of the different mechanisms to the cross section of the ${}^9\text{Be}(d, \alpha){}^7\text{Li}_{g.s.}$ reaction. See Fig. 6.7 for explanation of the curve notations.	78

List of Tables

2.1	Parameters of the M3Y-Paris [61] NN-potential with the Direct and Exchange terms.	43
3.1	The ground state energies E_{gs} of the three-body systems and the weights of the wave function components found by means of the SVM for the ${}^6\text{He}$, ${}^6\text{Li}$ and ${}^9\text{Be}$ nuclei. The set of quantum numbers $\gamma \equiv \{\lambda l LS\}$, the dimension N_γ and the component weights \mathcal{W}_γ (1.32) are listed.	45
3.2	Comparison of the calculated rms charge $\langle r_{ch}^2 \rangle$ and matter $\langle r_{ch}^2 \rangle$ radii obtained within the three-body model with experimental data.	51
4.1	The parameters of the potentials used in OM calculations for both $\alpha + {}^6\text{He}$ and $\alpha + {}^6\text{Li}$ nuclear reactions. For more details, see the text	57
6.1	Parameterized double-folding potentials of the $d+{}^9\text{Be}$ system used in the OM, CC and DWBA calculations.	67
6.2	Spectroscopic amplitudes used in CRC calculations for the Composite = Core + Nucleon system. The one-nucleon SA have been calculated by means of the <i>ANTOINE</i> code [84]. The alpha spectroscopic amplitudes were taken from [86, 87].	71
B.1	The three-body wave function parameters found by means of variational approach for the ground state of ${}^6\text{He}$	88

List of Abbreviations

NCSM	No Core Shell Model
RGM	Resonating Group Method
GCM	Generator Coordinate Method
SVM	Stochastic Variational Method
DWBA	distorted wave Born approximation
CRC	coupled reaction channels
OM	optical model
DF	double folding
CC	coupled channel
SA	spectroscopic amplitude
cm	center of mass
rms	root-mean-square

Physical Constants

Elementary electric charge $e = 1.602 \cdot 10^{-16}$ C

Reduced Planck constant $\hbar = 6.582 \cdot 10^{-16}$ eV·s

List of Symbols

Symbol	Name	Unit
r	distance	fm
k	wavenumber	fm^{-1}
E	energy	MeV
$\rho(r)$	density function	fm^{-3}
A	atomic mass	u
σ	cross section	mb
$d\sigma \setminus d\Omega$	differential cross section	mb \ sr

To the memory of my mother

Introduction

Humanity has always been interested in the structure of the Universe - how it works, what it consists of. The understanding and naming of modern objects such as molecules and atoms began in antiquity. The meaning of the word atom, in Greek *ατομος*, is indivisible, or the uncut particle of matter. Modern science has gone much deeper and determined that the atom is actually a complex particle. According to the standard model, the fundamental particles are now six quarks, six leptons and their corresponding anti-particles (for more details, see [1–3]). This has been achieved mainly through theoretical predictions and the development of integrated complex technology, detection systems designed to detect even the smallest particle of fundamental interactions. Particularly, in the modern nuclear physics the experimental techniques have also been successfully developed in the field of the production of secondary beams. Secondary beams, being rare and unstable nuclei, allow studying the properties and characteristics of the dripline nuclei, challenging the nuclear physics.

In recent years, the study of light weakly bound nuclei has not become less interesting due to the successful development of experimental facilities [4–8]. It is known that in nuclei the nucleons tend to group into clusters. A well known manifestation of the cluster structure in heavy nuclei is the α -decay of ^{238}U , first experimentally discovered by E. Rutherford [9]. The α -decay means that α -cluster can be formed in the uranium nucleus as an individual subsystem with the following emission. The first quantitative theory of α -decay was developed by G. Gamov (see [10]). In addition to α -decay, there is also a cluster decay,

where an emitted particle can be a heavy nucleus, for example – ^{12}C [11].

There are many theoretical approaches [12–16] devoted to studying the structure of exotic nuclei. In particular, the nuclear excitation function for light exotic nuclei is well reproduced by the No Core Shell Model (NCSM) [17–20]. The method uses one-particle basis function of the harmonic oscillator, realistic NN, NNN interactions. This method is reduced to solving the A -nucleon Schrödinger equation on the basis containing all possible configurations of A -nucleon oscillator functions. However, the size of the basis grows rapidly with the number of nucleons, the reliability of the NCSM model calculations decreases in the case of heavy nuclei. At present, the capabilities of modern computational machines make it possible to calculate with sufficient accuracy for nuclei with masses $A \leq 16$. For example, in Ref. [18] within the framework of this model, the excitation spectrum of the one-particle basis for the ^9Be nucleus is in good agreement with the experimental data [21].

The microscopic description, that is, taking into account the NN effective potential, of the break-up reaction is presented in the Resonating Group Method (RGM) [22–24]. Generalization of the RGM consists in constructing overall mathematically equivalent methods for the simultaneous calculation in the nuclear structures and nuclear reactions. The practical application of this method is also limited in the region of the lightest nuclei due to the lack of computational power in the antisymmetrization process. In the work [25] the algebraic RGM was successfully applied in describing the internal structure ^6He , ^6Li , and ^8He nuclei, their rms matter and proton and neutron radii, as well as nuclear matter distribution density were calculated. Also the fusion reactions at low energies with ^6He involved were presented.

Similar to the RGM [22], is the Generator Coordinate Method (GCM), if one takes the full model space of the basis Bloch-Brink wave functions [26]. In the framework of the GCM it is possible to carry out calculations for the nuclei

with medium masses taking into account a few clusters. For scattering problems, the RGM can be applied rather straightforwardly because the inter-cluster wave function is explicitly treated. On the other hand, in the application of the GCM to scattering problems, it is necessary to connect the basis wave functions in the internal region with continuum states in the asymptotic region at a chosen channel radius [27]. Microscopic three-body calculations for two valence neutrons around a core nucleus have been achieved by many groups to investigate the neutron halo and two-neutron correlation in drip-line nuclei such as ^6He and ^{14}Be [28, 29]. The ^{12}Be using the GCM has been studied [12]. In this work a negative-parity band was found, electromagnetic transition probabilities and partial widths of molecular states were calculated.

In addition to the above theoretical approaches, there is the Stochastic Variational Method (SVM) [30–33]. The SVM uses the Gaussian function as a basis function, which is convenient for deriving analytically matrix elements of the Hamiltonian. The corresponding Hamiltonian contains a Pauli projector [34], that removes forbidden states. The variational method describes well the internal structures of ^6He , ^6Li and ^9Be [31–33]. In particular, the electromagnetic properties, geometric parameters and configuration weights are in good agreement with the methods, where they are obtained by exact solutions of three-body problems.

To describe the elastic scattering in the field of a complex potential, one usually uses the Optical Model (OM), first presented in Ref. [35]. Within the framework of this model, the nucleus is considered as a transparent substance that has the ability to absorb. In practice, this method describes the experimental data well providing the direct information on the nucleus-nucleus interaction potential. However, the ambiguity of the optical potential parameters reduces

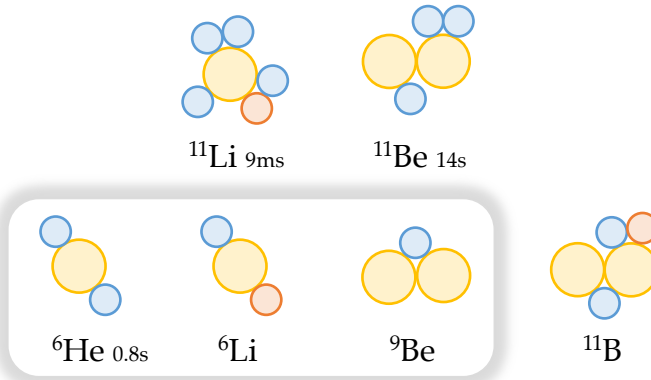


FIGURE 1: Schematic representation of the cluster structure of some nuclei, and their half-life, if unstable. Alpha particle, proton and neutron are marked in yellow, red and orange, respectively. The allocation of ^6He , ^6Li and ^9Be nuclei means the selected as objects of study. Read the text for more details..

the merits of optical model. To study the inelastic channels, transfer reactions and their use to describe experimental data the Distorted Wave Born Approximation (DWBA) method has been successfully applied [36]. The DWBA method proved to be appropriate and successful in describing the cross section of nuclear reactions involving the ground and low-lying excited nuclear states of single-particle as well as collective nature. The method becomes inadequate, since the reaction leads to the broad or strongly overlapped final states. In this case the couples channel formalism has to be applied.

In light nuclei, the cluster structure can often clearly manifest itself in the dripline region of the nuclear map. These series include such nuclei as ^6He , ^{11}Li , ^{12}Be and other exotic nuclei. However, there are also stable nuclei with apparent cluster structures. These include such nuclei as ^6Li , ^9Be , ^{11}B and others. Numerous experimental data [37–39] allow us to treat such nuclei as multi-cluster systems, including tightly bound α -clusters and valence nucleons. A visual representation of how these nuclei can be arranged in the cluster model is illustrated in Fig 1. For these nuclei the relative motion of internal subsystems determines the property and mechanisms of nuclear reactions. In the figure, we

see that the simplest nuclei with a cluster structure are ^6He , ^6Li , and ^9Be . Their structures are ideally suited to consideration within the framework of the three-body model. Moreover, it should be noted that the interaction of pairs inside these nuclei is well known, which can be used in constructing a solution to the Schrödinger equation. An important factor is also the number of scattering experiments conducted to study the structures of these nuclei. Therefore, the objects for investigation in this work have been taken ^6He , ^6Li , and ^9Be nuclei.

The experimental data of elastic scattering of the $^6\text{He} + \alpha$ and $^6\text{Li} + \alpha$ data is available at laboratory energies 151 MeV and 166 MeV [40, 41]. This experimental data can be used to show the elastic transfer phenomenon through two-neutron transfer between the two α core. The main motivation of these studies was to probe the relative importance of the "di-neutron" and "cigar" configurations of the valence neutrons in the ^6He ground state. The data show the backward angle rise in cross section. Usually it is considered as an indication of characteristic of elastic transfer. The DWBA analysis using the ^6He and ^6Li wave functions built on hyper-spherical harmonics [16], showed good agreement with the backward angle data. Consequently, it is concluded that the di-neutron configuration dominates the ^6He ground state wave function. The more detailed study of the $^6\text{He} + \alpha$ scattering data has carried out in Ref. [42] in the framework of the Coupled Reaction Channels (CRC) method. In this work the spectroscopic information of the di-neutron was obtained, a sequential transfer of the di-neutron was implemented in CRC calculations. It was concluded that the two valence neutrons are transferred mainly simultaneously, the rising of cross section at backward angles comes due to the elastic transfer of the $2n$ system.

Based on the Borromean structure of ^9Be , special attention was paid to the breakup processes resulting from the $^9\text{Be}(^6\text{Li}, ^6\text{Li}')^9\text{Be}^*$ nuclear reaction [38, 39]. The excited nucleus $^9\text{Be}^*$ can decay either directly into the $\alpha + \alpha + n$

three-body system or through one of the unstable nuclei, such as ${}^5\text{He}$ and ${}^8\text{Be}$. These relatively recent experimental studies explicitly confirm the cluster structure of ${}^9\text{Be}$. The calculated branching ratios show that the low-lying excited states, at $E_x < 4.0$ MeV, are mostly populated with the ${}^8\text{Be} + \text{n}$ configuration. In other conditions, the ${}^5\text{He} + \alpha$ configuration plays a significant role. Another aspect of finding the cluster structure is its effect on the nuclear reaction mechanisms. The investigations of works [43, 44] show that the multi-particle-multi-hole structures are expected at rather low excitation energies in nuclei. In such a case, it can be understood that the correlated nucleons are transferred as a whole strongly correlated cluster, which has the internal quantum numbers of a free particle.

In the present work, the three-body structure of nuclei and their role in the mechanisms of nuclear reactions are investigated. Usually, in the descriptions of the cross sections for nuclear reactions, the intrinsic structure of colliding nuclei in the interaction potentials is neglected, taking them in a phenomenological way, for example, in Gaussian form, or in the form of the Woods-Saxon potential [41]. In such cases, one should take the potential corresponding to the realistic shapes of colliding nuclei. To describe direct nuclear reactions, we proceed from the realistic shape of colliding nuclei within the three-body model. Therefore, the motivation for this work is to minimize the number of free parameters in the calculations of nuclear reactions as much as possible, and to use the density distribution functions of nuclear matter based on the three-body model. And also the main goal of this work is to understand how the mechanisms of interaction of nuclear reactions with the participation of weakly bound nuclei ${}^6\text{He}$, ${}^6\text{Li}$, and ${}^9\text{Be}$ occur.

This work is organized as follows. The first chapter is devoted to an introduction to the three-body model based on the SVM method. This chapter describes

the advantage of using the Gaussian basis function, the Hamiltonian, which includes the Pauli principle, the transformation of the basis function, and provides formulae for calculating the density function of nuclear matter within the three-body model. The next chapter presents widely used theoretical approaches to describe the scattering wave function. Methods for calculating differential cross sections are presented: for elastic scattering – Optical model, inelastic scattering – Coupled channel, and nuclear transfer reactions – Coupled Reactions Channels. For a complete understanding of how one-particle spectroscopic amplitudes (SA) are calculated within the framework of the shell model used in CRC calculations, a separate section is devoted. The details of building the potential of interaction in the framework of DF model are presented. The last three chapters present the results of the calculations. The comparative analysis of experimental data and theoretical calculations has been performed. Finally, the main findings are presented in the conclusion.

Some parts of this work have been published as follows:

- Urazbekov, B. A., Denikin, A. S., Lukyanov, S. M., Itaco, N., Janseitov, D. M., Mendibayev, K., ... and Harakeh, M. N. (2019). Journal of Physics G: Nuclear and Particle Physics, 46(10), 105110.
- Urazbekov, B. A., Denikin, A. S. (2018). Eurasian Journal of Physics and Functional Materials, 2(1), 17-22.
- Urazbekov, B.A., Denikin A.S., Itaco, N., Janseitov, D., (2021) Physics of Atomic Nuclei, to be published.
- Janseitov, D. M., Urazbekov, B.A., Lukyanov, S. M., Mendibayev, K., Penionzhkevich, Y. E., Skobelev, N. K., Sobolev, Y. G., ... and Khlebnikov, S. V. (2018). International Journal of Modern Physics E, 27(10), 1850089.

- Lukyanov, S. M., Urazbekov, B.A., Denikin, A. S., Naumenko, M. A., Burjan, V., Trzaska, W. H., Harakeh, M., ... and Glagolev, V. (2017). Exotic Nuclei, pp. 74-80 (2019).
- Urazbekov, B. A., Denikin, A. S., Itaco, N., and Tursunbayev, N. T. (2020). Eurasian Journal of Physics and Functional Materials, 4(3), 201-212.
- Burtebayev, N., Janseitov, D. M., Urazbekov, B. A., Kerimkulov, Z., Alimov, D., Nassurlla, M., Valiolda, D. S., ... and Danilov, A. N. (2020). Journal of Physics: Conference Series (Vol. 1555, p. 012032).

The materials of this work have been presented in the international conferences:

- International conference "Nucleus – 2018" "Fundamental problems of nuclear physics, nuclear energy industry, and nuclear technology", 2-6 July 2018, Voronezh, Russia;
- The LXIX International Conference "Nucleus-2019" on Nuclear Spectroscopy and Nuclear Structure "Fundamental Problems of Nuclear Physics, Nuclei at Borders of Nucleon Stability, High Technologies", 1-5 July 2019, Dubna, Russia;
- The LXX International conference "NUCLEUS – 2020. Nuclear physics and elementary particle physics. Nuclear physics technologies", 11-17 October 2020, online;
- The XXIV International Scientific Conference of Young Scientists and Specialists (AYSS-2020), 9 - 13 November 2020, online;

Chapter 1

The three body model

The wave function for the three-body system in the current work was calculated within the model proposed in Ref. [30]. The work based on the three body model provides great progress in understanding the structure and properties of the light weakly bound nuclei, like ^6He , ^6Li , ^9Be nuclei. In addition, a lot of research has been done in different directions of physics [30–33, 45–50] using this wave function. Below we list some of them:

- electromagnetic properties;
- low lying excitation spectra;
- root-mean-square charge radii $\langle r_{ch}^2 \rangle^{1/2}$, magnetic μ , quadrupole Q and octupole Ω moments;
- processes of ^6Li interaction with hadrons, including quasi-elastic scattering $(\alpha, 2\alpha)$, (p, d) and $(p, p\alpha)$;
- high energy proton and the lightest nuclei scattering on ^6Li
- scattering of π^\pm -mesons and μ -capture by ^6Li
- parameters of β -decay of ^6He ;
- the thermonuclear reactions in the D- ^3He - ^9Be plasma;
- properties of the six-quark dibaryons in nuclei with $A=6$ and *etc.*

Since this wave function was widely used, we chose it as the wave function to describe the three-body system in this work.

1.1 Three body wave function

Consider a three body system containing k , p , and q particles. A total wave function of this system with total spin J and spin projection M can be represented as a sum of components

$$\Psi^{JM}(\mathbf{x}_k, \mathbf{y}_k) = \sum_{\gamma} \Psi_{\gamma}^{JM}(\mathbf{x}_k, \mathbf{y}_k). \quad (1.1)$$

The vector \mathbf{x}_k is a vector of the relative distance between the pair of particles pq and k , and \mathbf{y}_k is the vector of the relative distance between the center of mass of the pair pq and the particle k (see Fig. 1.1). The designation γ is equivalent to the set of quantum numbers λLLS . The momenta λ, l are the orbital momenta conjugated to the coordinates \mathbf{x}_k and \mathbf{y}_k respectively, L is the total orbital momentum of the system and S is the total spin of three body system. The each component defines spatial and spin parts as follow

$$\begin{aligned} \Psi_{\gamma}^{JM}(\mathbf{x}_k, \mathbf{y}_k) &= \left[\Phi_L^{(\lambda, l)}(\mathbf{x}_k, \mathbf{y}_k) \otimes \chi_S(k, pq) \right]_{JM} = \\ &= \sum_{M_L M_S} (LM_L S M_S | JM) \Phi_{LM_L}^{(\lambda, l)}(\mathbf{x}_k, \mathbf{y}_k) \chi_{SM_S}(k, pq) \end{aligned} \quad (1.2)$$

The spin function of three body system having two fermions is given by

$$\chi_{SM_S}(k, pq) = \left[\chi_{\frac{1}{2}}(p) \otimes \chi_{\frac{1}{2}}(q) \right]_{SM_S}. \quad (1.3)$$

In the case of system, which has only fermion k , the total spin function becomes

$$\chi_{SM_S}(k, pq) = \chi_{\frac{1}{2}m_s}(k). \quad (1.4)$$

The spatial part of the wave function is chosen to be multidimensional Gaussian functions of the form

$$\begin{aligned} \Phi_{LM_L}^{(\lambda,l)} (\mathbf{x}_k, \mathbf{y}_k) = & x^\lambda y^l \sum_i C_i \exp \left(-\alpha_i^{(k)} x_k^2 - \beta_i^{(k)} y_k^2 \right) \times \\ & \times [Y_\lambda(\hat{x}_k) \otimes Y_l(\hat{y}_k)]_{LM_L}. \end{aligned} \quad (1.5)$$

Here, the coefficients C_i are the parameters of the wave function expansion and are found as a result of solving the generalized eigenvalue problem. The linear parameters $\alpha_i^{(k)}, \beta_i^{(k)}$ make the wave function more complete, if they are represented in the following form

$$\alpha_i^{(k)} = \alpha_0 \tan \left(\frac{\pi}{2} \frac{2i-1}{2N_\gamma} \right), \quad (1.6)$$

$$\beta_i^{(k)} = \beta_0 \tan \left(\frac{\pi}{2} \frac{2i-1}{2N_\gamma} \right), \quad i = 1, \dots, N_\gamma. \quad (1.7)$$

A pair of the three body system may have forbidden states according to the principle Pauli. For instance, lets say, the pair (kp) has the state ℓ_f must be excluded. This forbidden state ℓ_f is projected out by implementing the pseudo-potential [34]:

$$\tilde{V}_{kp} = V_{kp} + \lambda \Gamma_{\ell_f}, \quad (1.8)$$

where V_{kp} is a regular interaction potential between p and k particles, λ – a constant usually equal to 10^5 . By varying this parameter the binding energy of

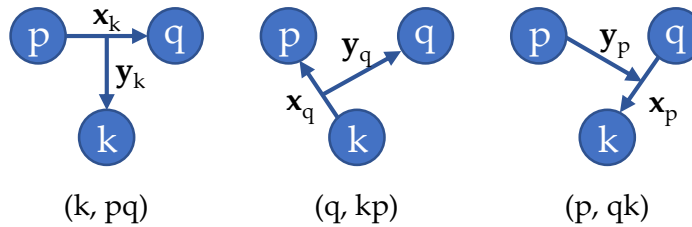


FIGURE 1.1: The schemes of Jacobi coordinate sets for the three body system.

three body system remains stable. The operator Γ_f is given by:

$$\Gamma(\ell_f) = \sum_{m_f} |\phi_{\ell_f m_f}(\mathbf{x})\rangle \langle \phi_{\ell_f m_f}(\mathbf{x}')| \delta(\mathbf{y} - \mathbf{y}'). \quad (1.9)$$

So the three body Hamiltonian including kinetic energy and pseudo potentials looks as

$$H = H_0 + \sum_{k < p} \tilde{V}_{kp}. \quad (1.10)$$

The Pauli principle plays a huge role in the structure of the nucleus, particularly it does not allow overlapping of two constituent particles, while maintaining the Pauli principle. This approach, so-called method of orthogonalizing pseudo-potentials, was previously developed by the group of V. Kukulin [34]. The method widely used not only in the construction of the wave function of the bound state, but also in the scattering theory [51, 52].

1.2 Transformation of the basis function

The main advantage of the Gaussian basis functions, is in simplicity of transformation into an alternative set of Jacobi coordinates [53]. The transformation from the sets (k, pq) to (p, qk) may be accomplished as follows:

$$\begin{pmatrix} \mathbf{x}_k \\ \mathbf{y}_k \end{pmatrix} = \mathbf{T}^{(kp)} \begin{pmatrix} \mathbf{x}_p \\ \mathbf{y}_p \end{pmatrix}, \quad (1.11)$$

where, the $\mathbf{T}^{(kp)}$ matrix elements is given by [54]

$$\mathbf{T}^{(kp)} = \begin{pmatrix} c_{kp} & s_{kp} \\ -s_{kp} & c_{kp} \end{pmatrix}, \quad (1.12)$$

where the coefficients c_{kp} and s_{kp} are given by

$$c_{kp} = - \left(\frac{m_k m_p}{(m_k + m_q)(m_p + m_q)} \right)^{1/2} \quad (1.13)$$

$$s_{kp} = (-1)^{k-p} \operatorname{sign}(k-p)(1 - c_{kp}^2)^{1/2}. \quad (1.14)$$

Consequently, these coefficients are depended only on the masses of particles.

Moreover the coefficients follow rules as

$$-1 < c_{kp} < 0, \quad s_{kp}^2 = 1 - c_{kp}, \quad c_{kp} = c_{pk}, \quad s_{kp} = -s_{pk}. \quad (1.15)$$

The transformation of the spatial part (1.5) of the wave function can be expressed in the following way [53, 55]

$$\Phi_{LM_L}^{(\lambda,l)}(\mathbf{x}_k, \mathbf{y}_k) = \sum_{\tilde{\lambda}, \tilde{l}} A_{\mathbf{T}^{(kq)}}^{\tilde{\lambda} \tilde{l} \lambda l} \Phi_{LM_L}^{(\tilde{\lambda}, \tilde{l})}(\mathbf{x}_q, \mathbf{y}_q), \quad (1.16)$$

where the summation is proceeded over new quantum numbers $\tilde{\lambda}, \tilde{l}$ in condition $\lambda + l = \tilde{\lambda} + \tilde{l}$, and the new spacial part is given by

$$\begin{aligned} \Phi_{LM_L}^{(\tilde{\lambda}, \tilde{l})}(\mathbf{x}_q, \mathbf{y}_q) = & x_q^{\tilde{\lambda}} y_q^{\tilde{l}} \sum_{i=1}^{N_\gamma} C_i \exp \left(-\frac{1}{2} \alpha_i^{(q)} x_q^2 - \frac{1}{2} \beta_i^{(q)} y_q^2 - \rho_i^{(q)} \mathbf{x}_q \cdot \mathbf{y}_q \right) \times \\ & \times [Y_{\tilde{\lambda}}(\hat{x}_k) \times Y_{\tilde{l}}(\hat{y}_k)]_{LM_L}. \end{aligned} \quad (1.17)$$

where new linear parameters can be expressed as

$$\begin{pmatrix} \alpha_i^{(q)} & \rho_i^{(q)} \\ \rho_i^{(q)} & \beta_i^{(q)} \end{pmatrix} = (\mathbf{T}^{(kq)})^T \times \begin{pmatrix} \alpha_i^{(k)} & \rho_i^{(k)} \\ \rho_i^{(k)} & \beta_i^{(k)} \end{pmatrix} \times \mathbf{T}^{(kq)}. \quad (1.18)$$

Note, that for the initial coordinate set (k, pq) the radial wave function (1.5) does not include the scalar product $\mathbf{x}_k \cdot \mathbf{y}_k$, which means $\rho_i^{(k)} = 0$.

The coupling coefficient $A_{\mathbf{T}^{(kq)}}^{\tilde{\lambda}\tilde{l}\lambda l}$ given in (1.16) is defined as follows

$$A_{\mathbf{T}^{(kq)}}^{\tilde{\lambda}\tilde{l}\lambda l} = \sum_{\lambda_1\lambda_2l_1l_2} \left(T_{11}^{(kq)}\right)^{\lambda_1} \left(T_{12}^{(kq)}\right)^{\lambda_2} \left(T_{21}^{(kq)}\right)^{l_1} \left(T_{22}^{(kq)}\right)^{l_2} \times \\ \times E_{\tilde{\lambda}\tilde{l}}^{\lambda_1\lambda_2\lambda l_1l_2lL} \mathcal{D}(\lambda, \lambda_1, \lambda_2) \mathcal{D}(l, l_1, l_2). \quad (1.19)$$

Here, the summation is satisfied to the conditions $\lambda_1 + \lambda_2 = \lambda$, $l_1 + l_2 = l$, $\lambda + l = \tilde{\lambda} + \tilde{l}$, the coefficients $E_{\tilde{\lambda}\tilde{l}}^{\lambda_1\lambda_2\lambda l_1l_2lL}$ and $\mathcal{D}(\lambda, \lambda_1, \lambda_2)$ come from re-coupling of the solid spherical harmonics , which are given in Appendix A. Switching into the Jacobi set (p, qk) is carried out in analogous way.

The spin part $\chi_{SM_S}(pq)$ of the wave function transforms as

$$\chi_{SM_S}(pq) = (-1)^{s_p+s_q-S} \chi_{SM_S}(qp). \quad (1.20)$$

As for the one fermionic system the spin part remains unchanged.

1.3 Overlap matrix elements

For the convenience of further expressions for the matrix elements we define a basis function for the three body system (k, pq) in form

$$\phi_{\gamma i}^{JM}(k, pq) = C_i \varphi_i^{(\lambda, l)}(x_k, y_k) [[Y_\lambda(\hat{x}_k) \otimes Y_l(\hat{y}_k)]_L \otimes \chi_S(k, pq)]_{JM}. \quad (1.21)$$

Here, the coordinate arguments, \mathbf{x}_k and \mathbf{y}_k , are down for convenience, and the radial part of the basis function has form

$$\varphi_i^{(\lambda, l)}(x_k, y_k) = x^\lambda y^l \exp\left(-\frac{1}{2}\alpha_i^{(k)}x_k^2 - \frac{1}{2}\beta_i^{(k)}y_k^2\right) \quad (1.22)$$

The overlap matrix elements for the basis function (1.21) is expressed as follows

$$\begin{aligned} \langle \phi_{\gamma i}^{JM}(k, pq) | \phi_{\gamma' j}^{JM}(k, pq) \rangle &= \int \int d\mathbf{x}_k d\mathbf{y}_k \phi_{\gamma i}^{JM}(k, pq) (\phi_{\gamma' j}^{JM}(k, pq))^* = \quad (1.23) \\ &= \int_0^\infty \int_0^\infty dx_k dy_k x_k^{2\lambda+2} y_k^{2l+2} \exp\left(-\frac{1}{2}\alpha_{ij}^{(k)} x_k^2 - \frac{1}{2}\beta_{ij}^{(k)} y_k^2\right) \delta_{\gamma\gamma'} = \\ &= C_i C_j \mathcal{I}\left(2\lambda + 2, \alpha_{ij}^{(k)}\right) \mathcal{I}\left(2l + 2, \beta_{ij}^{(k)}\right), \end{aligned}$$

where $\alpha_{ij}^{(k)} = \alpha_i^{(k)} + \alpha_j^{(k)}$ and $\beta_{ij}^{(k)} = \beta_i^{(k)} + \beta_j^{(k)}$, the table integral $\mathcal{I}(\lambda, \alpha)$ is given in Eq. (A.16).

It is also useful to give an expression of overlap matrix elements for alternative Jacobi coordinate set. For instance, the matrix elements for the (q, kp) three body system may be given as follows

$$\langle \phi_{\gamma i}^{JM}(k, pq) | \phi_{\gamma' j}^{JM}(k, pq) \rangle = \sum_{\tilde{\gamma}\tilde{\gamma}'} A_{\mathbf{T}^{(kq)}}^{\tilde{\lambda}'\tilde{l}'\lambda'\lambda'} A_{\mathbf{T}^{(kp)}}^{\tilde{\lambda}\tilde{l}\lambda l} \langle \phi_{\tilde{\gamma} i}^{JM}(q, kp) | \phi_{\tilde{\gamma}' j}^{JM}(q, kp) \rangle \quad (1.24)$$

The Jacobian matrix $\mathbf{J}^{(kq)}$ for transformation from the $\mathbf{x}_k, \mathbf{y}_k$ coordinates to the $\mathbf{x}_q, \mathbf{y}_q$ coordinates gives the $\mathbf{T}^{(kq)}$ matrix

$$\mathbf{J}^{(kq)} = \begin{pmatrix} \frac{\partial \mathbf{x}_k(\mathbf{x}_q, \mathbf{y}_q)}{\partial \mathbf{x}_q} & \frac{\partial \mathbf{x}_k(\mathbf{x}_q, \mathbf{y}_q)}{\partial \mathbf{y}_q} \\ \frac{\partial \mathbf{y}_k(\mathbf{x}_q, \mathbf{y}_q)}{\partial \mathbf{x}_q} & \frac{\partial \mathbf{y}_k(\mathbf{x}_q, \mathbf{y}_q)}{\partial \mathbf{y}_q} \end{pmatrix} = \mathbf{T}^{(kq)}. \quad (1.25)$$

Accordingly, the determinant $|\mathbf{J}^{(kq)}|$ is a determinant of the $\mathbf{T}^{(kq)}$ matrix, which equals to 1:

$$|\mathbf{J}^{(kq)}| = |\mathbf{T}^{(kq)}| = 1. \quad (1.26)$$

Therefore, the integration variables in Eq. (1.24) can be changed without any factorization.

The spacial part (1.28) in the alternative coordinate set has the scalar product, $\exp\left(-\alpha_i^{(q)}\beta_i^{(q)}\mathbf{x}_q \cdot \mathbf{y}_q\right)$. With this form the overlap matrix elements can be calculated directly, using the expansion of the exponential function [53]. However

it is possible to project the scalar product into \mathbf{T} matrix [55] as follows:

$$\mathbf{Q}_i^{(kq)} = \mathbf{T}^{(kq)} \times \begin{pmatrix} 1 & 0 \\ -\frac{\rho_i^{(q)}}{\alpha_i^{(q)}} & 1 \end{pmatrix}. \quad (1.27)$$

Consequently, the radial part (1.28) of the wave function can be rewritten without the scalar product term as

$$\begin{aligned} \Phi_{LM_L}^{(\tilde{\lambda}, \tilde{l})} (\mathbf{x}_q, \mathbf{y}_q) = & x_q^{\tilde{\lambda}} y_q^{\tilde{l}} \sum_{i=1}^{N_\gamma} C_i \exp \left(-\frac{1}{2} \alpha_i'^{(q)} x_q^2 - \frac{1}{2} \beta_i^{(q)} y_q^2 \right) \times \\ & \times [Y_{\tilde{\lambda}}(\hat{x}_k) \times Y_{\tilde{l}}(\hat{y}_k)]_{LM_L}. \end{aligned} \quad (1.28)$$

with

$$\alpha_i'^{(q)} = \alpha_i^{(q)} - \frac{\left(\rho_i^{(q)} \right)^2}{\beta_i^{(q)}} \quad (1.29)$$

One can get easily then an expression for the overlap matrix element in alternative Jacobi coordinate set as follows

$$\begin{aligned} \langle \phi_{\tilde{\gamma}i}^{JM} (q, kp) | \phi_{\tilde{\gamma}'j}^{JM} (q, kp) \rangle = & \\ = & C_i C_j \mathcal{I} \left(2\tilde{\lambda} + 2, \alpha_{ij}'^{(q)} \right) \mathcal{I} \left(2\tilde{l} + 2, \beta_{ij}^{(q)} \right) \delta_{\tilde{\gamma}\tilde{\gamma}'}. \end{aligned} \quad (1.30)$$

Taking into account Eq.(1.30) the matrix element (1.24) can be then rewritten as follows

$$\begin{aligned} \langle \phi_{\gamma i}^{JM} (k, pq) | \phi_{\gamma' j}^{JM} (k, pq) \rangle = & \sum_{\tilde{\gamma}\tilde{\gamma}'} A_{\mathbf{T}^{(kq)}}^{\tilde{\lambda}'\tilde{l}'\lambda'\lambda'} A_{\mathbf{T}^{(kq)}}^{\tilde{\lambda}\tilde{l}\lambda l} \langle \phi_{\tilde{\gamma}i}^{JM} (q, kp) | \phi_{\tilde{\gamma}'j}^{JM} (q, kp) \rangle = \\ = & \sum_{\substack{\tilde{\gamma}\tilde{\gamma}' \\ i=1..N_\gamma \\ j=1..N_{\gamma'}}} A_{\mathbf{Q}_{ij}^{(kq)}}^{\tilde{\lambda}'\tilde{l}'\lambda'\lambda'} A_{\mathbf{Q}_{ij}^{(kq)}}^{\tilde{\lambda}\tilde{l}\lambda l} C_i C_j \mathcal{I} \left(2\tilde{\lambda} + 2, \alpha_{ij}'^{(q)} \right) \mathcal{I} \left(2\tilde{l} + 2, \beta_{ij}^{(q)} \right) \delta_{\tilde{\gamma}\tilde{\gamma}'}. \end{aligned} \quad (1.31)$$

Notably, the coefficient $A_{\mathbf{Q}_{ij}^{(kq)}}^{\tilde{\lambda}\tilde{l}\lambda l}$ should now become depended on the rotation

matrix $\mathbf{Q}_{ij}^{(kq)}$. For simplicity the indexes of the rotation matrix are down in the next sections, consequently, the recoupling coefficient turns $A_{\mathbf{Q}}^{\tilde{\lambda}\tilde{l}\lambda l}$.

1.4 Normalization and correlation density function

By means of the overlap matrix elements (1.23) the weight of the component γ may be represented as follows

$$\mathcal{W}_\gamma = \sum_{\substack{i=1..N_\gamma \\ j=1..N_\gamma}} C_i C_j \mathcal{I} \left(2\lambda + 2, \alpha_{ij}^{(k)} \right) \mathcal{I} \left(2l + 2, \beta_{ij}^{(k)} \right). \quad (1.32)$$

This, in turn, gives the the normalization of the total three-body wave function as follows

$$\mathcal{W} = \sum_{\gamma} \mathcal{W}_\gamma^{(k)} = 1. \quad (1.33)$$

A correlation density function of the total wave function (1.1) can be expressed in the following way

$$W(x_k, y_k) = \int \int x_k^2 y_k^2 d\hat{x}_k d\hat{y}_k |\Psi_{tot}^{JM}|^2 = \sum_{\gamma} W_{\gamma}(x_k, y_k) \quad (1.34)$$

with

$$W_{\gamma}(x_k, y_k) = \sum_{ij} C_i C_j x_k^{2+2\lambda} y_k^{2+2l} \exp \left(-\frac{1}{2} \alpha_{ij}^{(k)} x_k^2 - \frac{1}{2} \beta_{ij}^{(k)} y_k^2 \right). \quad (1.35)$$

Here, the summation goes over $i = 1, \dots, N_\gamma$ and $j = 1, \dots, N_\gamma$.

1.5 Density distribution functions

The density distribution function of nuclear matter within the three body model can be expressed as follows

$$\rho(\mathbf{R}) = \sum_{\iota=\{k,p,q\}} \rho^{(\iota)}(\mathbf{R}) \quad (1.36)$$

where $\iota = \{k, p, q\}$. The density function of a cluster is given by

$$\rho^{(\iota)}(\mathbf{R}) = \langle \Psi_{tot}^{JM} | \hat{\rho}_i | \Psi_{tot}^{JM} \rangle, \quad (1.37)$$

here, the operator of density is defined as

$$\hat{\rho}_i \equiv \begin{cases} \delta \left(\mathbf{y}_i - y_0^{(i)} \mathbf{R} \right) & \text{for } i\text{-th nucleons,} \\ \rho_\alpha \left(\mathbf{y}_i - y_0^{(i)} \mathbf{R} \right) & \text{for } i\text{-th } \alpha\text{-clusters,} \end{cases} \quad (1.38)$$

where $\delta(\mathbf{z})$ – delta function, $\rho_\alpha(\mathbf{r})$ – internal density distribution function of α -cluster:

$$\rho_\alpha(\mathbf{r}) = \rho_0 \exp(-\gamma_0 \mathbf{r}^2) \quad (1.39)$$

The α -particle density function is normalized to unity with the following parameters

$$\gamma_0 = \frac{3}{2} \frac{1}{\langle r_\alpha^2 \rangle}, \quad \rho_0 = \left(\frac{\gamma_0}{\pi} \right)^{\frac{3}{2}}. \quad (1.40)$$

Here, the square root of $\langle r_\alpha^2 \rangle$ – rms matter radius of α -particle, which equals to 1.461 fm [56].

Write a matrix element of the nucleon operator $\delta \left(\mathbf{y}_k - y_0^{(k)} \mathbf{R} \right)$ via the basis functions:

$$\begin{aligned} & \langle \phi_{\gamma i}^{JM}(k, pq) | \delta \left(\mathbf{y}_k - y_0^{(k)} \mathbf{R} \right) | \phi_{\gamma' j}^{JM}(k, pq) \rangle = \\ &= C_i C_j \int \int dx_k dy_k x_k^2 y_k^2 \varphi_i^{(\lambda, l)}(x_k, y_k) \varphi_j^{(\lambda, l)}(x_k, y_k) \frac{\delta \left(y_k - y_0^{(k)} R \right)}{y_k^2} \delta_{\gamma \gamma'} = \\ &= C_i C_j \left(y_0^{(k)} \right)^{2l} R^{2l} \exp \left(-\frac{1}{2} y_0^{(k)2} \beta_{ij}^{(k)} R^2 \right) \mathcal{I} \left(2\lambda + 2, \frac{1}{2} \alpha_{ij}^{(k)} \right) \delta_{\gamma \gamma'}. \end{aligned} \quad (1.41)$$

Based on this expression the density function $\rho_k(R)$ of the nucleon $k \equiv N_k$ has form

$$\rho^{(N_k)}(R) = \sum_{\gamma} \rho_{\gamma}^{(N_k)}(R), \quad (1.42)$$

where

$$\rho_{\gamma}^{(N_k)}(R) = \sum_{ij} C_i C_j \left(y_0^{(k)} \right)^{2l} R^{2l} \exp \left(-\frac{1}{2} y_0^{(k)2} \beta_{ij}^{(k)} R^2 \right) \mathcal{I} \left(2\lambda + 2, \frac{1}{2} \alpha_{ij}^{(k)} \right).$$

If the cluster k is α -particle, a relevant matrix element has form

$$\begin{aligned} & \langle \phi_{\gamma i}^{JM}(k, pq) | \rho_{\alpha} \left(\mathbf{y}_k - y_0^{(k)} \mathbf{R} \right) | \phi_{\gamma' j}^{JM}(k, pq) \rangle = \\ &= \rho_0 C_i C_j \exp \left(-\gamma_0 R^2 \right) \int \int dx_k dy_k x_k^2 y_k^2 \varphi_i^{(\lambda, l)}(x_k, y_k) \varphi_j^{(\lambda, l)}(x_k, y_k) \times \\ & \times \exp \left(-\gamma_0 y_0^{(k)2} y_k^2 \right) i_0(2\gamma_0 y_0^{(k)} y_k R) \delta_{\gamma \gamma'}, \end{aligned} \quad (1.43)$$

where, $i_l(x)$ is the modified spherical Bessel function of the first kind (A.15).

The density function of the α -particle k is built as follows

$$\rho^{(\alpha_k)}(R) = \sum_{\gamma} \rho_{\gamma}^{(\alpha_k)}(R), \quad (1.44)$$

where

$$\rho_{\gamma}^{(\alpha_k)}(R) = 4\pi\rho_0 \exp(-\gamma_0 R^2) \sum_{ij} C_i C_j \mathcal{I}\left(2\lambda + 2, \frac{1}{2}\alpha_{ij}^{(k)}\right) \times \mathcal{I}\left(l, 0, \beta_{ij}^{(k)} + 2y_0^{(k)2}\gamma_0, 2\gamma_0 y_0^{(k)} R\right). \quad (1.45)$$

Here, $\mathcal{I}(n, l, v, |w|)$ is given in Eq. (A.17).

Let's turn to the density functions of q particles. In order to calculate the matrix elements for these particle, one must switch basis functions into (q, kp) Jacobi coordinate set, as in the case with overlap matrix element (1.24). In particular, the matrix element for the nucleon q may be represented in the form

$$\langle \phi_{\gamma i}^{JM}(k, pq) | \delta\left(\mathbf{y}_q - y_0^{(q)} \mathbf{R}\right) | \phi_{\gamma' j}^{JM}(k, pq) \rangle = \sum_{\tilde{\gamma}\tilde{\gamma}'} A_{\mathbf{Q}}^{\tilde{\lambda}'\tilde{l}'\lambda'\lambda'} A_{\mathbf{Q}}^{\tilde{\lambda}\tilde{l}\lambda l} \langle \phi_{\tilde{\gamma}i}^{JM}(q, kp) | \delta\left(\mathbf{y}_q - y_0^{(q)} \mathbf{R}\right) | \phi_{\tilde{\gamma}'j}^{JM}(q, kp) \rangle. \quad (1.46)$$

Analogously to the Eq. (1.41) the density function of the nucleon q may be represented as follows

$$\rho_{\gamma}^{(N_q)}(R) = \sum_{\gamma} \rho_{\gamma}^{(N_q)}(R), \quad (1.47)$$

where the component γ is

$$\rho_{\gamma}^{(N_q)} = \sum_{\tilde{\gamma}ij} A_{\mathbf{Q}}^{\tilde{\lambda}\tilde{l}\lambda l^2} C_i C_j \left(y_0^{(q)}\right)^{2\tilde{l}} R^{2\tilde{l}} \exp\left(-\frac{1}{2}y_0^{(q)2}\beta_{ij}^{(q)} R^2\right) \times \mathcal{I}\left(2\tilde{\lambda} + 2, \frac{1}{2}\alpha'_{ij}^{(q)}\right). \quad (1.48)$$

Here, it should be reminded that the rotation matrix \mathbf{Q} also depends on ij indexes (see. Eq. (1.27) and (1.31)). And, the matrix element of the density

operator for α -cluster q may be introduced in the following expression

$$\langle \phi_{\gamma i}^{JM}(k, pq) | \rho_\alpha \left(\mathbf{y}_q - y_0^{(q)} \mathbf{R} \right) | \phi_{\gamma' j}^{JM}(k, pq) \rangle = \\ \sum_{\tilde{\gamma} \tilde{\gamma}'} A_{\mathbf{Q}}^{\tilde{\lambda} \tilde{\nu} \lambda' \nu'} A_{\mathbf{Q}}^{\tilde{\lambda} \tilde{l} \lambda l} \langle \phi_{\tilde{\gamma} i}^{JM}(q, kp) | \rho_\alpha \left(\mathbf{y}_q - y_0^{(q)} \mathbf{R} \right) | \phi_{\tilde{\gamma}' j}^{JM}(q, kp) \rangle. \quad (1.49)$$

Following simple derivations one may write the density function of the α -cluster of three body system in the scheme (q, kp) as

$$\rho^{(\alpha_q)}(R) = \sum_{\gamma} \rho_{\gamma}^{(\alpha_q)}(R), \quad (1.50)$$

where the function $\rho_{\gamma}^{(\alpha_q)}(R)$ is

$$\rho_{\gamma}^{(\alpha_q)}(R) = 4\pi\rho_0 \exp(-\gamma_0 R^2) \sum_{\tilde{\gamma} i j} A_{\mathbf{Q}}^{\tilde{\lambda} \tilde{l} \lambda l} C_i C_j \mathcal{I}\left(2\tilde{\lambda} + 2, \frac{1}{2}\alpha'_{ij}^{(q)}\right) \times \\ \times \mathcal{I}\left(\tilde{l}, 0, \beta_{ij}^{(q)} + 2 y_0^{(q)2} \gamma_0, 2\gamma_0 y_0^{(q)} R\right). \quad (1.51)$$

Density functions for the nucleons N_p and α -clusters α_p are obtained in the similar way, as with density functions for the nucleon N_q and α -cluster α_q .

1.6 Root mean square radii

The above deduced density functions are useful for deriving the root mean square (rms) radii. Moreover, the explicit form of some integrals allows to express the rms radius in a convenient form. This would enable the exact value than the value obtained numerically.

The matter rms radius of in the framework of three body system in this work are defined as follows

$$\langle r^2 \rangle_m = \frac{m_k}{m} \langle r_k^2 \rangle + \frac{m_p}{m} \langle r_p^2 \rangle + \frac{m_q}{m} \langle r_q^2 \rangle, \quad m = m_k + m_p + m_q, \quad (1.52)$$

while the charge radius is

$$\langle r^2 \rangle_{ch} = \frac{z_k}{z} \langle r_k^2 \rangle + \frac{z_p}{z} \langle r_p^2 \rangle + \frac{z_q}{z} \langle r_q^2 \rangle, \quad z = z_k + z_p + z_q, \quad (1.53)$$

where z – charge of the three body system, the rms radii in general way are determined as follows

$$\langle r_i^2 \rangle = \int_0^\infty dr r^4 \rho^{(i)}(r), \quad i \equiv \{k, p, q\}. \quad (1.54)$$

In particular, using the Eq. (1.42) the rms radius $\langle r_{N_k} \rangle$ for the nucleon $k \equiv N_k$ is defined as follows

$$\langle r_{N_k}^2 \rangle = \sum_{\gamma ij} C_i C_j \left(y_0^{(k)} \right)^{2l+3} \mathcal{I}(2l+4, \frac{1}{2} y_0^{(k)2} \beta_{ij}^{(k)}) \mathcal{I}\left(2\lambda+2, \frac{1}{2} \alpha_{ij}^{(k)}\right). \quad (1.55)$$

In the case of the α -cluster q , by means of the Eq. (1.44) its rms radii is calculated as follows

$$\begin{aligned} \langle r_{\alpha_k}^2 \rangle = & 4\pi\rho_0 \sum_{\gamma ij} \mathcal{I}\left(2\lambda+2, \frac{1}{2} \alpha_{ij}^{(k)}\right) \times \\ & \times \mathcal{I}\left(1, l, 0, 2\gamma_0, \beta_{ij}^{(k)} + 2y_0^{(k)2} \gamma_0, 2\gamma_0 y_0^{(k)}\right) \end{aligned} \quad (1.56)$$

where the integral depending on six arguments is expressed in Appendix A (see Eq. (A.19)).

Likewise, the rms radii for the particle q in the three body system may be expressed through the density functions $\rho^{(q)}$. For instance, putting the Eq. (1.47) into the Eq. (1.54) we can get the rms radius $\langle r_{N_q}^2 \rangle$ for the nucleon q :

$$\begin{aligned} \langle r_{N_q}^2 \rangle = & \sum_{\gamma\tilde{\gamma}} \sum_{ij} A_{\mathbf{Q}}^{\tilde{\lambda}\tilde{\lambda}l^2} C_i C_j \left(y_0^{(q)} \right)^{2\tilde{l}+3} \mathcal{I}(2\tilde{l}+4, \frac{1}{2} y_0^{(q)2} \beta_{ij}^{(q)}) \times \\ & \times \mathcal{I}\left(2\tilde{\lambda}+2, \frac{1}{2} \alpha'_{ij}^{(q)}\right). \end{aligned} \quad (1.57)$$

Inserting Eq. (1.50) into Eq. (1.54) we obtain the rms radius $\langle r_{\alpha_q}^2 \rangle$ for the α -cluster q the following expression

$$\begin{aligned} \langle r_{\alpha_q}^2 \rangle = & 4\pi\rho_0 \sum_{\gamma\tilde{\gamma}} \sum_{ij} A_{\mathbf{Q}}^{\tilde{\lambda}\tilde{l}\lambda l^2} C_i C_j \mathcal{I} \left(2\tilde{\lambda} + 2, \frac{1}{2}\alpha'_{ij}^{(q)} \right) \times \\ & \times \mathcal{I} \left(1, \tilde{l}, 0, 2\gamma_0, \beta_{ij}^{(q)} + 2y_0^{(q)2}\gamma_0, 2\gamma_0 y_0^{(q)} \right) \end{aligned} \quad (1.58)$$

As regards for the particles p in the three body system the rms radii $\langle r_q^2 \rangle$ may be extracted in analogous way as in the case with the particles q .

For calculating charge radii one must use the different parametrizations ρ_0 and γ_0 . Provided the α -particle has Gaussian density distribution, the parameters may be obtained by using the charge rms radius $\langle r^2 \rangle_{ch}^{1/2} = 1.67$ [56] in the Eq. (1.40).

Chapter 2

Theoretical models describing nuclear reactions

2.1 Description of elastic scattering

In this chapter the description of scattering of two nuclei is given by a complex potential U . The potential may depend on the spins of the two nuclei but not on their internal coordinates. Thus, it cannot excite the nuclei internally or cause the transfer between them. It can only change their relative motion and, perhaps, reorient spins to each other or to the orbital motion [57].

In the case of colliding $a + A$ particles without spin the potential $U(r)$ is central, depending only on the magnitude of the channel coordinate \mathbf{r} . The corresponding Schrödinger equation may be written explicitly

$$\left(E + \frac{\hbar^2}{2\mu} \nabla^2 - U(r) \right) \chi(\mathbf{r}) = 0 \quad (2.1)$$

where μ is the reduced mass of the $a+A$ system, E is the energy in the centre-of-mass system. The $\chi(\mathbf{r})$ wave function is known as distorted waves describing elastic scattering. The expression "distorted wave" is meant to denote distortion away from the plane wave form due to the presence of the distorting potential $U(r)$ (see Fig. 2.1). Asymptotically, it has the form of an incident plane wave

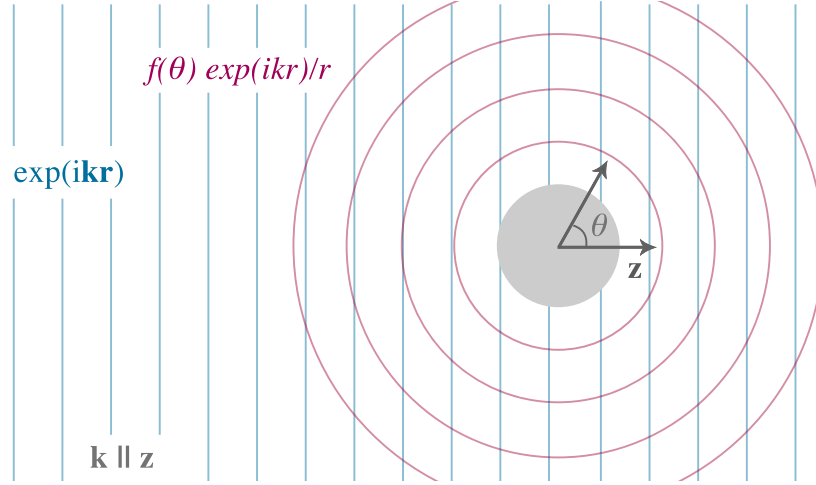


FIGURE 2.1: An incoming plane wave scattering off a body making a distorted wave

plus outgoing (scattered) spherical waves

$$\chi^{(+)}(\mathbf{k}, \mathbf{r}) \rightarrow e^{i\mathbf{k}\cdot\mathbf{r}} + f(\theta) \frac{1}{\mathbf{r}} e^{ikr}, \quad \mathbf{r} \rightarrow \infty \quad (2.2)$$

where $f(\theta)$ is the scattering amplitude. The (+) superscript stands for outgoing plane wave, while incoming spherical waves is the time-reverse of the $\chi^{(+)}$

$$\chi^{(-)}(\mathbf{k}, \mathbf{r}) = (\chi^{(+)}(-\mathbf{k}, \mathbf{r}))^* \quad (2.3)$$

Using the partial wave expansion

$$\chi^{(+)}(\mathbf{k}, \mathbf{r}) = \frac{4\pi}{kr} \sum_{LM} i^L \chi_L(k, r) Y_{LM}(\hat{\mathbf{r}}) \left(Y_{LM}(\hat{\mathbf{k}})\right)^*, \quad (2.4)$$

A solution for Eq. (2.1) in the absence of any interaction potential, $U(r) = 0$, is given by

$$\chi^{(+)}(\mathbf{k}, \mathbf{r}) \rightarrow e^{i\mathbf{k}\cdot\mathbf{r}}, \quad \mathbf{r} \rightarrow \infty, \quad (2.5)$$

for radial part only is written as

$$\chi_L(k, r) \rightarrow kr j_L(kr), \quad r \rightarrow \infty, \quad (2.6)$$

where $j_L(kr)$ is the usual spherical Bessel function. The $\chi_L(k, r)$ radial function satisfies the radial Schrödinger equation

$$\left(\frac{d^2}{dr^2} + k^2 - \frac{L(L+1)}{r^2} - \frac{2\mu}{\hbar^2} U(r) \right) \chi_L(k, r) = 0, \quad (2.7)$$

where $k^2 = \frac{2\mu E}{\hbar^2}$.

In the case of the interaction potential has a more sophisticated form, including both Coulomb and nuclear short-range potentials, the radial Schrödinger equation (2.7) may be rewritten as

$$\left(\frac{d^2}{dr^2} + k^2 - \frac{2\eta k}{r} - \frac{L(L+1)}{r^2} - \frac{2\mu}{\hbar^2} U(r) \right) \chi_L(k, r) = 0, \quad (2.8)$$

where η is the usual Sommerfeld parameter with the Z charge numbers

$$\eta = \frac{Z_a Z_A e^2 \mu}{\hbar^2 k}$$

At the radius r_0 , where the nuclear potential is negligible, Eq. (2.8) has the solution, which can be expressed in terms of the H_L outgoing and H_L^* incoming Coulomb functions, as follow

$$\chi_L(k, r) \rightarrow \frac{i}{2} e^{i\sigma_L} (H_L(kr_0)^* - S_L H_L(kr_0)), \quad r \rightarrow r_0 \quad (2.9)$$

where σ_L is the Coulomb phase shift, and it is given with the Γ Gamma function as follow

$$\sigma_L = \text{Arg}(\Gamma(L+1+i\eta))$$

In practice, the radial Eq. (2.8) is solved by numerical integration from $r \approx 0$, then, matched the value and the slope of the result onto the form (2.9) at $r = r_0$. This procedure then gives a value for the S_L scattering matrix elements. Having the S_L matrix elements, the amplitude of the elastic scattering, analogous from

Eq. (2.2), for the $\chi_L(k, r)$ wave function in the Eq. (2.8) is given by

$$f(\theta) = \frac{1}{2ik} \sum_L (2L + 1) e^{2i\sigma_L} (S_L - 1) P_L(\cos(\theta)) \quad (2.10)$$

where $P_L(x)$ is the Legendre polynomials, which are solutions to the Legendre differential equation. By means of the Rutherford scattering amplitude

$$f_C(\theta) = -\frac{\eta}{2k \sin^2\left(\frac{1}{2}\theta\right)} e^{\left(i\eta \ln\left(\sin^2\left(\frac{1}{2}\theta\right)\right) + 2i\sigma_0\right)} \quad (2.11)$$

the differential cross section of the elastic scattering has the form

$$\frac{d\sigma_\alpha}{d\Omega} = |f_C(\theta) + f(\theta)|^2. \quad (2.12)$$

The expression (2.12) allows thus to provide comparison with the obtained experimental data.

2.2 The coupled channels method for inelastic scattering

The elastic scattering of the projectile a by the nucleus A has been denoted by $\alpha = a + A$. Let $\alpha' = a + A^*$ be an inelastic channel, in which only the A nucleus has an extra excitation. In the framework of the coupled channel (CC) approach the total wave function Ψ for the system may be written as

$$\Psi = \phi_\alpha(x) \chi_\alpha(\mathbf{r}_\alpha) + \phi_{\alpha'}(x) \chi_{\alpha'}(\mathbf{r}_{\alpha'}) \quad (2.13)$$

where \mathbf{r} is the channel coordinate for the partitions α or α' , x represents the corresponding internal coordinates. The total wave function can be part of the Schrödinger equation kind of

$$H\Psi = E\Psi \quad (2.14)$$

with the Hamiltonian appropriate particular for the α partition

$$H = H_\alpha + K_\alpha + V_\alpha. \quad (2.15)$$

where $H_\alpha \equiv H_a + H_A$ is the internal Hamiltonian for the nuclei a and A , K_α is the kinetic energy operator of relative motion and V_α is the interaction potential operator. The wave functions of ground $\phi_\alpha(x)$ and excited state $\phi_{\alpha'}(x)$, being eigenfunctions of the internal Hamiltonian H_α

$$\begin{aligned} H_\alpha \phi_\alpha(x) &= \varepsilon_\alpha \phi_\alpha(x) \\ H_\alpha \phi_{\alpha'}(x) &= \varepsilon_{\alpha'} \phi_{\alpha'}(x), \end{aligned} \quad (2.16)$$

have an orthonormality property of the form

$$\int dx (\phi_\alpha(x))^* \phi_{\alpha'}(x) = \delta_{\alpha\alpha'}. \quad (2.17)$$

Using the expression of total wave function (2.13), multiplying Eq. (2.14) from the left by the ϕ_α^* function, then, by the $\phi_{\alpha'}^*$ function, the two coupled equations can be defined in the following form

$$\begin{aligned} (E - \varepsilon_\alpha - K_\alpha - \langle \alpha | V_\alpha | \alpha \rangle) \chi_\alpha(\mathbf{r}) &= \langle \alpha | V_\alpha | \alpha' \rangle \chi_{\alpha'}(\mathbf{r}) \\ (E - \varepsilon_\alpha - K_\alpha - \langle \alpha' | V_\alpha | \alpha' \rangle) \chi_{\alpha'}(\mathbf{r}) &= \langle \alpha' | V_\alpha | \alpha \rangle \chi_\alpha(\mathbf{r}) \end{aligned} \quad (2.18)$$

where $\langle \alpha | V_\alpha | \alpha \rangle$, or $\langle \alpha' | V_\alpha | \alpha \rangle$, is the matrix element of V_α . In particular, the matrix element $\langle \alpha' | V_\alpha | \alpha \rangle$ is given by

$$\begin{aligned} \langle \alpha' | V_\alpha | \alpha \rangle &= \int dx \phi'_{\alpha'}(x) V_\alpha(x, \mathbf{r}) \phi_\alpha(x) = \\ &= V_{\alpha'\alpha}(\mathbf{r}). \end{aligned} \quad (2.19)$$

An expansion of the coupling potential $V_{\alpha'\alpha}(\mathbf{r})$ into the λ multipoles can be given as follow

$$V_{\alpha'\alpha}(\mathbf{r}) = \sum_{\lambda\mu} V_{\alpha'\alpha}^{\lambda\mu}(r) Y_{\lambda\mu}(\hat{r}) \quad (2.20)$$

If the potential shape has a deformation, the nuclear potential can be constructed as

$$V_\alpha(\mathbf{x}, \mathbf{r}) = U(r - \Delta(\hat{r}')) \quad (2.21)$$

where \hat{r}' denotes the angular part of \mathbf{r} referred to the intrinsic coordinates \mathbf{x} .

The shift function $\Delta(\hat{r}')$ is normally expanded in multipoles

$$\Delta(\hat{r}') = \sum_{\lambda} \delta_{\lambda} Y_{\lambda 0}(\hat{r}'). \quad (2.22)$$

In the collective model, the ground and excited states are characterized by their angular momenta I_i and I_f with projections M_i and M_f , respectively. For these state the relevant matrix element of the $V_{\alpha'\alpha}^{\lambda\mu}$ operator is described using the Wigner-Eckart theorem by

$$\langle I_i M_i | V_{\alpha'\alpha}^{\lambda\mu} | I_f M_f \rangle = \sqrt{2I_i + 1} \langle I_f M_f \lambda \mu | I_i M_i \rangle \langle I' | V_{\alpha'\alpha}^{\lambda} | I \rangle. \quad (2.23)$$

Using the definitions, (2.21) and (2.22), the reduced matrix element of radial multipoles from Eq. (2.23) can be rewritten as follow

$$\langle I_i | V_{\alpha'\alpha}^{\lambda\mu} | I_f \rangle = -\frac{\langle I_i | \delta_{\lambda} | I_f \rangle}{\sqrt{4\pi}} \frac{dU(r)}{dr} \quad (2.24)$$

where

$$\langle I_i | \delta_{\lambda} | I_f \rangle = \sqrt{2I_f + 1} \langle I_f M_f \lambda 0 | I_i M_i \rangle \langle \chi | \delta_{\lambda} | \chi \rangle \delta_{M_i M_f}. \quad (2.25)$$

The matrix element $\langle \chi | \delta_{\lambda} | \chi \rangle$ is the expectation value of the operator δ_{λ} in the internal state of the deformed nucleus. In the framework of the rotational model

it can be given with the deformation length β_λ as follow

$$\langle \chi | \delta_\lambda | \chi \rangle = R_0 \beta_\lambda \quad (2.26)$$

where R_0 is an average radius of the interaction potential.

The general asymptotic behaviour of the χ_α elastic channel can be taken from Eq. (2.2), while the inelastic channel $\chi_{\alpha'}$ may have

$$\chi_{\alpha'}(\mathbf{r}_{\alpha'}) \rightarrow f_{\alpha'}(\theta) \frac{e^{ikr_{\alpha'}}}{r}, \quad \mathbf{r}_{\alpha'} \rightarrow \infty \quad (2.27)$$

Note, that the plane wave expression doesn't present in this equation - only outgoing wave presents. A relevant differential cross section for the inelastic channel is obtained from the coefficient of the outgoing wave as follow

$$\frac{d\sigma_{\alpha'}(\theta)}{d\Omega} = \frac{k_{\alpha'}}{k_\alpha} |f_{\alpha'}(\theta)|^2. \quad (2.28)$$

The wave numbers k_α and $k_{\alpha'}$ follow from the energy conservation

$$E = \varepsilon_\alpha + \frac{\hbar^2 k_\alpha}{2\mu} = \varepsilon_{\alpha'} + \frac{\hbar^2 k_{\alpha'}}{2\mu}. \quad (2.29)$$

2.3 The coupled-reaction-channels method for the transfer reactions

Consider a model for the $a + A \rightarrow b + B$ nuclear reaction, in which entrance and exit channels are denoted as α and β respectively. The Ψ total wave function for this model may be given as

$$\Psi = \chi_\alpha(\mathbf{r}_\alpha) \phi_\alpha(x_\alpha) + \chi_\beta(\mathbf{r}_\beta) \phi_\beta(x_\beta). \quad (2.30)$$

with a model Hamiltonian H such that $(E - H)\Psi = 0$. From the projections of this equation onto the two channels,

$$\begin{aligned}\langle \chi_\alpha | (E - H) | \Psi \rangle &= 0 \\ \langle \chi_\beta | (E - H) | \Psi \rangle &= 0\end{aligned}\tag{2.31}$$

with the two equivalent forms of H ,

$$\begin{aligned}H &= H_\alpha + K_\alpha + V_\alpha \\ H &= H_\beta + K_\beta + V_\beta\end{aligned}\tag{2.32}$$

one can get a pair of coupled equations for χ_α and χ_β :

$$\begin{aligned}[(E - \varepsilon_\alpha) - K_\alpha - \langle \alpha | V_\alpha | \alpha \rangle] \chi_\alpha(\mathbf{r}_\alpha) &= \langle \alpha | H - E | \beta \rangle \chi_\beta \\ [(E - \varepsilon_\beta) - K_\beta - \langle \beta | V_\beta | \beta \rangle] \chi_\beta(\mathbf{r}_\beta) &= \langle \beta | H - E | \alpha \rangle \chi_\alpha.\end{aligned}\tag{2.33}$$

These are *the coupled-reaction-channels* (CRC) equations. They are integro-differential equations, as may be seen more explicitly in the form

$$\begin{aligned}[(E - \varepsilon_\alpha) - K_\alpha - \langle \alpha | V_\alpha | \alpha \rangle] \chi_\alpha(\mathbf{r}_\alpha) &= \int d\mathbf{r}_\beta K_{\alpha\beta}(\mathbf{r}_\alpha, \mathbf{r}_\beta) \chi_\beta(\mathbf{r}_\beta) \\ [(E - \varepsilon_\beta) - K_\beta - \langle \beta | V_\beta | \beta \rangle] \chi_\beta(\mathbf{r}_\beta) &= \int d\mathbf{r}_\alpha K_{\beta\alpha}(\mathbf{r}_\beta, \mathbf{r}_\alpha) \chi_\alpha(\mathbf{r}_\alpha)\end{aligned}\tag{2.34}$$

where the kernels are

$$\begin{aligned}K_{\alpha\beta}(\mathbf{r}_\alpha, \mathbf{r}_\beta) &= J_{\alpha\beta} \int d\zeta_\alpha \phi_\alpha^*(x_\alpha) (H - E) \phi_\beta(x_\beta) \\ K_{\beta\alpha}(\mathbf{r}_\beta, \mathbf{r}_\alpha) &= J_{\beta\alpha} \int d\zeta_\beta \phi_\beta^*(x_\beta) (H - E) \phi_\alpha(x_\alpha).\end{aligned}\tag{2.35}$$

Here the internal coordinates have been transformed from the set x_α to the set $(\zeta_\alpha, \mathbf{r}_\beta)$, where the ζ_α are independent of \mathbf{r}_β . Also, $J_{\alpha\beta}$ is the Jacobian of

this transformation. Then $J_{\beta\alpha}$ is the Jacobian for the analogous transformation from x_β to $(\zeta_\beta, \mathbf{r}_\alpha)$.

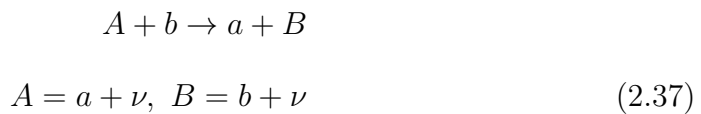
Since the off-diagonal matrix elements of V_α are small, they have little effect on the elastic scattering and may be neglected on the right side. This implies that the elastic scattering in the entrance α channel is described well by the potential $\langle\alpha|V_\alpha|\alpha\rangle$, and the potential $\langle\beta|V_\beta|\beta\rangle$ describes well the elastic scattering in the β channel. By doing this approximation, Eq. (2.33) may be rewritten as

$$\begin{aligned} [(E - \varepsilon_\alpha) - K_\alpha - \langle\alpha|V_\alpha|\alpha\rangle] \chi_\alpha(\mathbf{r}_\alpha) &\approx 0 \\ [(E - \varepsilon_\beta) - K_\beta - \langle\beta|V_\beta|\beta\rangle] \chi_\beta(\mathbf{r}_\beta) &\approx \langle\beta|H - E|\alpha\rangle \chi_\alpha \\ &\approx \langle\beta|V_\alpha|\alpha\rangle \chi_\alpha + \langle\beta|\alpha\rangle (H_\alpha - E_\alpha) \chi_\alpha \\ &\approx \langle\beta|V_\alpha|\alpha\rangle \chi_\alpha \end{aligned} \quad (2.36)$$

Here the prior interaction, that is the interaction of the α channel, is used. The non-orthogonal term $\langle\beta|\alpha\rangle(H_\alpha - E_\alpha)\chi_\alpha$ vanishes because of the χ_α is on-shell. The usual Green function techniques may then be used to solve these equations and give *the distorted wave Born approximation transition* (DWBA) amplitude. A detailed representation of the amplitude will be done in the next section.

2.4 Distorted Wave Born Approximation

Let consider the nuclear reaction of transfer ν particle from a A nucleus into a B nucleus:



In the case of weak coupling between intermediate channels, it is reasonable to evaluate the transition amplitude in Born Approximation.

In the rearrangement reactions there are few ways to describe the interaction between the different fragments, one for each partition. For example, if we choose to describe the scattering in terms of the nuclei of the entrance partition, the projectile-target interaction will be written as

$$V_{Ab} = V_{\nu b} + U_{ab}. \quad (2.38)$$

Here, $V_{\nu b}$ – a binding potential of the ν valence particle with the b core, and it is real potential, U_{ab} – a complex optical potential describing the scattering state of the $a + b$ system. In this representation, known as the prior form, the transition amplitude for the transfer process is given by

$$\begin{aligned} T_{prior} &= \langle \chi_{\beta}^{(-)} \phi_a \phi_B | V_{\nu b} + U_{ab} - U_{\alpha} | \chi_{\alpha}^{(+)} \phi_A \phi_b \rangle = \\ &= \int \int d\mathbf{r}_{\alpha} d\mathbf{r}_{\beta} \chi_{\beta}^{-}(\mathbf{r}_{\beta})^* I_{\beta\alpha}((\mathbf{r}_{\beta}, \mathbf{r}_{\alpha})) \chi_{\alpha}^{+}(\mathbf{r}_{\alpha}), \end{aligned} \quad (2.39)$$

where \mathbf{r}_{α} and \mathbf{r}_{β} – the radius vectors, illustrated in Fig.2.2, describing relative distance of the $b + A$ and $a + B$ systems respectively, U_{α} – the optical potential describing elastic scattering of α -channel, and $I_{\beta\alpha}$ is the kernel function having form

$$I_{\beta\alpha}((\mathbf{r}_{\beta}, \mathbf{r}_{\alpha})) = (\phi_a \phi_B | V_{\nu b} + U_{ab} - U_{\alpha} | \phi_A \phi_b). \quad (2.40)$$

Analogously, for the exit channel with $V_{aB} = V_{a\nu} + U_{ab}$ the transition amplitude turns to

$$T_{post} = \langle \chi_{\beta}^{(-)} \phi_a \phi_B | V_{a\nu} + U_{ab} - U_{\beta} | \chi_{\alpha}^{(+)} \phi_A \phi_b \rangle. \quad (2.41)$$

Here, U_{β} stands for the optical potential corresponding to β elastic channel.

The differential cross section for the rearrangement nuclear reaction within the DWBA, in particular for prior form, may be written as

$$\frac{d\sigma}{d\Omega_{DWBA}} = \frac{\mu_{\beta}\mu_{\alpha}}{2\pi\hbar^2} \left(\frac{k_{\beta}}{k_{\alpha}} \right) |T_{prior}(\mathbf{k}_{\beta}, \mathbf{k}_{\alpha})|^2 \quad (2.42)$$

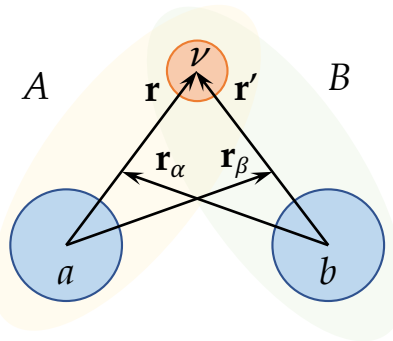


FIGURE 2.2: The arrangement of radial vectors in the DWBA on example of the $A+b \rightarrow a+B$ nuclear reaction. Here $A = a+\nu$ and $B = b+\nu$.

For the post form the differential cross section is written analogously replacing the corresponding transition amplitude.

In accordance with the DWBA calculations the main ingredients are internal wave functions for both initial (ϕ_A, ϕ_b) and final (ϕ_a, ϕ_B) nuclei. In this scheme, the valence particle ν is bound to the b core to give the composite B . In the simplest picture, the valence particle can be considered a pure single-particle state. This means that within this model there is only one possible configuration of the core and valence particle to give the nucleus B . Thus, the wave function for the nucleus B can be written as

$$\phi_B^{JM}(\xi, \mathbf{r}') = [\phi_b^I(\xi) \times \phi_{lsj}(\mathbf{r}')]_{JM}, \quad (2.43)$$

where ξ is the intrinsic coordinate of the b nucleus. In a more sophisticated model, however, the state of the composite contains components of many single particle states coupled to all possible core states. Therefore, the wave function

$\phi_B^{JM}(\xi, \mathbf{r})$ may be built as a superposition of the form

$$\phi_B^{JM}(\xi, \mathbf{r}') = \frac{1}{\sqrt{n_B}} \sum_{Ilj} \mathcal{A}_{lsj}^{IJ} [\phi_b^I(\xi) \times \phi_{lsj}(\mathbf{r}')]_{JM} \quad (2.44)$$

where the coefficient \mathcal{A}_{lsj}^{IJ} is the coefficient of fractional parentage or spectroscopic amplitudes. More information about the SA will be introduced in the next section. The squared value of the amplitude is

$$S_{lsj}^{IJ} = |\mathcal{A}_{lsj}^{IJ}|^2, \quad (2.45)$$

which is called spectroscopic factors. The spectroscopic factors can be regarded as the probability of finding the valence particle ν in a single particle state l, s, j coupled to the core with spin I . The quantity n_B is the number of nucleons or clusters in the composite system.

Note that the kernel function $I_{\beta\alpha}(\mathbf{r}_\beta, \mathbf{r}_\alpha)$ involve the overlap between the composite and core wave functions. Using the Eq.2.44 the internal variable ξ in the integral can be explicitly performed giving just unity by normalization

$$(\phi_B^{JM}(\xi, \mathbf{r}'), \phi_b^I(\xi)) \equiv \int d\xi \phi_B^{JM}(\xi, \mathbf{r}') \phi_b^I(\xi) = \frac{1}{\sqrt{n_B}} \sum_{Ilj} \mathcal{A}_{lsj}^{IJ} \phi_{lsj}(\mathbf{r}') \quad (2.46)$$

The bound wave function $\phi_{lsj}(\mathbf{r}')$ obey the Schrödinger equation

$$(T + V_{\nu b}(\mathbf{r}') + \epsilon - E) \phi_{lsj}(\mathbf{r}) = 0 \quad (2.47)$$

where ϵ is binding energy of the valence particle ν .

The spectroscopic amplitude \mathcal{A}_{lsj}^{IJ} is an important ingredient of the DWBA method. Since the further calculations take into account the transfer reactions of one particle, it is possible to obtain the spectroscopic amplitude using the Shell model calculations. This allows to reduce the number of free parameters in

the CRC calculations. The next section is devoted to defining how spectroscopic amplitudes can be obtained within the Shell model.

2.5 Spectroscopic Amplitudes within the Shell Model

Spectroscopic amplitudes for nuclear reactions can be obtained by calculations within the shell model. However, this approach is limited in calculating the amount of transferred particles. The calculation of matrix elements for the creation operator is suitable only in the case of the one-particle transfers, or at best two particle transfer. In nuclear reactions with the cluster transfer, one should use other theoretical approaches, or achieve certain values by fitting for the best reproduction of the observables [58].

Observables for the removal or addition of a nucleon from a specific initial state to a specific final state are related to the matrix elements of the creation and destruction operators. The creation operator a_{km}^+ is a tensor of rank j since it creates the single-particle state $|km\rangle$. Here, k stands for the set of single-particle quantum numbers nlj . The destruction operator a_{km} is not a tensor of rank j , however,

$$\tilde{a}_{km} = (-1)^{j+m} [a_{k,-m}^+]^+ = (-1)^{j+m} a_{k,-m} \quad (2.48)$$

is a tensor of rank j . And its inverse is $a_{km} = (-1)^{j-m} \tilde{a}_{k,-m}$. Corresponding matrix elements of these operators can be written as

$$\langle k^{n-1} \omega' J' || \tilde{a}_k || k^n \omega J \rangle = (-1)^{j+J'-J} \langle k^n \omega J || a_k^+ || k^{n-1} \omega' J' \rangle \quad (2.49)$$

where ω – the harmonic oscillator parameter chosen to reproduce the observed mean-square charge radius, J – total spin of the n -particle state. All many-body

matrix elements of a^+ can be reduced to these involving a single k -state.

Wave-function expansion relations and sum-rules for the states in the $n - 1$ particle system can be obtained by operating with the number operator

$$\hat{N}_k = \sum_m a_{km}^+ a_{km} \quad (2.50)$$

on the k^n configuration and then inserting a complete set of states with $n - 1$ particles

$$\begin{aligned} \hat{N}_k |k^n \omega JM\rangle &= \sum_m a_{km}^+ a_{km} |k^n \omega JM\rangle = n |k^n \omega J\rangle = \\ &= \sum_{m\omega' J' M'} a_{km}^+ |k^{n-1} \omega' J' M'\rangle \langle k^{n-1} \omega' J' M'| a_{km} |k^n \omega JM\rangle. \end{aligned} \quad (2.51)$$

The matrix element of $a_{k,m}$ can be reduced with the Wigner-Eckhart theorem

$$\begin{aligned} \langle k^{n-1} \omega' J' M' | a_{km} | k^n \omega JM \rangle &= (-1)^{j-m+J'-M'} \begin{pmatrix} J' & j & J \\ -M' & -m & M \end{pmatrix} \times \\ &\quad \times \langle k^{n-1} \omega' J' | | a_{km} | | k^n \omega J \rangle. \end{aligned} \quad (2.52)$$

By Eq. 2.49 the reduced matrix element of \tilde{a} can be converted in a reduced matrix element of a^+ to obtain the final result:

$$\begin{aligned} \hat{N}_k |k^n \omega JM\rangle &= n |k^n \omega JM\rangle = \sum_{m\omega JM} (-1)^{-m-M'+J} \begin{pmatrix} J' & j & J \\ -M' & -m & M \end{pmatrix} \times \\ &\quad \times a_{km}^+ |k^{n-1} \omega' J' M'\rangle \langle k^n \omega' J | | a_k^+ | | k^{n-1} \omega' J' M \rangle. \end{aligned} \quad (2.53)$$

Denoting the n -particle wave function by

$$|k^n \omega JM\rangle \equiv Z^+(k^n \omega JM) |\rangle \quad (2.54)$$

where Z^+ is the linear combination of a^+ operator which create the antisymmetric n -particle state, we can thus expand the k^n wave function in terms of those in the k^{n-1} basis:

$$|k^n\omega JM\rangle = (-1)^n \sum_{\omega' J'} \frac{\langle k^n\omega' J || a_k^+ || k^{n-1}\omega' J' M \rangle}{n\sqrt{2J+1}} [Z^+(k^{(n-1)}\omega' J') \times a_k^+]_{JM} | \rangle \quad (2.55)$$

A phase factor $(-1)^{n-1}$ arises from commuting a^+ with the $n - 1$ particles in the state k^{n-1}

A sum rule for the matrix elements of a^+ can be obtained by multiplying both sides of Eq. 2.53 by $\langle k^n\omega'' J'' M'' |$ to obtain

$$\begin{aligned} n\delta_{JJ''}\delta_{MM''}\delta_{\omega\omega''} &= \sum_{m\omega' J'M'} (-1)^{-m-M'+J} \begin{pmatrix} J' & j & J \\ -M' & -m & M \end{pmatrix} \times \\ &\times \langle k^n\omega'' J'' M'' | a_{km}^+ | k^{n-1}\omega' J' M' \rangle \langle k^n\omega J || a_k^+ || k^{n-1}\omega' J' \rangle = \\ &= \sum_{m\omega' J'M'} \begin{pmatrix} J' & j & J \\ -M' & -m & M \end{pmatrix} \begin{pmatrix} J'' & j & J' \\ -M'' & -m & M' \end{pmatrix} \times \\ &\times \langle k^n\omega'' J'' || a_k^+ || k^{n-1}\omega' J' \rangle \langle k^n\omega J || a_k^+ || k^{n-1}\omega' J' \rangle = \\ &= \frac{\delta_{JJ''}\delta_{MM''}}{2J+1} \sum_{\omega' J'} \langle k^n\omega'' J'' || a_k^+ || k^{n-1}\omega' J' \rangle \langle k^n\omega J || a_k^+ || k^{n-1}\omega' J' \rangle. \end{aligned} \quad (2.56)$$

Then, one finds the sum-rule:

$$\sum_{\omega' J'} \langle k^n\omega'' J'' || a_k^+ || k^{n-1}\omega' J' \rangle \langle k^n\omega J || a_k^+ || k^{n-1}\omega' J' \rangle = n(2J+1)\delta_{\omega\omega''}\delta_{JJ''} \quad (2.57)$$

Thus:

$$\sum_{\omega' J'} |\langle k^n\omega J || a_k^+ || k^{n-1}\omega' J' \rangle|^2 = \sum_{\omega' J'} |\langle k^{n-1}\omega' J' || \tilde{a}_k || k^n\omega J \rangle|^2 = n(2J+1) \quad (2.58)$$

The matrix elements in which the sum over final states is normalized to unity are historically called coefficients of fractional parentage [59] (CFP) defined by:

$$\mathcal{A}_{lsj}^{JJ'} = \frac{\langle k^n \omega J | |a_k^+| |k^{n-1} \omega' J' \rangle}{\sqrt{n(2J+1)}} \quad (2.59)$$

The reduced matrix elements of the creation and destruction operators are used to define the SA associated with nuclear reactions. They are also building blocks for the more complicated operators associated with one-body (such as electromagnetic and β -decay) and two-body transition amplitudes.

2.6 Double folding potential

The numerical calculations of elastic scattering can be performed in the framework of the OM with the optical potential given by:

$$U(R) = -V^V(R) - iW^V(R) + V^{SO}(R)(\mathbf{l} \cdot \boldsymbol{\sigma}) + V^C(R), \quad (2.60)$$

where V^V , W^V , V^{SO} , and V^C are real volume, imaginary volume, spin-orbit and Coulomb potentials, respectively. The volume potentials of colliding two spherical nuclei may be represented as parametrized function. For example, in practice the Woods-Saxon potential is often used, and it has the form

$$V^V(r) = V_0^V f_{r_V, a_V}(r), \\ W^V(r) = V_0^W f_{r_W, a_W}(r), \\ f_{r_0, a_0}(r) = \frac{1}{1 + \exp\left(\frac{r-r_0}{a_0}\right)}, \quad (2.61)$$

where V_0 is depth of the potential, r_0 is average distance and a_0 is diffusion parameter.

The spin-orbit term of the OM potential has standard form

$$V^{SO}(r) = V_0^{SO} \left(\frac{\hbar}{m_\pi c} \right)^2 \frac{1}{r} \frac{d}{dR} f_{R_{SO}a_{SO}}(r). \quad (2.62)$$

The Coulomb term has been taken as the interaction of a point-charge with a uniformly charged sphere

$$V^C(r) = \begin{cases} \frac{Z_1 Z_2 e^2}{2r_C} \left(3 - \frac{r^2}{r_C^2} \right), & \text{for } r \leq r_C, \\ \frac{Z_1 Z_2 e^2}{r}, & \text{for } r > r_C. \end{cases}$$

The situation changes, when the colliding nuclei have sophisticated shape. Assume, that there are nuclear matter distribution of the projectile $\rho_a(r_a)$ and target $\rho_A(r_a)$, depending on internal their own radii. Folding the nucleon-nucleon interaction potential V_{nn} over the density distributions of nuclear matter, in the framework of *the Double folding model* an interaction potential may be constructed as follow

$$\begin{aligned} V^V(r) &= N_f V^{DF}(r) \\ V^{DF}(\mathbf{r}) &= \int \int d\mathbf{r}_a d\mathbf{r}_A \rho_a(\mathbf{r}_a) V_{nn}(r_{aA}) \rho_A(\mathbf{r}_A). \end{aligned} \quad (2.63)$$

where $r_{aA} = |\mathbf{r} + \mathbf{r}_A - \mathbf{r}_a|$ (see Fig. 2.3). The N_f normalization parameter is usually fitted in accordance with the dynamics of nuclear reaction of elastic scattering.

The form of DF potential (2.63) used in this work is the Direct folding potential. In addition, if one takes into account the effects of nucleon exchange, the Exchange term of the DF potential must be added (for more, see [60]). The DF potential may be calculated using the effective M3Y-Paris [61] nucleon-nucleon potential and the nuclear-matter-densities of projectile and target nuclei.

The V_{nn} effective nucleon-nucleon interactions usually are taken as a sum of the

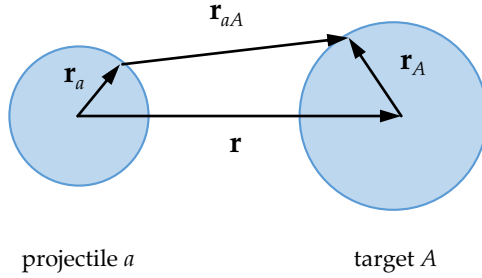


FIGURE 2.3: Radius vectors for the double folding model.

three Yukawa potentials, i.e. M3Y-potentials. For both isoscalar ($T=0$) and isovector ($T=1$) the M3Y-potentials have a form as

$$V_{nn}(r) = \sum_{i=1}^3 N_i \frac{\exp(-\mu_i r)}{\mu_i r}. \quad (2.64)$$

The parameters N_i , μ_i of the M3Y-Paris effective NN-potential [61], often used in the double folding calculations, are given in Tab.2.1.

The dependence $g(E)$ of the folding potential on the collision energy and an additional dependence on the nuclear matter density in the region of their overlap $F(\rho)$ have been phenomenologically established. The folding potential is usually taken as the real part of the optical potential, adjusting its depth to better reproduce the experimental data. The imaginary part of the optical potential is selected in the form of the Woods-Saxon potential, or the same folding potential, while varying its depth.

The potential depending on the collision energy of the projectile, undergoes a change by multiplying a factor

$$g(E) = 1 - 0.003 \frac{E}{A}. \quad (2.65)$$

An additional dependence of the V_{nn} potential on the total density of colliding nuclei in the region of their overlap may be given as

$$F(\rho) = C (1 + \alpha \exp(-\beta\rho) - \gamma\rho(\mathbf{r})). \quad (2.66)$$

with the parameters

$$C = 0.2658 \quad \alpha = 3.8033 \quad \beta = 1.4099 \quad \gamma = 4.0 \quad (2.67)$$

For the particles t , ${}^3\text{He}$, α , which have simple structure, the density distribution of nuclear matter can be represented as parametrized Gaussian function as follows

$$\rho(r) = \rho_0 \exp(-\alpha_0 r^2) \quad (2.68)$$

where the parameters ρ_0 and α_0 are defined in condition to reproduce the rms matter radii

$$\alpha_0 = \frac{3}{2\langle r_m^2 \rangle}, \quad \rho_0 = a \left(\frac{\alpha_0}{\pi} \right)^{3/2} \quad (2.69)$$

here a – atomic number of projectile.

The density distributions in (2.63) are normalized so that

$$\int \rho_a(\mathbf{r}) d\mathbf{r} = a \quad (2.70)$$

where a is atomic mass of projectile. For the target nucleus A normalization has the equivalent form.

As regards target nuclei, having cluster structure, the density distribution of nuclear matter is calculated by means of the three body wave function, and its details are set out in the Section 1.5 .

TABLE 2.1: Parameters of the M3Y-Paris [61] NN-potential
with the Direct and Exchange terms.

i	N_i , MeV				μ_i, fm^{-1}
	Direct T=0	Exchange T=0	Direct T=1	Exchange T=1	
1	11061.60	-1524.25	313.62	-4118.9	4.0000
2	-2537.5	-518.75	223.5	1054.75	2.5000
3	0.0	-7.84	0.0	2.62	0.7072

Chapter 3

The three-body wave functions and their properties

3.1 The three-body wave functions

The three-body wave functions are calculated within the SVM. The obtained parameters C_i for ground state of the ${}^6\text{He}$ nucleus are listed in Application B. The calculations were done using the RSC potential [62] for nucleon-nucleon interaction, the SBB potential [63] for α - N interaction and the BFW potential [64] for α - α interaction. In Tab. 3.1 the relative weights of the ground state wave function components and eigenvalues the three body systems are listed¹.

¹The obtained data of the variational calculations are not the subject of our research, since the results, perhaps better ones, have already been published and discussed. The purpose of the section result of the three-body wave function is to familiarize with what wave function we are dealing with, and its features will be needed in further discussions.

TABLE 3.1: The ground state energies E_{gs} of the three-body systems and the weights of the wave function components found by means of the SVM for the ${}^6\text{He}$, ${}^6\text{Li}$ and ${}^9\text{Be}$ nuclei. The set of quantum numbers $\gamma \equiv \{\lambda l L S\}$, the dimension N_γ and the component weights \mathcal{W}_γ (1.32) are listed.

${}^6\text{He}$			${}^6\text{Li}$			${}^9\text{Be}$		
$E_{gs} = -0.228$			$E_{gs} = -3.258$			$E_{gs} = -1.417$		
$E_{exp} = -0.970$			$E_{exp} = -3.70$			$E_{exp} = -1.570$		
$\lambda l L S$	N_γ	\mathcal{W}_γ	$\lambda l L S$	N_γ	\mathcal{W}_γ	$\lambda l L S$	N_γ	\mathcal{W}_γ
0 0 0 0	81	0.884	0 0 0 1	64	0.898	0 1 1 1/2	49	0.403
1 1 1 1	81	0.102	2 0 2 1	49	0.073	2 1 1 1/2	49	0.328
2 2 0 0	25	0.010	1 1 1 0	49	0.021	2 1 2 1/2	49	0.235
3 3 1 1	25	0.004	2 2 0 1	25	0.005	2 3 1 1/2	36	0.017
			2 2 1 1	25	0.002	2 3 2 1/2	25	0.004
						4 3 1 1/2	16	0.009
						4 3 2 1/2	16	0.003

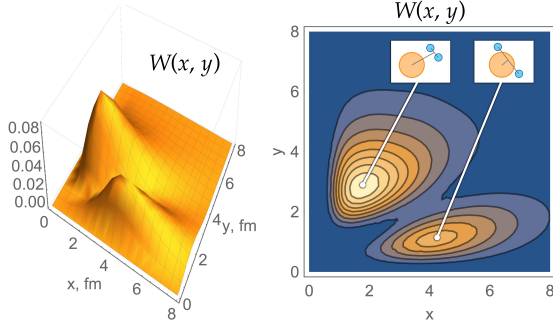


FIGURE 3.1: The correlation function $W(x, y)$ for the ground state of ${}^6\text{He}$.

The data in Tab. 3.1 show good agreement between calculated and measured values of the ground state energy for the ${}^9\text{Be}$ nucleus. However, the corresponding values given for the ${}^6\text{He}$ and ${}^6\text{Li}$ nuclei underestimate the experimental data approximately by 0.5–0.7 MeV. The discrepancy, probably, due to the non-completeness of the basis function. In this work it has no symmetrization, and doesn't enfold an alternative coordinate space. Other reasons might be in the presence of other cluster components, which has not been included in the variational calculations, and the NNN -body forces. For example, ${}^6\text{He}$ can contain two cluster such as ${}^3\text{H} + {}^3\text{H}$, the ${}^6\text{Li}$ nucleus can have ${}^3\text{He} + {}^3\text{H}$, and the ${}^9\text{Be}$ nucleus can be represented as the ${}^5\text{He} + {}^4\text{He}$ system. These kind of structures cannot be explicitly included in the current model. In particular, for ${}^6\text{He}$ and ${}^6\text{Li}$ within the SVM the authors Kakenov *et al* [50] managed to move closer to experimental values of binding energies by implementing the NNN -force.

In Figures 3.1, 3.2 and 3.3 the correlation densities $W(x_k, y_k)$ (1.34) of the three-body wave functions are illustrated in the 3D-Plot form for the ${}^6\text{He}$, ${}^6\text{Li}$ and ${}^9\text{Be}$ nuclei. For the purpose of proper visualization the contour-plot are given along.

In Figures 3.1 and 3.2, two main geometric configurations can be distinguished, cigar-like component with maximum at the coordinates ($x_k \simeq 4.0 \text{ fm}$, $y_k \simeq 1.0 \text{ fm}$), and di-nucleon component around the coordinates (1.8 fm , 3.0 fm),

both for ${}^6\text{He}$ and ${}^6\text{Li}$ nuclei. The striking highlight of such geometrical configurations is clear evidence of the cluster structure. In particular, we see that in ${}^6\text{He}$, the effect of pairing two nucleons stands out against the background of comparison with ${}^6\text{Li}$. Similar results were described in works [30, 65], and were obtained in particularly within the hyperspherical harmonics method [16].

The Fig. 3.3 shows the spatial correlation function for the bound state of ${}^9\text{Be}$. The single maximum of the correlation density function is located at the coordinates ($x_k \simeq 3.0 \text{ fm}$, $y_k \simeq 2.0 \text{ fm}$). In contrast with the ${}^6\text{He}$ and ${}^6\text{Li}$ nuclei the ${}^9\text{Be}$ nucleus has only one pronounced spatial configuration corresponding to the two α -clusters (${}^8\text{Be}$ ground state) glued by the valence neutron. A very similar picture has been found in Ref. [66].

3.2 Density Function of Nuclear Matter

On the basis of the three-body wave function 1.1, the nuclear matter density distributions are calculated for ${}^6\text{He}$, ${}^6\text{Li}$, and ${}^9\text{Be}$ in the ground states using Equations 1.42, 1.44, 1.47, and 1.50. The results are shown in the Figures 3.4, 3.5, and 3.6 respectively. The plotted the density functions are normalized to their own atomic masses.

A distinctive feature of the obtained results is in the extended tail of the density function for the ${}^6\text{He}$ and ${}^6\text{Li}$ nuclei in Figures 3.4 and 3.5. This is caused by the

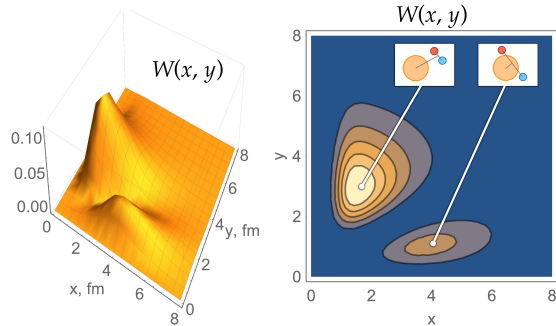


FIGURE 3.2: The same caption as in the Fig.3.1, but for ${}^6\text{Li}$.

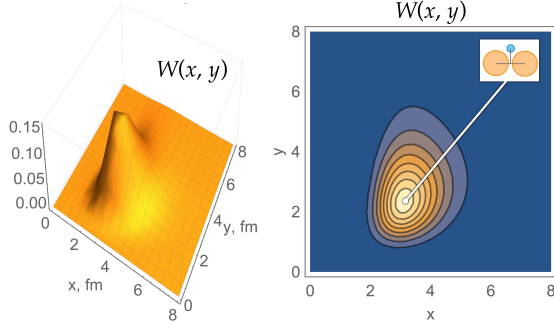


FIGURE 3.3: The same caption as in the Fig.3.1, but for ${}^9\text{Be}$.

properties of the valence nucleons in the three-body system. In particular, the density function of the core $\rho^\alpha(r)$ tends to zero rapidly as the radius r increases in comparison with the nucleon density function ρ^N . As regards of ${}^6\text{Li}$, it testifies stronger contribution of the deuteron-cluster component, in contrast, the ${}^6\text{He}$ has less contribution of di-neutron cluster. The main contribution to the density functions beginning from $r \simeq 3.0 \text{ fm}$ is due to two valence nucleons. Another point of behaviour of density function of nuclei with $A = 6$ is a maximum in the density functions ρ^N at $r \simeq 1.8 \text{ fm}$. In particular, the bump of ${}^6\text{Li}$ is sufficiently remarkable. This character of function explains that the valence nucleons are moved apart from the cm. The view disappears, if the plot of function is built as $r^2\rho^N(r)$. It should be noted that the similar plot are absent elsewhere.

The density function $\rho(r)$ of ${}^9\text{Be}$ has a different shape than the other two previous nuclei (see Fig. 3.6). The alpha particle density function has become much more voluminous. The specific feature of the obtained density function is an extended tail at large distances determined by the valence neutron. The neutron is thus mainly located far from the cm and determines the low binding energy of ${}^9\text{Be}$ nucleus. The density function ρ^N begins from zero, getting the maximum at $r \simeq 3.0 \text{ fm}$, what is characteristic for p -shell nucleons. Another peculiarity of the ${}^9\text{Be}$ structure is in minimum of the function $\rho(r)$ at the start. Such minima are strongly manifested in stable carbon, nitrogen, and oxygen

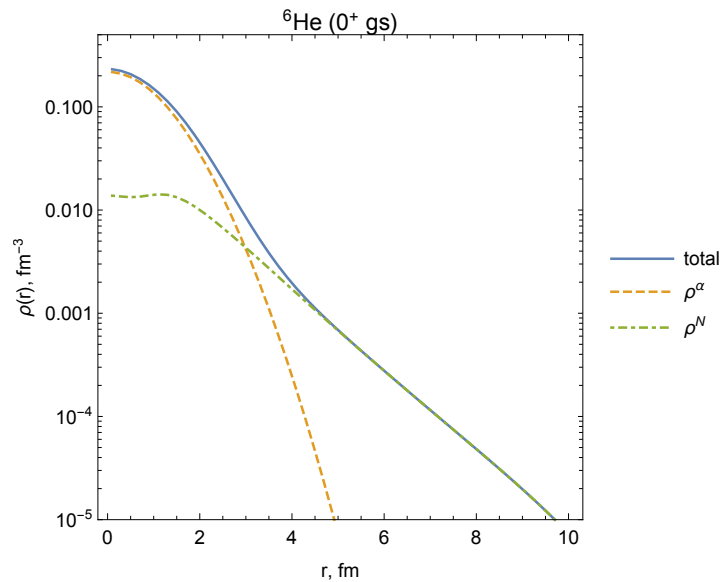


FIGURE 3.4: The nuclear matter density distribution of ${}^6\text{He}$ with the cluster component contributions;

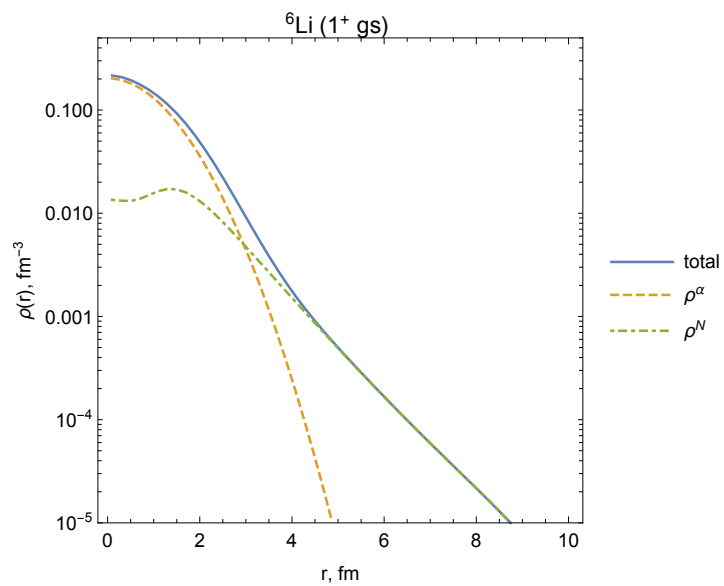


FIGURE 3.5: The same caption as in Fig. 3.4, but for ${}^6\text{Li}$.

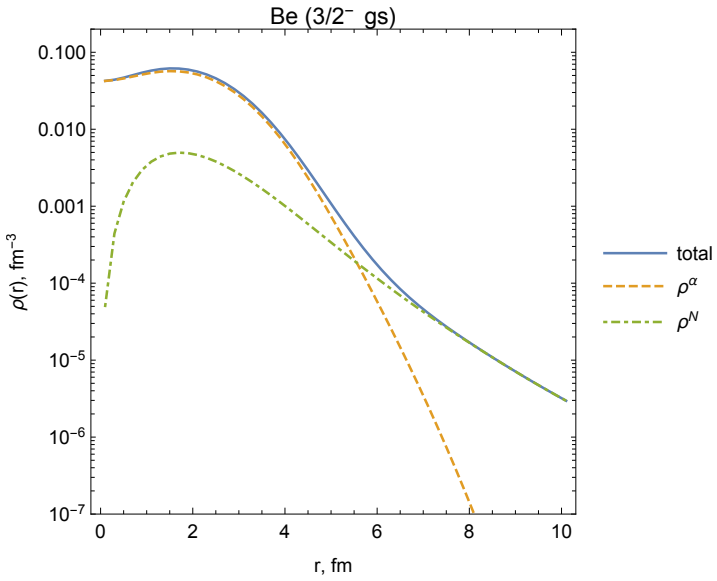


FIGURE 3.6: The same caption as in Fig. 3.4, but for ${}^9\text{Be}$.

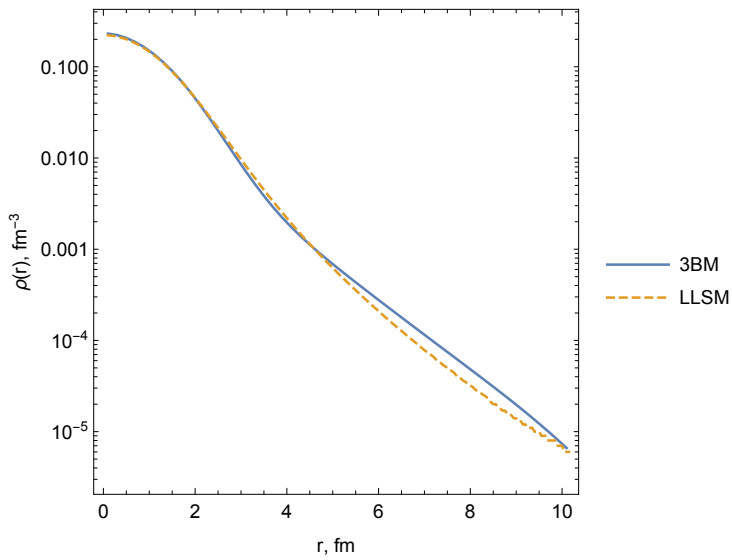


FIGURE 3.7: Comparison of the total nuclear matter density distribution function of ${}^6\text{He}$ with the LLSM calculations [67].

isotopes. For ${}^9\text{Be}$ considered within the three body model, the minimum testifies to its cluster structure and noticeable deformation, reflecting that both valence neutron and α -clusters are displaced with respect to the cm. Such kind of feature for ${}^9\text{Be}$ were obtained also with in the framework of the AMD model [68].

A comparison of the total density function $\rho(r)$ for ${}^6\text{He}$ with the density function calculated in the framework of the Large-Scale Shell-Model (LSSM), (for more, see Ref. [67]), is illustrated in Fig.3.7. Both functions are in good agreement. However, starting from $r \simeq 5.0 - 10.0 \text{ fm}$ the three body model overestimates slightly.

The density function of nuclear matter is an excellent subject for studying rms matter radii. Corresponding formulae for calculating $\langle r^2 \rangle$ are given by Eq.(1.54). The calculated results are presented in Tab.3.2. Here, it should be reminded that the rms radii for α -cluster are taken as: $\langle r_\alpha^2 \rangle_m^{1/2} = 1.461 \text{ fm}$ for nuclear matter, $\langle r_\alpha^2 \rangle_{ch}^{1/2} = 1.67 \text{ fm}$ for charge radius [56]. Obtained results are in good agreement with the experimental data. Except that the rms matter radius of ${}^9\text{Be}$ overestimates for 0.1 fm . It should be noted that similar theoretical estimation was obtained by means of the AMD model [68]. The rms matter radius within this model is $\langle r^2 \rangle_m^{1/2} = 2.61 \text{ fm}$.

TABLE 3.2: Comparison of the calculated rms charge $\langle r_{ch}^2 \rangle$ and matter $\langle r_{ch}^2 \rangle$ radii obtained within the three-body model with experimental data.

	${}^6\text{He} (0^+, gs)$	${}^6\text{Li} (1^+, gs)$	${}^9\text{Be} (\frac{3}{2}^-, gs)$
$\langle r_{ch}^2 \rangle^{1/2}, \text{ fm}$	2.03	2.57	2.48
$\langle r_{ch}^2 \rangle_{exp}^{1/2}, \text{ fm}$	2.066 [69]	2.57(10) [70]	2.50(9) [71]
$\langle r_m^2 \rangle^{1/2}, \text{ fm}$	2.75	2.49	2.58
$\langle r_m^2 \rangle^{1/2}, \text{ fm} [72]$	2.75 ± 0.01	2.54 ± 0.03	2.49 ± 0.01

It worth to note that matrix elements of the rms radii may be obtained also in the following way

$$\langle \phi_{\gamma i}^{JM}(k, pq) | r^2 | \phi_{\gamma' j}^{JM}(k, pq) \rangle, \quad (3.1)$$

where $r = -y_0^{(k)} y_k$. This method gives results in easier way, but doesn't go into the density distribution function of the α -clusters. But, eventually, the rms radii calculated with both Eq. (1.54) and (3.1) give the same results. More detailed derivation of Eq. (3.1) is provided in Ref. [73].

In the further calculations the components of three body wave function, contributing less than 10%, have been omitted (see Tab.3.1), since their influence on the results is insignificant.

Chapter 4

$\alpha + {}^6\text{He}$ nuclear reactions

4.1 Elastic scattering

The differential cross section of elastic scattering (2.12) for the ${}^6\text{He} + \alpha$ nuclear reaction has been calculated within the framework of the OM. The calculations were carried out by means of the code *FRESCO*¹ [74].

The optical potential for the ${}^6\text{He} + \alpha$ system was obtained within the DF model (2.63) using the density functions of nuclear matter (see Eq. 1.44 and 1.47). For the NN-force the density depended DDM3Y-Paris potential was chosen [61]. The DF potential may have terms depending on the interaction of projectile with the clusters of the three body system. In particular, for the ${}^6\text{He} + \alpha$ system, the DF potential can be defined as

$$V^{DF}(r) = V_{\alpha+\alpha}^{DF}(r) + V_{2N+\alpha}^{DF}(r) \quad (4.1)$$

The calculated results are demonstrated in Fig. 4.1. The folding potential of α -core and two valence nucleon with the projectile ${}^4\text{He}$ show specific feature of the interaction. The potential of the α -cluster with the projectile provides

¹Further, when it comes to calculations within the framework of the OM, CC and CRC methods, it means that all calculations have been performed using the code FRESCO.

strong central part, while the interaction with halo neutrons is localized at the peripheral region.

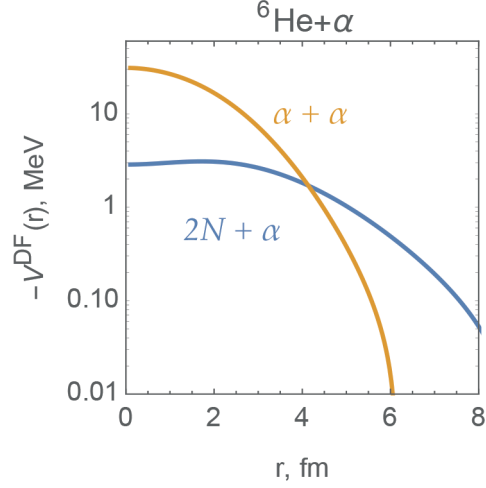


FIGURE 4.1: The folding potential V^{DF} calculated with the density functions of nuclear matter of ${}^6\text{He}$. The $\alpha+\alpha$ designation is for the $V_{\alpha+\alpha}^{DF}$ potential, while $2N+\alpha$ is for the $V_{2N+\alpha}^{DF}$ potential.

Obtained potential was used to calculate the differential cross section for elastic scattering of ${}^6\text{He}$ by α -particles at energy $E_{lab} = 151 \text{ MeV}$. As the real part of the optical potential the folding potential with the parameter N_r was used. For the imaginary part of the optical potential we used again the folding potential, but with the parameter N_i . The corresponding results are shown in Fig. 4.2. In addition to the folding potential, two other potentials (WS1- ${}^6\text{He}$ and WS2- ${}^6\text{He}$) are presented as the Woods-Saxon potential taken from [41]. The potential parameters used in the OM calculations are presented in Tab. 4.1. Calculated results with the both double folding and Woods-Saxon potentials are in good agreement with the experimental data at forward scattering angles. Except the potential WS2- ${}^6\text{He}$, it underestimates the cross section in the range of $50^\circ - 100^\circ$.

The advantage of folding potential in comparison with others is in a less number of adjustable optical parameters. Instead of six parameters fitted in the case of Woods-Saxon potentials, the folding potential allows to reproduce data within two parameters.

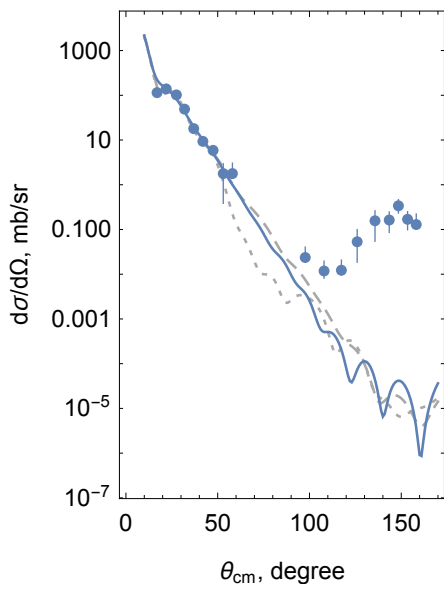


FIGURE 4.2: The differential cross section of the elastic scattering of ${}^6\text{He}$ by α -particles at $E_{\text{lab}} = 151\text{MeV}$ calculated with the different potentials: the double folding potential (blue solid), the WS1- ${}^6\text{He}$ (gray dashed) [41] and WS2- ${}^6\text{He}$ (gray dotted) [41]. Experimental data were taken from [41].

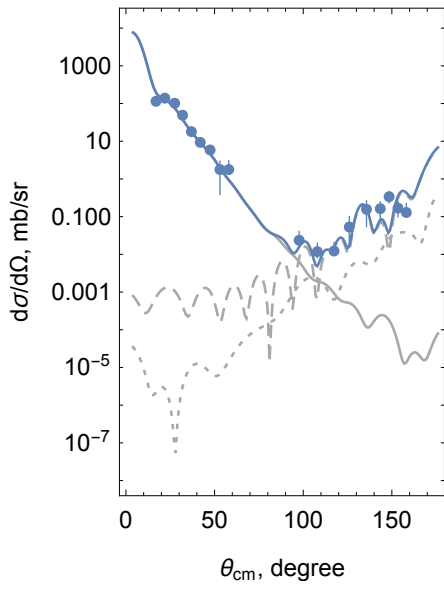


FIGURE 4.3: The cross sections of the elastic channel taking into account few possible reaction mechanisms: elastic scattering (solid gray), simultaneous transfer of di-neutron (gray dashed), sequential transfer of di-neutron (dotted) and their coherent sum (solid blue). Experimental data were taken from [41].

4.2 Elastic transfer

Theoretical curves in Fig. 4.2 could show a good result in describing the experimental data on elastic scattering within the framework of the optical model. However, this is true only at the front scattering angles, while the backscattering angles are far from description of optical calculations. Therefore, in order to explain the disagreement, we propose the following transfer mechanisms of two nucleons: the sequential and simultaneous transfer.

The schematic representation of mechanisms can be seen in Fig. 4.4. Taking into account these mechanisms, the differential cross section can be written as follows

$$\frac{d\sigma}{d\Omega}(\theta) = |f(\theta)_{OM} + f_{sim}(\pi - \theta) + f_{seq}(\pi - \theta)|^2, \quad (4.2)$$

where the amplitude f_{sim} – an amplitude of the finite-range transfer, which may be calculated within the DWBA method (2.39), f_{seq} – an amplitude of two step transfer mechanisms (see, i.e. [57, 74]).

Obtained calculation results for the differential cross section of the elastic transfer were carried out within the framework of the CRC method. Potential for the input and output channels was chosen to be the double folding potential ${}^6\text{He-DF}$. The potential for the intermediate channel was taken as the optical potential with global optical parametrizations for α particles [75]. Trial calculations have shown that the results depend insignificantly on the selected potential for the intermediate channel. The wave function of the bound states was chosen by fitting the potential depth to the binding energy of the composite systems. In particular, the binding energy of one neutron with ${}^6\text{He}$ was chosen 1.8 MeV, neutron with ${}^5\text{He}$ – 0.1 MeV, and two neutrons with α – 0.9 MeV.

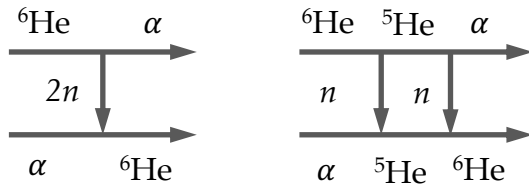


FIGURE 4.4: Schematic representation of the elastic transfer nuclear reaction, on the left - the simultaneous transfer of two nucleons, on the right - the sequential transfer of two nucleons.

TABLE 4.1: The parameters of the potentials used in OM calculations for both $\alpha + {}^6\text{He}$ and $\alpha + {}^6\text{Li}$ nuclear reactions. For more details, see the text

	$-V_0$, MeV	R_v , fm	a_v , fm	$-W_0$, MeV	R_w , fm	a_w , fm	χ^2/N
DF- ${}^6\text{He}$		$N_r=1.4$			$N_i=0.5$		7.32
DF- ${}^6\text{Li}$		$N_r=2.0$			$N_i=1.8$		11.61
WS1- ${}^6\text{He}$	102.5	1.78	0.920	13.0	3.85	0.5	5.75
WS2- ${}^6\text{He}$	102.5	1.54	0.904	7.0	4.28	0.569	6.31
WS1- ${}^6\text{Li}$	102.5	1.78	0.820	11.8	4.11	0.950	15.43

The results of the CRC calculations for elastic transfer are shown in Fig. 4.3. As mentioned in the previous section, the elastic collision mechanism prevails at the forward scattering angles. Beginning from the angle 90° , the contribution to the cross section is mainly caused by the simultaneous transfer of two nucleons. It is worth noting here that two neutrons have the nlj $2S_0$ configuration, which, possibly, leads to an oscillatory cross section. One magnitude less is the contribution of the sequential transfer of di-neutron. In this case both neutrons have $1P_{\frac{3}{2}}$ configuration. For the best reproduction of the experimental data, the SA of di-neutrons was taken $\mathcal{A}_{2S_0}^{00} = 1.0$. The extracted value correspond with the value from Ref. [41, 42].

Thus, it was possible to achieve good agreement between the calculated differential cross section, using the double-folding potential DF- ${}^6\text{He}$ and the proposed transfer mechanisms, with the experimental data [41].

Chapter 5

$\alpha + {}^6\text{Li}$ nuclear reactions

5.1 Elastic scattering

To calculate the elastic scattering cross section we used again the folding potential with the density depended DDM3Y-Paris effective NN-potential [61]. The three body density functions of nuclear matter used to calculate the potential similarly to Eq. (4.1). Therefore, it was possible to look into the interaction of the α -projectile with deuteron and α clusters inside the nucleus ${}^6\text{Li}$ (see, Fig. 5.1). The function of the interaction potential of the projectile with the internal alpha particle rapidly tends to zero, while the function of the interaction potential of the projectile with the internal deuteron slowly decreases. It should also be noted that, starting from the distance $r \simeq 4.0$, the main contribution is due to the interaction of the projectile with the internal deuteron.

The folding potential was chosen to be the real part of the optical potential with the N_r fitting parameter. As regards the imaginary part, the same shape of real part was used, but with the parameters N_i . The Woods-Saxon potential with six parametrizations was taken from [41] as comparison to DF- ${}^6\text{Li}$. The results of calculating the differential cross section of elastic collision of the $\alpha + {}^6\text{Li}$ system are shown in Fig. 5.2. The theoretical curves based on the potentials DF- ${}^6\text{Li}$ and WS1- ${}^6\text{Li}$ show good agreement with the experimental

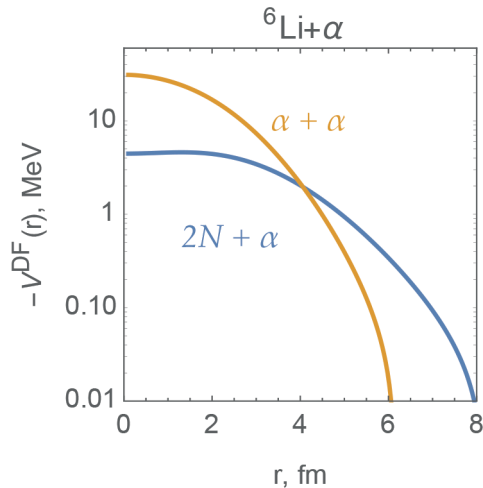


FIGURE 5.1: The folding potential $V^{DF}(r)$ calculated with the density functions of nuclear matter of ${}^6\text{Li}$. The $\alpha + \alpha$ designation is for the $V_{\alpha+\alpha}^{DF}$ potential, while $2N + \alpha$ is for the $V_{2N+\alpha}^{DF}$ potential.

data. It should be noted that the double folding potential DF- ${}^6\text{Li}$ for the elastic scattering $\alpha + {}^6\text{Li}$ reaction depends only on two parameters rather than the Woods-Saxon potential WS1- ${}^6\text{Li}$ with six parameters.

The ${}^6\text{Li}$ structure is very similar to ${}^6\text{He}$. Therefore, as in the case of ${}^6\text{He}$, the calculations made in the framework of the OM are well described only at the forward scattering angles. The potential parameters are listed in Tab. 4.1.

Differential cross sections belonging to the backward angles have the character of another mechanism - the transfer of d from ${}^6\text{Li}$. How exactly this subsystem is transferred will be discussed in the next section devoted to elastic transfer for the $\alpha + {}^6\text{He}$ reaction.

5.2 Elastic transfer

An increase in the cross section for the elastic scattering $\alpha + {}^6\text{Li}$ reaction starting from 90° suggests the existence of additional reaction mechanisms. In this case, in order to register the same particle as the elastically scattered projectile,

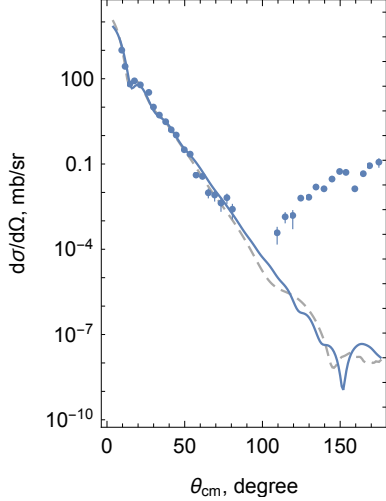


FIGURE 5.2: The differential cross section of the elastic scattering of ${}^6\text{Li}$ by α -particles at $E_{lab} = 166\text{MeV}$ with the different potentials: the double folding potential DF- ${}^6\text{Li}$ (blue solid), the WS1- ${}^6\text{Li}$ (gray dashed) [41]. Experimanetal data taken from [41].

a deuteron particle must be transferred to the target at angles above 90° . The transfer mechanisms are shown schematically in Fig 5.4.

As in the case of ${}^6\text{He}$, calculations for obtaining the differential cross section of the elastic transfer were carried out within the framework of the CRC method. For the input and output channels the double folding potential was taken, and for the intermediate channel the optical potential with global optical parametrizations for α particles [75] was chosen. The calculations have shown that the cross sections depend insignificantly on the selected potential for the intermediate channel. The wave function of the bound states was chosen by fitting the potential depth to the binding energy of the composite systems. In particular, the binding energy of one neutron with ${}^5\text{Li}$ was 5.663 MeV, as neutron with ${}^5\text{He}$ taken 0.9 MeV, and as d with α taken 1.474 MeV. The differential cross section for this reaction is determined using the same formula 4.2.

The results of calculations for elastic transfer are shown in Fig. 5.3. The mechanism of elastic collision in the reaction of $\alpha + {}^6\text{Li}$ prevails over other mechanisms at the forward scattering angles. However, starting from 90° we see that the

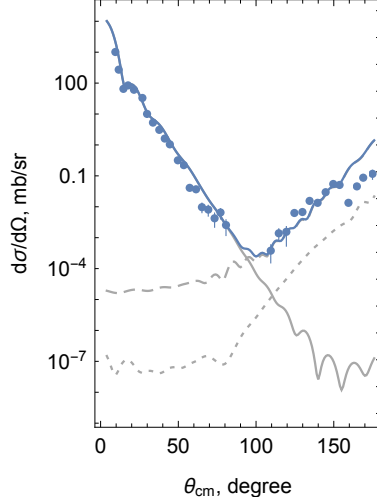


FIGURE 5.3: The cross sections of the elastic transfer reaction are represented in terms of the transfer mechanisms: elastic scattering (solid gray), simultaneous transfer of d (gray dashed), sequential transfer of $2N$ (dotted) and their coherent sum (solid blue). Experimanetal data taken from [41].

main contribution to the cross section is caused by the simultaneous transfer of two nucleons of ${}^6\text{Li}$, that is, the deuteron. The difference from the reaction $\alpha + {}^6\text{He}$ is in the spin structures of the composite nucleus ${}^6\text{Li}(1^+) = \alpha(0^+) + d(1^+)$. Accordingly, deuteron can be transferred by $2S1$ and $2D1$ configurations.

At the backward scattering angles the domination of the simultaneous transfer on sequential transfer mechanism is seen. That makes total sense because deuteron is less bound than neutron with ${}^6\text{Li}$ - $E_{BE}(d) = 1.5\text{MeV}$ and $E_{BE}(n) = 5.7\text{MeV}$. Moreover, two step mechanisms are typically few order magnitude lower than the one step transfers. The best agreement with the experimental data is obtained if one uses the SA for the configuration $2S1$ $\mathcal{A}_{2S1}^{10} \simeq 0.7$, and for the configuration $2D1$ $\mathcal{A}_{2D1}^{10} \simeq 0.5$. As for the sequential transfer of the d system, it has a contribution much less than the simultaneous transfer by one order of magnitude. Taken results based on the three body model are in good agreement with the experimental data.

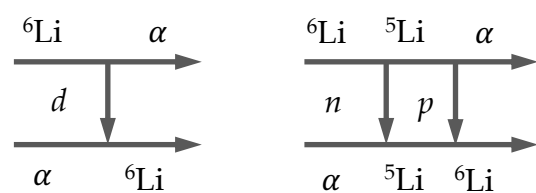


FIGURE 5.4: Schematic representation of the elastic transfer nuclear reaction, on the left - the simultaneous transfer of two nucleons, on the right - the sequential transfer of two nucleons.

Chapter 6

$d + {}^9\text{Be}$ nuclear reactions

6.1 Elastic channel

The DF potential was calculated using the effective DDM3Y-Paris nucleon-nucleon potential [61] and the nuclear-matter-densities of projectile and target nuclei (see Eq. (1.42) and (1.50)). The matter density distribution of the deuteron projectile was chosen to be of the form

$$\rho\left(\frac{1}{2}r\right) = \int |\Psi^d(\mathbf{r})|^2 d\Omega_r. \quad (6.1)$$

where $\Psi^d(\mathbf{r})$ – a wave function of deuteron, \mathbf{r} – a relative distance between proton and neutron. The calculated results of the DF potential for $d + {}^9\text{Be}$ are plotted in Fig. 6.1. It is seen that the main contribution of the $d + {}^9\text{Be}$ interaction starting at $r \simeq 6.0 fm$ is caused by N .

For convenience, in the OM and CC (CRC) calculations the DF potentials have been fitted by means of the sum of three Woods-Saxon potentials:

$$V^V(R) = \sum_{i=1}^3 V^i f^{R_i, a_i}(R), \quad (6.2)$$

$$f^{R_V, a_V}(R) = \frac{1}{1 + \exp \frac{R - R_V}{a_V}}. \quad (6.3)$$

Here, the parameters of the imaginary part of the optical potential were ob-

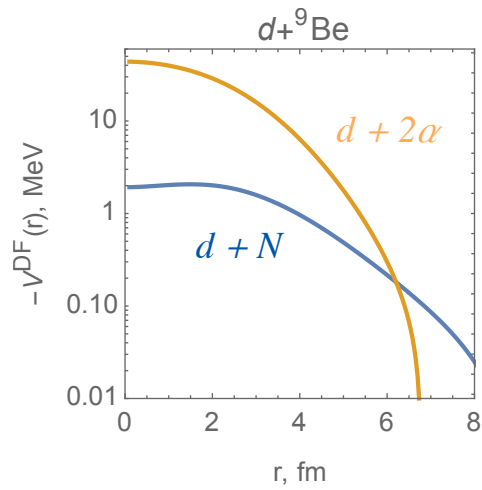


FIGURE 6.1: The folding potential $V^{DF}(r)$ calculated with the density functions of nuclear matter of ${}^9\text{Be}$. The $d + 2\alpha$ designation is for the $V_{d+2\alpha}^{DF}$ potential, while $d + N$ is for the V_{d+N}^{DF} potential, see Eq. (4.1).

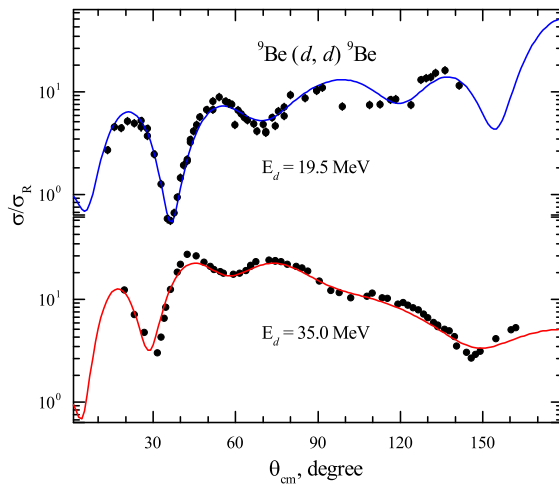


FIGURE 6.2: The angular distribution of elastic scattering data of d from ${}^9\text{Be}$ at laboratory energy 19.5 MeV in comparison with theoretical calculations within the OM (solid curve).

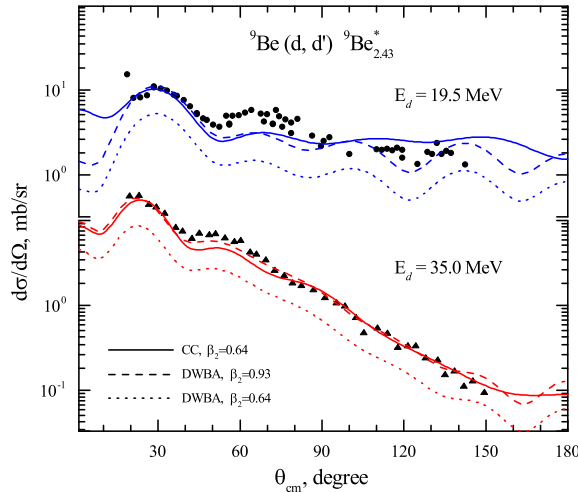


FIGURE 6.3: The cross sections of inelastic scattering ${}^9\text{Be}(d, d') {}^9\text{Be}^*$ ($E_{exc}=2.43$ MeV) at laboratory energies 19.5 MeV (full circle) and 35 MeV (full triangle). Theoretical curves are described in the text.

tained by fitting the theoretical cross sections to the experimental data at 19.5 MeV and 35 MeV incident energies. As a starting point, the same parameterizations of the real part were used. The obtained potential parameters after fitting are listed in Table 6.1 for both 19.5 MeV and 35.0 MeV incident energies.

The comparison of the results of the theoretical calculations with the measured data for elastic scattering at 19.5 MeV and 35.0 MeV energies are plotted in Fig. 6.2. The cross sections obtained in the framework of the OM with the DF potential are shown as solid curves. Theoretical results obtained by means of the OM give an excellent agreement, $\chi^2 \approx 2.5$, with the experimental data. The parameters of parameterized double-folding potential are listed in Table 6.1.

6.2 Inelastic scattering

The CC and DWBA approaches have been applied to analyse the measured inelastic scattering data corresponding to the ${}^9\text{Be}(5/2^-, 2.43$ MeV) excitation. Calculations were performed employing the FRESCO code [74] and the DWUCK5 code [76] which are available in the NRV knowledge-base [77].

In order to describe the measured experimental data one has to consider the ${}^9\text{Be}$ target having a quadrupole deformation. Thus, the ${}^9\text{Be}$ spectrum consists of the rotational band including the $3/2^-$ ground state, $5/2^-$ state at 2.43 MeV and $7/2^-$ state at 6.38 MeV. Couplings to these states were taken into account within the CC approach. The spin reorientations were also taken into account. The coupling interaction has the usual form:

$$V_\lambda(R) = -\beta_\lambda R_V \left| \frac{dV^V}{dR} \right| - i\beta_\lambda R_W \left| \frac{dW^D}{dR} \right|, \quad (6.4)$$

where β_λ is the deformation parameter of λ multipole describing the target-nucleus form. Here, we neglect as usual the contribution of the Coulomb interaction.

The calculated cross sections for inelastic scattering to the $5/2^-$ state at 2.43 MeV are shown in Fig. 6.3. The solid curves correspond to the results obtained within the CC approach, while the dashed and dotted curves were obtained within the DWBA approach using different values of the deformation parameter β_2 . The used potential parameters are listed in Table 6.1.

All the results in Fig. 6.3 are in good agreement with the experimental data, except for the cross sections around 60° at 19.5 MeV incident energy. The

TABLE 6.1: Parameterized double-folding potentials of the $d+{}^9\text{Be}$ system used in the OM, CC and DWBA calculations.

E_d , MeV	i	V_0 , MeV	r_v^a , fm	a_v , fm	W_0 , MeV	r_w^a , fm	a_w , fm	V_0^{SO} , MeV	N_R	r_C^a , fm	χ^2/N
19.5	16.18	0.328	0.308	3.99	25.50 (17.5 ^b)	0.328	0.127	3.275	1.22	0.809	2.490
	270.97	0.746	0.831	0.746		0.766					
	30.605	1.491	1.724	0.924		1.491	2.238				
35.0	15.941	0.328	0.308	7.07	22.50 (17.5 ^b)	0.612	0.108	3.275	1.17	0.809	2.503
	268.68	0.746	0.831	0.838		0.731					
	30.58	1.491	1.724	0.999		1.377	1.856				

^a Radii are defined as $R_i = r_i \left(A_P^{1/3} + A_T^{1/3} \right)$.

^b The values are used in CRC calculations.

quadrupole deformation parameter $\beta_2 = 0.64$ extracted within the coupled-channel model is consistent with the previous studies [78, 79].

In the case of DWBA calculations, one uses the DF potential (see Table 6.1) for both the entrance and the exit channels. The DWBA angular distributions very well reproduce the structure of experimental data but clearly underestimate them when the deformation parameter $\beta_2 = 0.64$ is used (see the dotted curves in Fig. 6.3). In order to get the best fit the deformation parameter must be increased up to $\beta_2 = 0.93$, which is quite close to the values reported in previous studies (see, for example, [80, 81]).

Thus, one may confirm that channel coupling and the effects of spin reorientation enhance the cross section that results in the reduction of the deformation parameter. However, the DWBA approach takes into account only first-order contributions to the transition amplitude. In particular, it also describes only general features of the angular distributions and overestimates the deformation parameter in order to compensate the difference between the experimental data and the DWBA cross sections.

6.3 One-nucleon transfer reactions

The one-neutron pick-up ${}^9\text{Be}(d, t){}^8\text{Be}$ and stripping ${}^9\text{Be}(d, p){}^{10}\text{Be}$ reactions were analyzed here within the framework of the CRC method.

The double-folding potential given in Table 6.1 was used in the CRC calculations for the entrance channel and the global optical parameterizations from Ref. [82, 83] were used for the exit channels. The coupling schemes of target and daughter nuclei for the ${}^9\text{Be}(d, p){}^{10}\text{Be}$ and ${}^9\text{Be}(d, t){}^8\text{Be}$ reactions are illustrated in Fig. 6.4. The states of ${}^{10}\text{Be}$, 2_1^+ and 2_2^+ , as well as the low-lying excited states of ${}^8\text{Be}$, 2^+ and 4^+ , were included in the coupling scheme. Also, the schemes take into account the spin reorientations of states on the condition $J \neq 0$.

In order to construct the bound-state wave functions of the transferred particle in the entrance and exit channels, the common method, i.e. fitting the depth of the corresponding Woods-Saxon potential to the known binding energy, was employed. The reduced radius and diffuseness in this case are set to be $r = 1.25$ fm and $a = 0.65$ fm, respectively. If the transfer takes place to a final unbound state, the depth of the potential for this state was adjusted to yield a binding energy equal to -0.1 MeV in accordance with the procedure used in Ref. [79].

If the core and the composite nuclei have internal excitation energies, a renewed binding energy BE^* of the transferred particle is expressed by the formula:

$$BE^* = BE - E_{com}^* + E_{core}^* \quad (6.5)$$

where BE – the binding energy of the transferred particle, E_{com}^* , E_{core}^* – excitation energies of the composite and core nuclei, respectively.

The SA (2.59) for the addition of a particle to a core with angular momentum J_{core} to form a composite with J_{com} is related to the matrix element of the creation operator \hat{a}^\dagger :

$$\mathcal{A}_{Nlj} = \frac{\langle J_{com} | \hat{a}_{Nlj}^\dagger | J_{core} \rangle}{\sqrt{2J_{com} + 1}} \quad (6.6)$$

where Nlj is the set of particle quantum numbers. The spectroscopic amplitudes for one particle states were calculated by means of the *ANTOINE* code [84] using the effective Cohen-Kurath interaction for p -shell nuclei [85]. The calculated SA for the one-nucleon transfer reactions are listed in Table 6.2.

Angular distributions of the ${}^9\text{Be}(d, p){}^{10}\text{Be}$ nuclear reaction at $E_d=19.5$ MeV are shown in comparison with the theoretical curves calculated in the framework of the CRC method in Fig. 6.5.

In order to study the couplings of the input channels, the outputs were fixed

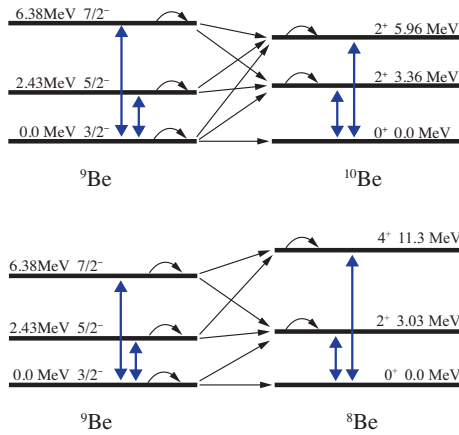


FIGURE 6.4: The target coupling schemes in the ${}^9\text{Be}(d, p){}^{10}\text{Be}$ (upper) and the ${}^9\text{Be}(d, t){}^8\text{Be}$ (lower) nuclear reactions. The bold two-headed arrows indicate $E\lambda$ transitions. The spin re-orientation effects are indicated as back-pointing arrows.

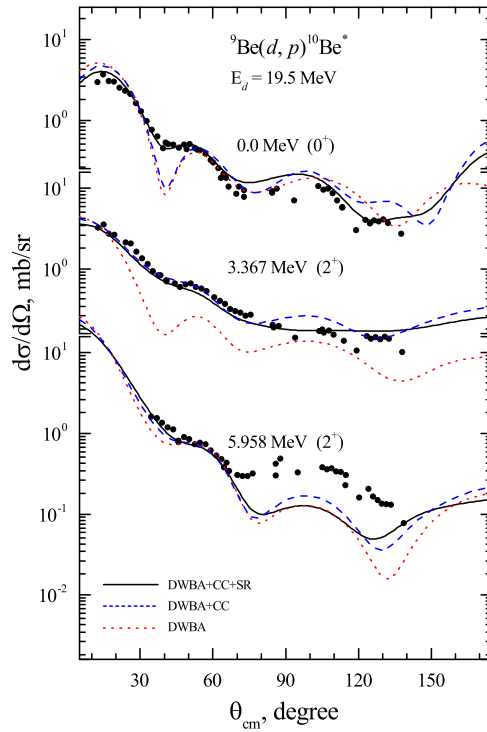


FIGURE 6.5: Differential cross sections for the ${}^9\text{Be}(d, p){}^{10}\text{Be}^*$ reactions at 19.5 MeV leading to different final states (labelled in the figure) in ${}^{10}\text{Be}$. The experimental data are shown in comparison with theoretical results obtained within the CRC method.

TABLE 6.2: Spectroscopic amplitudes used in CRC calculations for the Composite = Core + Nucleon system. The one-nucleon SA have been calculated by means of the *ANTOINE* code [84]. The alpha spectroscopic amplitudes were taken from [86, 87].

Com	2J ₁	Core	2J ₂	N	2J	SA	Com	2J ₁	Core	2J ₂	N	2J	SA
⁹ Be	3	⁸ Be	0	<i>n</i>	3	-0.761	⁹ Be	3	⁸ Li	₂ ₁	<i>p</i>	1	-0.444
⁹ Be	3	⁸ Be	4	<i>n</i>	3	0.816	⁹ Be	3	⁸ Li	₆	<i>p</i>	3	-0.592
⁹ Be	3	⁸ Be	4	<i>n</i>	1	-0.242	⁹ Be	3	⁸ Li	₂ ₂	<i>p</i>	3	-0.236
⁹ Be	5	⁸ Be	4	<i>n</i>	3	0.986	⁹ Be	3	⁸ Li	₂ ₂	<i>p</i>	1	0.036
⁹ Be	5	⁸ Be	4	<i>n</i>	1	-0.417	⁹ Be	5	⁸ Li	₄	<i>p</i>	3	0.593
⁹ Be	5	⁸ Be	8	<i>n</i>	3	-0.374	⁹ Be	5	⁸ Li	₄	<i>p</i>	1	0.515
⁹ Be	7	⁸ Be	4	<i>n</i>	3	-0.457	⁹ Be	5	⁸ Li	₂ ₁	<i>p</i>	3	-0.672
⁹ Be	7	⁸ Be	8	<i>n</i>	3	0.919	⁹ Be	5	⁸ Li	₆	<i>p</i>	3	-0.571
⁹ Be	7	⁸ Be	8	<i>n</i>	1	-0.429	⁹ Be	5	⁸ Li	₆	<i>p</i>	1	-0.171
⁸ Be	0	⁷ Li	3	<i>p</i>	3	-1.204	⁹ Be	5	⁸ Li	₂ ₂	<i>p</i>	3	0.200
⁸ Be	0	⁷ Li	1	<i>p</i>	1	0.736	⁹ Be	7	⁸ Li	₄	<i>p</i>	3	-0.323
⁸ Be	4	⁷ Li	3	<i>p</i>	3	-0.748	⁹ Be	7	⁸ Li	₆	<i>p</i>	3	-0.899
⁸ Be	4	⁷ Li	3	<i>p</i>	1	-0.612	⁹ Be	7	⁸ Li	₆	<i>p</i>	1	-0.564
⁸ Be	4	⁷ Li	1	<i>p</i>	3	0.667	⁷ Li	₃	⁶ Li	₂	<i>n</i>	3	0.657
⁸ Be	4	⁷ Li	7	<i>p</i>	3	0.624	⁷ Li	₃	⁶ Li	₂	<i>n</i>	1	-0.538
⁸ Be	4	⁷ Li	5 ₂	<i>p</i>	3	0.079	⁷ Li	₃	⁶ Li	₆	<i>n</i>	3	0.744
⁸ Be	4	⁷ Li	5 ₂	<i>p</i>	3	-0.146	⁷ Li	₃	⁶ Li	₄	<i>n</i>	3	-0.032
⁸ Be	8	⁷ Li	7	<i>p</i>	3	0.864	⁷ Li	₃	⁶ Li	₄	<i>n</i>	1	0.399
⁸ Be	8	⁷ Li	7	<i>p</i>	1	0.687	⁷ Li	₁	⁶ Li	₂	<i>n</i>	3	-0.925
⁸ Be	8	⁷ Li	5 ₂	<i>p</i>	3	0.374	⁷ Li	₁	⁶ Li	₂	<i>n</i>	1	0.197
⁸ Li	4	⁷ Li	3	<i>n</i>	3	-0.988	⁷ Li	₁	⁶ Li	₄	<i>n</i>	3	-0.555
⁸ Li	4	⁷ Li	3	<i>n</i>	1	0.237	⁷ Li	₇	⁶ Li	₆	<i>n</i>	3	-0.936
⁸ Li	4	⁷ Li	1	<i>n</i>	3	0.430	⁷ Li	₇	⁶ Li	₆	<i>n</i>	1	0.645
⁸ Li	4	⁷ Li	7	<i>n</i>	3	-0.496	⁷ Li	₇	⁶ Li	₄	<i>n</i>	3	-0.456
⁸ Li	4	⁷ Li	5	<i>n</i>	3	-0.665	⁷ Li	_{5₂}	⁶ Li	₂	<i>n</i>	3	-0.650
⁸ Li	4	⁷ Li	5 ₂	<i>n</i>	1	-0.275	⁷ Li	_{5₂}	⁶ Li	₆	<i>n</i>	3	0.732
⁸ Li	2 ₁	⁷ Li	3	<i>n</i>	3	0.567	⁷ Li	_{5₂}	⁶ Li	₆	<i>n</i>	1	0.549
⁸ Li	2 ₁	⁷ Li	3	<i>n</i>	1	0.351	⁷ Li	_{5₂}	⁶ Li	₄	<i>n</i>	3	0.200
⁸ Li	2 ₁	⁷ Li	1	<i>n</i>	3	0.905	⁷ Li	_{5₂}	⁶ Li	₄	<i>n</i>	1	-0.114
⁸ Li	2 ₁	⁷ Li	1	<i>n</i>	1	0.331	⁶ Li	₂	<i>d</i>	₂	α	0	0.907
⁸ Li	2 ₁	⁷ Li	5 ₂	<i>n</i>	3	0.767	⁶ Li	₂	<i>d</i>	₂	α	4	0.077
⁸ Li	6	⁷ Li	3	<i>n</i>	3	0.581	⁶ Li	₆	<i>d</i>	₂	α	4	0.943
⁸ Li	6	⁷ Li	5 ₂	<i>n</i>	3	-0.660	⁶ Li	₆	<i>d</i>	₂	α	8	0.028
⁸ Li	6	⁷ Li	5 ₂	<i>n</i>	1	-0.541	⁶ Li	₄	<i>d</i>	₂	α	4	0.929
⁸ Li	6	⁷ Li	7	<i>n</i>	3	0.973	⁹ Be	3	⁵ He	₃	α	0	-0.925
⁸ Li	6	⁷ Li	7	<i>n</i>	1	-0.404	⁹ Be	3	⁵ He	₃	α	4	0.784
⁸ Li	2 ₂	⁷ Li	3	<i>n</i>	3	-0.617	⁹ Be	5	⁵ He	₃	α	4	0.974
⁸ Li	2 ₂	⁷ Li	3	<i>n</i>	1	-0.841	⁹ Be	5	⁵ He	₃	α	8	-0.260
⁸ Li	2 ₂	⁷ Li	1	<i>n</i>	3	0.178	⁹ Be	7	⁵ He	₃	α	4	0.882
⁸ Li	2 ₂	⁷ Li	1	<i>n</i>	1	0.331	⁹ Be	7	⁵ He	₃	α	8	-0.737
⁸ Li	2 ₂	⁷ Li	5	<i>n</i>	3	0.231	⁷ Li	₃	<i>t</i>	₁	α	1	0.970
⁹ Be	3	⁸ Li	4	<i>p</i>	3	-0.947	⁷ Li	₁	<i>t</i>	₁	α	1	0.961
⁹ Be	3	⁸ Li	4	<i>p</i>	1	-0.319	⁷ Li	₇	<i>t</i>	₁	α	3	0.952
⁹ Be	3	⁸ Li	2 ₁	<i>p</i>	3	0.454	⁷ Li	_{5₂}	<i>t</i>	₁	α	3	0.223

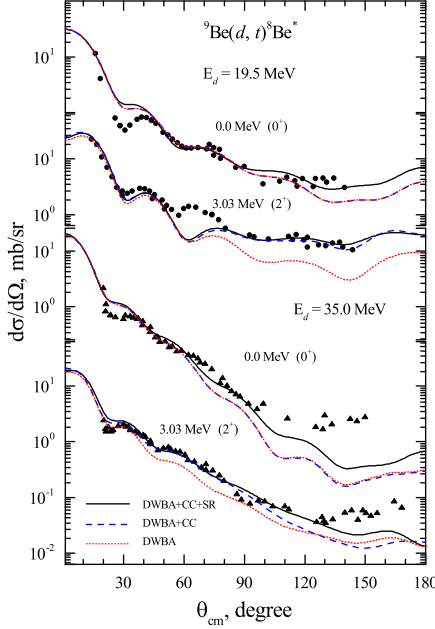


FIGURE 6.6: Differential cross sections for the ${}^9\text{Be}(d, t){}^8\text{Be}^*$ reactions at 19.5 and 35 MeV leading to different final states (labelled in the figure) in ${}^8\text{Be}$. The experimental data are shown in comparison with theoretical results obtained within the CRC method.

using the deformation parameter of ${}^8\text{Be}$ from Ref. [88], and for ${}^{10}\text{Be}$ from Ref. [79]. The direct transition from the ground state is indicated by the dotted line (DWBA). The contributions of the transitions from excited states (CC), and from spin reorientations (SR) are indicated by dashed and solid lines, respectively. During the analysis, it was found that spin reorientation has a significant contribution in the $p + {}^{10}\text{Be}_{gs}$ channel, especially in the range of 40-60 degrees.

It is interesting to note that we managed to describe within the CRC method the differential cross section of the ${}^9\text{Be}(d, p){}^{10}\text{Be}_{gs}$ reaction at all scattering angles, including the range 40° - 60° , where they were not covered in Refs. [80, 89].

An appreciable contribution of the $3/2^- \rightarrow 2_1^+$, $5/2^- \rightarrow 2_1^+$, $7/2^- \rightarrow 2_1^+$ transitions was observed in the $p + {}^{10}\text{Be}_{3.37}$ channel in the entire range of scattering

angles. In the cross section of the $p + {}^{10}\text{Be}_{5.96}$ channel, the theoretical calculation underestimates the experimental data starting from 70° . Possibly, other higher excited states of ${}^9\text{Be}$ should be taken into account.

Figure 6.6 displays the cross sections of the ${}^9\text{Be}(d,t){}^8\text{Be}$ nuclear reaction at both 19.5 MeV and 35 MeV incident energies. As in the case of the (d,p) reactions, the (d,t) reactions also show the strong channel-coupling effects. We see the manifestation of spin-reorientation effects in the $t + {}^8\text{Be}_{gs}$ channels and the significant contribution of the $3/2^- \rightarrow 2^+$, $5/2^- \rightarrow 2^+$, $7/2^- \rightarrow 2^+$ transitions in the $t + {}^8\text{Be}_{3.03}$ channel. Disagreements around 30° in the $t + {}^8\text{Be}_{gs}$ channel for both 19.5 MeV and 35 MeV incident energies and around 60° in the $t + {}^8\text{Be}_{3.03}$ channel for 19.5 MeV incident energy are possibly caused by the uncertainty in the $t + {}^8\text{Be}$ interaction potential.

Theoretical calculations made within the CRC method show, in general, good agreement with the experimental data for both (d,p) and (d,t) reactions. The analysis showed strong coupling effects in both entrance and exit channels. The effects of such couplings were also emphasized in Refs. [79, 90].

6.4 Cluster-transfer reaction

Differential cross sections for the nuclear reaction ${}^9\text{Be}(d,\alpha){}^7\text{Li}$ are of particular interest. This is due to the specific behaviour of the cross section at large scattering angles, which indicates a ${}^5\text{He}$ transfer. In addition, the cross section calculated within the DWBA approach underestimates the data even at forward scattering angles. Therefore, in order to understand the difference between theory and experiment, the following transfer mechanisms are suggested (see Fig. 6.7):

- the direct transfer of cluster d and of ${}^5\text{He}$ system;
- the sequential two-step transfer of $n-p$, $p-n$, $n-\alpha$ and $\alpha-n$;

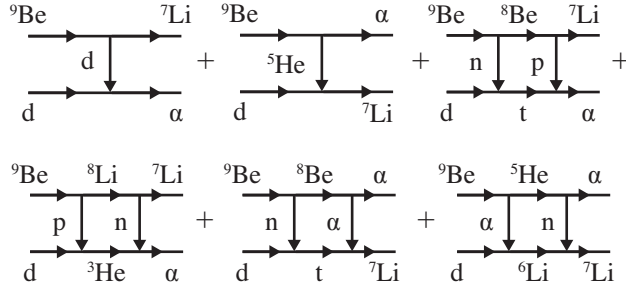


FIGURE 6.7: The scheme illustrates the reaction mechanisms taken into account in CRC calculations of the cross sections for ${}^9\text{Be}(d, \alpha){}^7\text{Li}$ reaction.

The resulting differential cross section for the ${}^9\text{Be}(d, \alpha){}^7\text{Li}$ reaction has the form of a coherent sum of two amplitudes

$$\frac{d\sigma}{d\Omega}(\theta) = |f_I(\theta) + f_{II}(\theta)|^2, \quad (6.7)$$

where the amplitude

$$f_I(\theta) = f_{^5\text{He}}(\pi - \theta) + f_{n-\alpha}(\pi - \theta) + f_{\alpha-n}(\pi - \theta) \quad (6.8)$$

describes the transfer of the ${}^5\text{He}$ nucleus and sequential two-step transfer of $n-\alpha$ and $\alpha-n$, and the amplitude

$$f_{II}(\theta) = f_d(\theta) + f_{n-p}(\theta) + f_{p-n}(\theta) \quad (6.9)$$

corresponds to the deuteron pick-up and sequential two-step transfer of $n-p$ and $p-n$.

The DF potential (see Table 6.1) for the entrance channel and global optical potential parameterizations from Refs. [83, 91, 92] for intermediate and exit channels were used in the analysis. The prior form for the first coupling and the post form for the second coupling were chosen for two-step transfer reactions in order to avoid the non-orthogonal terms in the calculations of transition

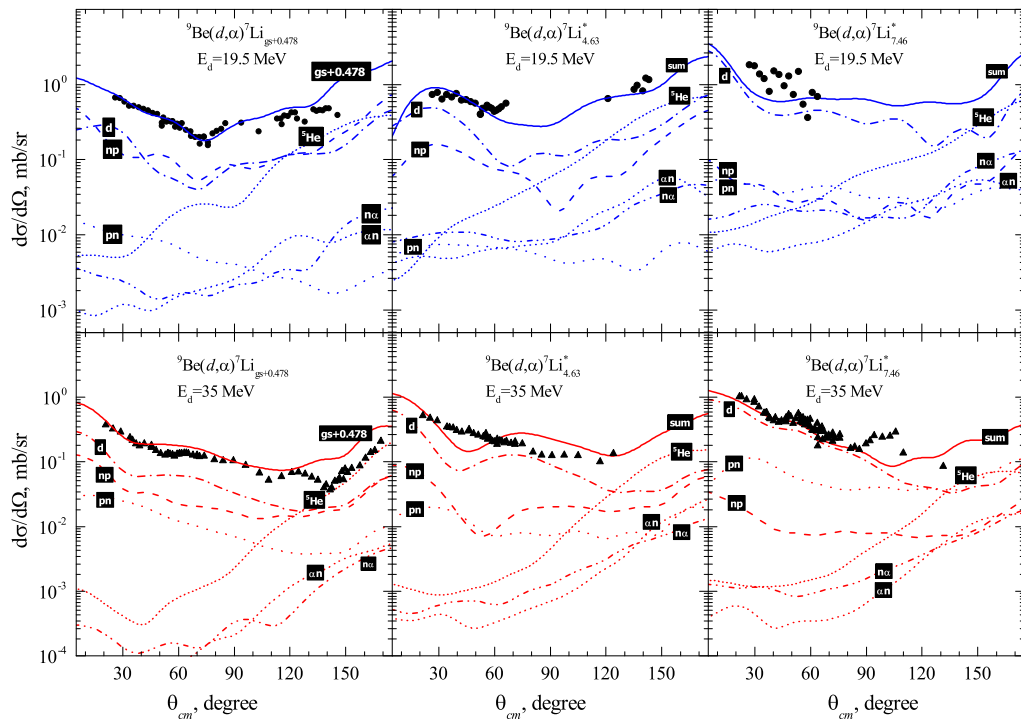


FIGURE 6.8: Differential cross sections for the ${}^9\text{Be}(d,\alpha){}^7\text{Li}$ reactions measured at 19.5 MeV and 35 MeV energy with the ${}^7\text{Li}$ observed in the ground or low-lying excited states in the exit channels.

amplitudes.

The spectroscopic amplitudes of the d and ${}^5\text{He}$ systems were taken from Ref. [93], while the alpha-cluster spectroscopic amplitudes given in Table 6.2 were provided by Dr. A. Volya within the method reported in Ref. [87].

The calculated cross sections are shown in Fig. 6.8 with the α -particle angular distributions formed in the ${}^9\text{Be}(d,\alpha){}^7\text{Li}^*$ reaction at incident energies of 19.5 and 35 MeV and corresponding to the low-lying excitation of the ${}^7\text{Li}$ nucleus in the exit channels. The transfer of the deuteron (dash-dotted curve) provides the dominant contribution in all the channels. Despite the fact that the spectroscopic amplitude of the deuteron $\mathcal{A}_{1D_3} = 0.558$ in the ${}^9\text{Be}$ nucleus is not of great importance, a noticeable cross section is due to the large value of the deuteron spectroscopic amplitude $\mathcal{A}_{1S_1} = 1.732$ of ${}^4\text{He}$.

The angular distribution of deuteron transfer has a significant cross section also at the backward scattering angles, which is mainly caused by the contribution of the D wave. This symmetrical behaviour of the cross section of D waves is very similar to the cross section of evaporation residues. Tanaka *et al* [94] analyzed the role of the compound process in ${}^9\text{Be}(d,\alpha){}^7\text{Li}$ reaction and claimed the domination of the compound nucleus channels at the energies of 12.17 MeV and 14.43 MeV. However, in Ref. [80] the negligible contribution of the compound-nucleus mechanism was shown at 7 MeV using the DWBA analysis. In this regard, our theoretical results based on the CRC method show that there is no need to take into account the mechanism through the compound-nucleus formation at energies of 19.5 and 35.0 MeV.

Starting from scattering angle $\theta_{c.m.} = 120^\circ$, the transfer of the ${}^5\text{He}$ system, labeled as ${}^5\text{He}$ in Fig. 6.8, has a predominant contribution in all channels. It should be noted that a similar result was reported earlier in Ref. [80]. One-step transfer of the ${}^5\text{He}$ nucleus was also indicated as a dominant process by Jarczyk *et al* [95] in studying the ${}^{12}\text{C}({}^{11}\text{B}, {}^6\text{Li}){}^{17}\text{O}$ and ${}^{12}\text{C}(d, {}^7\text{Li}){}^7\text{Be}$ reactions.

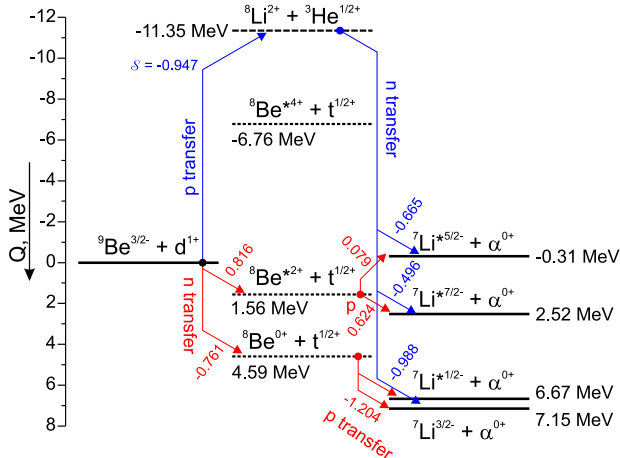


FIGURE 6.9: The scheme illustrates the energy balance of the different intermediate stages for the two-step mechanisms of ${}^9\text{Be}(d, \alpha){}^7\text{Li}$ transfer reaction. The Q -values for the different intermediate channels are shown near the corresponding lines. The numbers near the arrows correspond to the spectroscopic amplitudes of the heaviest reaction participants. For example, spectroscopic amplitude for the ${}^9\text{Be} = {}^8\text{Li} + p$ configuration is equal $\mathcal{A} = -0.947$.

Using the CRC method, we are able to estimate the contribution of the sequential transfer of ${}^5\text{He}$, which was not studied before. Corresponding cross sections are shown in Fig. 6.8 as curves labeled $n\alpha$ and αn . It turned out that the $n\text{-}\alpha$ and $\alpha\text{-}n$ transfer processes provide indeed a contribution more than one order of magnitude smaller in comparison with the one-step ${}^5\text{He}$ transfer. Nevertheless, it should be noted that the contribution of the $n\text{-}\alpha$ and the $\alpha\text{-}n$ transfer channels increases with the increase in the ${}^7\text{Li}$ excitation energy, where they should not be ignored.

The two-step n - p transfer is another mechanism providing a noticeable contribution to the cross section. It is due to the prominent cluster structure of the ^9Be nucleus having the weakly bound neutron. This structural feature explains also the weakness of the p - n sequential transfer contribution to the cross section corresponding to the $^7\text{Li}(\text{g.s.})$ in the exit channel. However, with increasing the ^7Li excitation energy these two mechanisms are interchanged in the significance of their contributions, as depicted by the curves in Fig. 6.8, and the p - n transfer

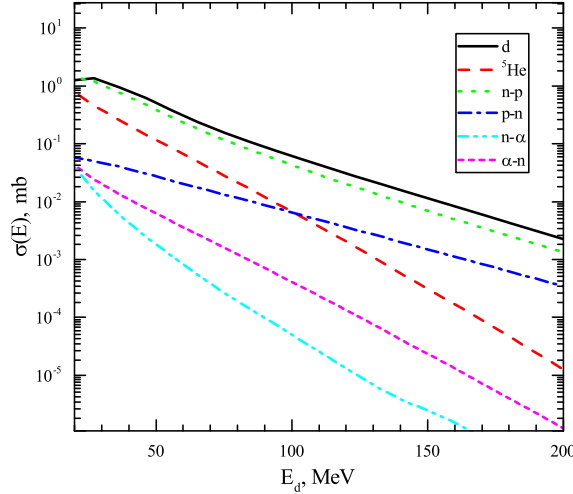


FIGURE 6.10: Contributions of the different mechanisms to the cross section of the ${}^9\text{Be}(d, \alpha){}^7\text{Li}_{g.s.}$ reaction. See Fig. 6.7 for explanation of the curve notations.

begins to play a leading role, providing, in particular, almost 10 times larger contribution in the case of reaction at $E_{lab} = 35$ MeV with ${}^7\text{Li}^*(7.46 \text{ MeV})$ in exit channel.

In Fig. 6.9, the possible scenarios for the $n-p$ and $p-n$ sequential transfer for the reaction under consideration are shown in respect to the Q -values. One may see that all the steps of the $n-p$ sequential transfer have positive Q -values, while the $p-n$ transfer goes through the intermediate channel ${}^8\text{Li} + {}^3\text{He}$ that has a considerably negative Q -value. Together with the large values of the spectroscopic amplitudes (shown near to the arrows in Fig. 6.9), this explains the leading role of the $(d, t; t, \alpha)$ mechanism in populating the ground state of ${}^7\text{Li}$ in the exit channel.

The situation becomes quite different in the case of the ${}^7\text{Li}^*(5/2^-)$ in the exit channel. First, the population of this state through the $n-p$ transfer involves the ${}^9\text{Be} = {}^8\text{Be}^*(2^+) + n$ intermediate configuration where the ${}^8\text{Be}$ cluster has to be in the 2^+ excited state. Note that the ${}^8\text{Be}(0^+)$ ground state is inappropriate because of angular-momentum-coupling mismatch in the entrance and exit configurations. Second, the extremely small spectroscopic amplitude of the

${}^8\text{Be}^*(2^+) = {}^7\text{Li}^*(5/2^-) + p$ configuration, which is $\mathcal{A} = 0.079$, influences the transfer amplitude. These two factors lead to the suppression of the contribution of $(d, t; t, \alpha)$ mechanism in population of the ${}^7\text{Li}^*(5/2^-)$ state in the exit channel. Therefore, the p - n sequential transfer prevails over the n - p one.

Figure 6.10 shows the contributions of all the mechanisms mentioned above to the total cross section of the ${}^9\text{Be}(d, \alpha){}^7\text{Li}_{g.s.}$ reaction (see Fig. 6.7) as a function of the deuteron energy. One may conclude that mainly four mechanisms contribute to the cross section of this reaction. The transfer of the deuteron-cluster is predominant channel at all collision energies. The sequential n - p and p - n transfers play a significant role at the high energies. The ${}^5\text{He}$ transfer gives almost 20% of the cross section at low energies and outdoes the sequential p - n transfer in this energy domain. This allows us to claim that the configurations $n + {}^8\text{Be}$ and $\alpha + {}^5\text{He}$ provide noticeable contributions to the ground-state wave function of the ${}^9\text{Be}$ nucleus. These conclusions agree well with the previous experimental studies [38, 39].

Summary and Conclusions

This work is dedicated to study the structure of weakly bound nuclei, such as ^6He , ^6Li , and ^9Be , and its impact on the direct nuclear reactions. The nuclei are considered as the three body systems: $^6\text{He} = \alpha + 2N$, $^6\text{Li} = \alpha + 2N$ and $^9\text{Be} = 2\alpha + N$. Their wave functions are chosen to be in the form of Gaussian basis. The three body wave functions are obtained within the stochastic variational method. Variational calculations underestimate the three body eigen-energies when compared to experimental values. Such results point to the presence of additional natures. In particular, the NNN -forces and other cluster configurations are not implemented explicitly in the current model. Taking into account such kind of specificities it may contribute to the properties of the nuclear systems under study.

The density functions of nuclear matter on the basis of the three body wave functions are derived in explicit form. The functions obtained for these nuclei demonstrate drastically different shapes in comparison with the spherical stable nuclei. Using the density functions the rms radii are expressed explicitly. Obtained values on both charge and matter radii are in good agreement with the available estimations from the well-known sources.

In the framework of the double folding model the interaction potentials, $\alpha + ^6\text{He}$, $\alpha + ^6\text{Li}$ and $d + ^9\text{Be}$, have been calculated. It should be pointed out that the large diffuseness of the double folding potentials are caused by the valence nucleons. The potential built on the three body density functions was used to calculate

the differential cross sections of elastic, inelastic scattering and nuclear transfer reactions.

The nuclear reactions ${}^6\text{He} + \alpha$ and $\alpha + {}^6\text{Li}$, at laboratory energies 151 MeV and 166 MeV, respectively, are excellent tools in terms of the theoretical study. By using them we could extract the optical potential parameters, the spectroscopic information of the three cluster configurations. The obtained optical potentials in calculations of elastic scattering and elastic transfer show the good agreement of corresponding differential cross sections with experimental data. The spectroscopic amplitude of di-neutron in ${}^6\text{He}$ is consistent with the spectroscopic information given in Ref. [41, 42].

The experimental data on elastic scattering of α -particles by ${}^6\text{He}$ and ${}^6\text{Li}$ demonstrate significant growth of cross section at backward angles. Such kind of behaviour is characterized by contribution of the elastic transfer channel. The analysis based on the CRC calculations show that the major contribution to the elastic transfer cross section is resulted from the di-nucleon transfer channel, whereas the sequential transfer is one order of magnitude lower. This confirms validity of the three body model, and the analysis is compatible with the conclusions of other authors from [41, 42].

The deuteron-induced reactions on a ${}^9\text{Be}$ target at the collision energies 19.5 and 35 MeV were studied. The calculated double-folding potential is applied successfully to describing the cross sections of elastic and inelastic scatterings, one-nucleon transfer and cluster-transfer reactions. The deformation parameter for the transition $3/2^- \rightarrow 5/2^-$ of ${}^9\text{Be}$ is extracted. The resulting deformation parameter is consistent with the parameters given in Ref. [78, 79].

The strong coupling effects have been shown for the (d, p) and (d, t) one-nucleon transfer reactions. In particular, the cross sections of the reaction (d, p) obtained within CRC method are in good agreement with the experimental data in wide angular range. It is due to taking into account all possible couplings including

the spin-reorientations. The spin reorientation coupling allows, particularly, to improve agreement with data significantly for the ${}^9\text{Be}(d,p){}^{10}\text{Be}_{gs}$ reaction. Such kind of effects occurs when a strong deformed and high spin valued nucleus, like ${}^9\text{Be}$, is involved.

The theoretical analysis of the nuclear reaction ${}^9\text{Be}(d, \alpha){}^7\text{Li}_{gs}$ shows that it goes basically through three reaction mechanisms, which are the transfer mechanism of $n-p$, the simultaneous and sequential transfer of ${}^5\text{He}$. It has become known that the light nucleus ${}^5\text{He}$ is transferred mainly simultaneously at the backward scattering angles, and the contribution of its sequential transfer is an order of magnitude lower. The $n-p$ transfer mechanism turned out to be competitive to the d transfer. Based on these observations from studying the $d + {}^9\text{Be}$ nuclear reactions, it can be concluded that ${}^9\text{Be}$ nucleus has a cluster structure.

Appendix A

Definitions from the quantum theory of angular momenta

The Appendix presents some definitions used in this work and the table integrals.

- A total angular momentum \mathbf{j} are decomposed into two angular momenta \mathbf{j}_1 and \mathbf{j}_2 by means of the Clebsch-Gordan coefficient. For example, to quote a basis $|jm\rangle$ with the angular momentum j with its z -component m , the Clebsch-Gordan coefficient can be represented as follow

$$|jm\rangle = \sum_{m_1 m_2} \langle j_1 m_1 j_2 m_2 | jm \rangle |j_1 m_1\rangle |j_2 m_2\rangle, \quad (\text{A.1})$$

For non-zero values of the coefficient (A.1) vectors \mathbf{j}_1 , \mathbf{j}_2 and \mathbf{j} must satisfy the rule of triangle:

$$|j_1 - j_2| \leq j \leq j_1 + j_2$$

$$|j - j_2| \leq j_1 \leq j + j_2$$

$$|j_1 - j| \leq j_2 \leq j_1 + j$$

and the condition

$$m = m_1 + m_2.$$

- If there are three vectors $\mathbf{j}_1, \mathbf{j}_2$ and \mathbf{j}_3 , one can get a total angular momentum \mathbf{j} in two ways

$$\mathbf{j} = (\mathbf{j}_1 + \mathbf{j}_2) + \mathbf{j}_3 = \mathbf{j}_{12} + \mathbf{j}_3 \quad (\text{A.2})$$

$$= \mathbf{j}_1 + (\mathbf{j}_2 + \mathbf{j}_3) = \mathbf{j}_1 + \mathbf{j}_{23} \quad (\text{A.3})$$

The Basis $|(j_1 j_2) j_{12}, j_3; jm\rangle$ and the basis $|j_1, (j_2 j_3); jm\rangle$ corresponding to Eq. (A.2) and Eq. (A.3) are related through a factor $U(j_1 j_2 j_3 j_{12}; j_{12} j_{23})$, which is the Racah coefficient:

$$|(j_1 j_2) j_{12}, j_3; jm\rangle = \sum_{j_{23}} U(j_1 j_2 j_3; j_{12} j_{23}) |j_1, (j_2 j_3); jm\rangle. \quad (\text{A.4})$$

Four angular momenta, $\mathbf{j}_1, \mathbf{j}_2, \mathbf{j}_3$ and \mathbf{j}_4 , are added into the total momentum \mathbf{j} by

$$\mathbf{j} = (\mathbf{j}_1 + \mathbf{j}_2) + (\mathbf{j}_3 + \mathbf{j}_4) = \mathbf{j}_{12} + \mathbf{j}_{34} \quad (\text{A.5})$$

$$= (\mathbf{j}_1 + \mathbf{j}_3) + (\mathbf{j}_2 + \mathbf{j}_4) = \mathbf{j}_{13} + \mathbf{j}_{24} \quad (\text{A.6})$$

- Two basis $|j_1 j_2(j_{12}), j_3 j_4(j_{34}); jm\rangle$ and $|j_1 j_3(j_{13}), j_2 j_4(j_{24}); jm\rangle$, constructed respectively on the scheme Eq. A.5 and Eq. A.6, are related as follow

$$|j_1 j_2(j_{12}), j_3 j_4(j_{34}); jm\rangle = \sum_{j_{13}, j_{24}} \begin{bmatrix} j_1 & j_2 & j_{12} \\ j_3 & j_4 & j_{34} \\ j_{13} & j_{24} & j \end{bmatrix} |j_1 j_3(j_{13}), j_2 j_4(j_{24}); jm\rangle \quad (\text{A.7})$$

where transformation coefficient with square brackets is called a unitary 9j-symbol.

- A spacial spherical harmonics is expressed like

$$\mathcal{Y}_{lm}(\mathbf{r}) = r^l Y_{lm}(\hat{r}) \quad (\text{A.8})$$

where $Y_{lm}(\hat{r})$ – spherical function, which is a eigenfunction of angular part the $\Delta_{\hat{r}}$ Laplace operator. For $\mathbf{r} = a\mathbf{r}_1 + b\mathbf{r}_2$ a decomposition of the spacial spherical harmonics $\mathcal{Y}_{lm}(\mathbf{r})$ leads to the following equality

$$\begin{aligned} \mathcal{Y}_{lm}(\mathbf{r} = a\mathbf{r}_1 + b\mathbf{r}_2) &= \sum_{l_1, l_2, m_1, m_2} a^{l_1} b^{l_2} \langle l_1 m_1 | l_2 m_2 | lm \rangle \mathcal{D}(l, l_1, l_2) \times \\ &\quad \times \mathcal{Y}_{l_1 m_1}(\mathbf{r}_1) \mathcal{Y}_{l_2 m_2}(\mathbf{r}_2) \\ &= \sum_{l_1, l_2} a^{l_1} b^{l_2} \mathcal{D}(l, l_1, l_2) [\mathcal{Y}_{l_1}(\mathbf{r}_1) \times \mathcal{Y}_{l_2}(\mathbf{r}_2)]_{lm} \end{aligned} \quad (\text{A.9})$$

with the condition $l = l_1 + l_2$, and $\mathcal{D}(l, l_1, l_2)$ is given by

$$\mathcal{D}(l, l_1, l_2) = \sqrt{\frac{4\pi(2l+1)!}{(2l_1+1)!(2l_2+1)!}} \quad (\text{A.10})$$

- Spherical harmonics with the momenta l_1 and l_2 are coupled as follow

$$[Y_{l_1}(\hat{r}) \times Y_{l_2}(\hat{r})]_{lm} = \mathcal{C}(l_1, l_2, l) Y_{lm}(\hat{r}) \quad (\text{A.11})$$

where the $\mathcal{C}(l_1, l_2, l)$ coefficient reads as

$$\mathcal{C}(l_1, l_2, l) = \sqrt{\frac{(2l_1+1)(2l_2+1)}{4\pi(2l+1)}} \langle l_1 0 | l_2 0 | l 0 \rangle \quad (\text{A.12})$$

- It would be useful also note a coupling between two spherical hyper harmonics kind of (see [53], p. 269)

$$\left[Y_{l_{12}}^{(l_1 l_2)}(\hat{\mathbf{r}}_1, \hat{\mathbf{r}}_2) \times Y_{l_{34}}^{(l_3 l_4)}(\hat{\mathbf{r}}_1, \hat{\mathbf{r}}_2) \right]_{lm} = \sum_{l_{13} l_{24}} E_{l_{13} l_{24}}^{l_1 l_2 l_{12} l_2 l_4 l_{34} l} Y_{lm}^{(l_1 l_2 l_3 l_4)}(\hat{\mathbf{r}}_1, \hat{\mathbf{r}}_2) \quad (\text{A.13})$$

where the coupling coefficient $E_{l_{13}l_{24}}^{l_1l_2l_{12}l_2l_4l_{34}l}$ is given as

$$E_{l_{13}l_{24}}^{l_1l_2l_{12}l_2l_4l_{34}l} = \begin{bmatrix} l_1 & l_2 & l_{12} \\ l_3 & l_4 & l_{34} \\ l_{13} & l_{24} & l \end{bmatrix} \mathcal{C}(l_1, l_3, l_{13}) \mathcal{C}(l_2, l_4, l_{24}). \quad (\text{A.14})$$

- The modified spherical Bessel function may be expressed as follows (see [53], p. 98)

$$i_l(x) = \sqrt{\frac{\pi}{2x}} I_{l+\frac{1}{2}}(x) = \sum_{k=0}^{\infty} \frac{x^{2k+l}}{(2k)!!(2k+2l+1)!!}, \quad (\text{A.15})$$

where $I_l(x)$ is a modified Bessel function of the first kind.

- The integral depending on the parameters λ and α

$$\int_0^\infty dx x^\lambda \exp(-\alpha x^2)$$

can be expressed in explicit form as follows

$$\mathcal{I}(\lambda, \alpha) = 2^{1+\lambda} \frac{\Gamma(1+\lambda)}{(\alpha)^{1+\lambda}}. \quad (\text{A.16})$$

where, $\Gamma(x)$ – the Gamma function.

- An integral kind of

$$\int_0^\infty dx x^{2n+l+2} \exp(-\frac{1}{2}vx^2) i_l(|w|y)$$

has the analytic form in the following (see [53], p. 270)

$$\mathcal{I}(n, l, v, |w|) = \frac{\pi}{2} \frac{(2n)!!|w|^l}{v^{n+l+3/2}} \exp\left(\frac{w^2}{2v}\right) L_n^{l+1/2}\left(-\frac{w^2}{2v}\right) \quad (\text{A.17})$$

where, $L_n^{l+1/2}(x)$ – is the associated Laguerre polynomial.

- The integral with six parameters

$$\int_0^\infty dx \int_0^\infty dy x^{2\lambda+l+2} y^{2n+l+2} \exp\left(-\frac{1}{2}\alpha x^2 - \frac{1}{2}\beta y^2\right) i_l(|\rho|xy) \quad (\text{A.18})$$

may be expressed explicitly as follow (see [53], p. 271)

$$\begin{aligned} \mathcal{I}(\lambda, l, n, \alpha, \beta, |\rho|) = & \sqrt{\frac{\pi}{8}} (2l)!! \Gamma(l + n + \frac{3}{2}) |\rho|^n \beta^{-l-n-\frac{3}{2}} \times \\ & \times \sum_{\kappa=0}^l \frac{\Gamma(\kappa + \lambda + n + \frac{3}{2})}{\kappa!(l-\kappa)!\Gamma(\kappa + n + \frac{3}{2})} \left(\frac{\rho^2}{2\beta}\right)^\kappa \left(\frac{\alpha}{2} - \frac{\rho^2}{2\beta}\right)^{-\kappa-\lambda-n-\frac{3}{2}}. \end{aligned} \quad (\text{A.19})$$

Appendix B

Parameters of the three body wave function for ${}^6\text{He}$

TABLE B.1: The three-body wave function parameters found by means of variational approach for the ground state of ${}^6\text{He}$

i	$\alpha_i^{(k)}$	$\beta_i^{(k)}$	C_i
$\gamma \equiv 0 \ 0 \ 0 \ 0$			
1	0.03872262	0.09444994	-0.1737337132E-04
2	0.03872262	0.28926931	-0.7746568943E-01
3	0.03872262	0.50341072	0.1537953138E+00
4	0.03872262	0.75592149	-0.2068222047E+00
5	0.03872262	1.07956780	0.1915099409E+00
6	0.03872262	1.54178260	-0.1186045848E+00
7	0.03872262	2.31514050	0.4377908070E-01
8	0.03872262	4.02900180	-0.8511508780E-02
9	0.03872262	12.33951600	0.8124669663E-03
10	0.11859473	0.09444994	0.1914598067E+00
11	0.11859473	0.28926931	-0.4142283997E-01
12	0.11859473	0.50341072	-0.9504287755E+00
13	0.11859473	0.75592149	0.5100204701E+00
14	0.11859473	1.07956780	0.4351961872E+00
15	0.11859473	1.54178260	-0.5512501566E+00
16	0.11859473	2.31514050	0.2353573699E+00
17	0.11859473	4.02900180	-0.3888384752E-01

Continued on next page

Table B.1 – continued from previous page

i	$\alpha_i^{(k)}$	$\beta_i^{(k)}$	C_i
18	0.11859473	12.33951600	0.2142226702E-02
19	0.20638850	0.09444994	-0.7243857878E+00
20	0.20638850	0.28926931	0.1811320023E+01
21	0.20638850	0.50341072	-0.2829679245E+00
22	0.20638850	0.75592149	0.6392623958E-01
23	0.20638850	1.07956780	-0.1629089089E+01
24	0.20638850	1.54178260	0.1304993071E+01
25	0.20638850	2.31514050	-0.4928065738E+00
26	0.20638850	4.02900180	0.1996819496E-01
27	0.20638850	12.33951600	0.1060241013E-01
28	0.30991295	0.09444994	0.1599423834E+01
29	0.30991295	0.28926931	-0.5264844147E+01
30	0.30991295	0.50341072	0.7012917232E+01
31	0.30991295	0.75592149	-0.4714686948E+01
32	0.30991295	1.07956780	-0.4796509839E+00
33	0.30991295	1.54178260	0.2065489512E+01
34	0.30991295	2.31514050	-0.8987555045E+00
35	0.30991295	4.02900180	0.4500233344E+00
36	0.30991295	12.33951600	-0.8218053258E-01
37	0.44260156	0.09444994	-0.1956103683E+01
38	0.44260156	0.28926931	0.7193813517E+01
39	0.44260156	0.50341072	-0.1163049706E+02
40	0.44260156	0.75592149	0.6193322640E+01
41	0.44260156	1.07956780	0.7415949805E+01
42	0.44260156	1.54178260	-0.8938587045E+01
43	0.44260156	2.31514050	0.3391887206E+01
44	0.44260156	4.02900180	-0.1168066181E+01
45	0.44260156	12.33951600	0.1744136293E+00
46	0.63210054	0.09444994	0.1402383982E+01
47	0.63210054	0.28926931	-0.5136700789E+01
48	0.63210054	0.50341072	0.8665026533E+01
49	0.63210054	0.75592149	-0.2933774272E+01
50	0.63210054	1.07956780	-0.8943836753E+01
51	0.63210054	1.54178260	0.8717580886E+01

Continued on next page

Table B.1 – continued from previous page

i	$\alpha_i^{(k)}$	$\beta_i^{(k)}$	C_i
52	0.63210054	2.31514050	-0.3215399907E+01
53	0.63210054	4.02900180	0.1165125187E+01
54	0.63210054	12.33951600	-0.1665816218E+00
55	0.94916212	0.09444994	-0.5455065421E+00
56	0.94916212	0.28926931	0.1973142226E+01
57	0.94916212	0.50341072	-0.3305486410E+01
58	0.94916212	0.75592149	0.5936725650E+00
59	0.94916212	1.07956780	0.4339113002E+01
60	0.94916212	1.54178260	-0.4005833236E+01
61	0.94916212	2.31514050	0.1671843031E+01
62	0.94916212	4.02900180	-0.6442299484E+00
63	0.94916212	12.33951600	0.8553541645E-01
64	1.65181150	0.09444994	0.1291465276E+00
65	1.65181150	0.28926931	-0.3358554818E+00
66	1.65181150	0.50341072	0.6888942468E+00
67	1.65181150	0.75592149	-0.1350120966E+00
68	1.65181150	1.07956780	-0.1153775517E+01
69	1.65181150	1.54178260	0.1271270643E+01
70	1.65181150	2.31514050	-0.7908870481E+00
71	1.65181150	4.02900180	0.2382269089E+00
72	1.65181150	12.33951600	-0.2472769828E-01
73	5.05895900	0.09444994	-0.1003954377E+00
74	5.05895900	0.28926931	-0.1270223362E+00
75	5.05895900	0.50341072	-0.3653418537E+00
76	5.05895900	0.75592149	0.6548391778E+00
77	5.05895900	1.07956780	-0.1837812114E+00
78	5.05895900	1.54178260	0.2724244480E+00
79	5.05895900	2.31514050	0.5022837020E-01
80	5.05895900	4.02900180	-0.1318577464E-01
81	5.05895900	12.33951600	-0.5334531276E-03
$\gamma \equiv 1 \ 1 \ 1 \ 1$			
1	0.03872262	0.09444994	-0.1209912997E-03
2	0.03872262	0.28926931	-0.2752286691E-03

Continued on next page

Table B.1 – continued from previous page

i	$\alpha_i^{(k)}$	$\beta_i^{(k)}$	C_i
3	0.03872262	0.50341072	0.8313112741E-03
4	0.03872262	0.75592149	-0.1569396728E-02
5	0.03872262	1.07956780	0.1841931183E-02
6	0.03872262	1.54178260	-0.1329878249E-02
7	0.03872262	2.31514050	0.5732118509E-03
8	0.03872262	4.02900180	-0.1407523317E-03
9	0.03872262	12.33951600	0.2464625078E-04
10	0.11859473	0.09444994	0.3780785946E-03
11	0.11859473	0.28926931	-0.1000393773E-01
12	0.11859473	0.50341072	0.1426933985E-01
13	0.11859473	0.75592149	-0.2639755490E-01
14	0.11859473	1.07956780	0.3639070623E-01
15	0.11859473	1.54178260	-0.3096578932E-01
16	0.11859473	2.31514050	0.1507393647E-01
17	0.11859473	4.02900180	-0.4078109925E-02
18	0.11859473	12.33951600	0.7893561124E-03
19	0.20638850	0.09444994	-0.1675476628E-02
20	0.20638850	0.28926931	0.3933745812E-01
21	0.20638850	0.50341072	-0.1092045673E+00
22	0.20638850	0.75592149	0.1542197135E+00
23	0.20638850	1.07956780	-0.1840525972E+00
24	0.20638850	1.54178260	0.1475223686E+00
25	0.20638850	2.31514050	-0.6976541581E-01
26	0.20638850	4.02900180	0.1855170403E-01
27	0.20638850	12.33951600	-0.3521003985E-02
28	0.30991295	0.09444994	0.4106806042E-02
29	0.30991295	0.28926931	-0.9266191014E-01
30	0.30991295	0.50341072	0.2815735552E+00
31	0.30991295	0.75592149	-0.4603450597E+00
32	0.30991295	1.07956780	0.5000169839E+00
33	0.30991295	1.54178260	-0.3928705377E+00
34	0.30991295	2.31514050	0.1830077652E+00
35	0.30991295	4.02900180	-0.4774102277E-01
36	0.30991295	12.33951600	0.7847255538E-02

Continued on next page

Table B.1 – continued from previous page

i	$\alpha_i^{(k)}$	$\beta_i^{(k)}$	C_i
37	0.44260156	0.09444994	-0.5723743876E-02
38	0.44260156	0.28926931	0.1267185089E+00
39	0.44260156	0.50341072	-0.4013118748E+00
40	0.44260156	0.75592149	0.6809541150E+00
41	0.44260156	1.07956780	-0.7658315705E+00
42	0.44260156	1.54178260	0.5861381351E+00
43	0.44260156	2.31514050	-0.2712619146E+00
44	0.44260156	4.02900180	0.7108163202E-01
45	0.44260156	12.33951600	-0.1022953848E-01
46	0.63210054	0.09444994	0.4677586570E-02
47	0.63210054	0.28926931	-0.1014186442E+00
48	0.63210054	0.50341072	0.3298241305E+00
49	0.63210054	0.75592149	-0.5616842239E+00
50	0.63210054	1.07956780	0.6411713372E+00
51	0.63210054	1.54178260	-0.4946856323E+00
52	0.63210054	2.31514050	0.2242477697E+00
53	0.63210054	4.02900180	-0.6092825450E-01
54	0.63210054	12.33951600	0.8592838651E-02
55	0.94916212	0.09444994	-0.2194397884E-02
56	0.94916212	0.28926931	0.4740184928E-01
57	0.94916212	0.50341072	-0.1572767288E+00
58	0.94916212	0.75592149	0.2605021995E+00
59	0.94916212	1.07956780	-0.2950306986E+00
60	0.94916212	1.54178260	0.2325275547E+00
61	0.94916212	2.31514050	-0.1002393441E+00
62	0.94916212	4.02900180	0.2887819798E-01
63	0.94916212	12.33951600	-0.4542642070E-02
64	1.65181150	0.09444994	0.5992856734E-03
65	1.65181150	0.28926931	-0.1164675896E-01
66	1.65181150	0.50341072	0.4636939204E-01
67	1.65181150	0.75592149	-0.5909598945E-01
68	1.65181150	1.07956780	0.7349403097E-01
69	1.65181150	1.54178260	-0.6253335023E-01
70	1.65181150	2.31514050	0.2300764414E-01

Continued on next page

Table B.1 – continued from previous page

i	$\alpha_i^{(k)}$	$\beta_i^{(k)}$	C_i
71	1.65181150	4.02900180	-0.6869029310E-02
72	1.65181150	12.33951600	0.1279464637E-02
73	5.05895900	0.09444994	-0.8739688325E-04
74	5.05895900	0.28926931	0.2659208242E-02
75	5.05895900	0.50341072	-0.4297540353E-02
76	5.05895900	0.75592149	0.1984703845E-01
77	5.05895900	1.07956780	-0.1802355036E-01
78	5.05895900	1.54178260	0.1173642602E-01
79	5.05895900	2.31514050	-0.7529136326E-02
80	5.05895900	4.02900180	0.1375626183E-02
81	5.05895900	12.33951600	-0.2653098521E-03
$\gamma \equiv 2\ 2\ 0\ 0$			
1	0.07010120	0.17098674	0.8287413344E-05
2	0.07010120	0.55006725	-0.2315910360E-03
3	0.07010120	1.07956780	0.2205912189E-03
4	0.07010120	2.11877100	-0.1546351743E-03
5	0.07010120	6.81612260	0.1309976070E-03
6	0.22551676	0.17098674	0.1592019751E-03
7	0.22551676	0.55006725	0.1457399081E-02
8	0.22551676	1.07956780	-0.6213676741E-02
9	0.22551676	2.11877100	0.5178724836E-02
10	0.22551676	6.81612260	-0.4694996433E-02
11	0.44260156	0.17098674	-0.3630365442E-03
12	0.44260156	0.55006725	0.5589096347E-03
13	0.44260156	1.07956780	0.9499448616E-02
14	0.44260156	2.11877100	-0.1099890159E-01
15	0.44260156	6.81612260	0.1241336217E-01
16	0.86865448	0.17098674	0.3996664351E-03
17	0.86865448	0.55006725	-0.4801971131E-03
18	0.86865448	1.07956780	-0.9127801910E-02
19	0.86865448	2.11877100	0.6666082171E-02
20	0.86865448	6.81612260	-0.1471088050E-01
21	2.79447630	0.17098674	-0.3154650054E-03

Continued on next page

Table B.1 – continued from previous page

i	$\alpha_i^{(k)}$	$\beta_i^{(k)}$	C_i
22	2.79447630	0.55006725	-0.8889072435E-04
23	2.79447630	1.07956780	0.1109393782E-01
24	2.79447630	2.11877100	-0.2003915591E-01
25	2.79447630	6.81612260	0.1595658076E-01
$\gamma \equiv 3\ 3\ 1\ 1$			
1	0.07010120	0.17098674	-0.2579335841E-06
2	0.07010120	0.55006725	-0.2765357271E-05
3	0.07010120	1.07956780	0.6139330639E-05
4	0.07010120	2.11877100	-0.7938375153E-05
5	0.07010120	6.81612260	0.1167298934E-04
6	0.22551676	0.17098674	0.5917355271E-06
7	0.22551676	0.55006725	-0.6483646762E-04
8	0.22551676	1.07956780	0.8695083699E-05
9	0.22551676	2.11877100	-0.4800513075E-05
10	0.22551676	6.81612260	0.6570347080E-06
11	0.44260156	0.17098674	-0.1470428346E-05
12	0.44260156	0.55006725	0.1350176334E-03
13	0.44260156	1.07956780	-0.2583695882E-03
14	0.44260156	2.11877100	0.1700235229E-03
15	0.44260156	6.81612260	-0.2196174841E-03
16	0.86865448	0.17098674	0.2122290583E-05
17	0.86865448	0.55006725	-0.1948661774E-03
18	0.86865448	1.07956780	0.3856831336E-03
19	0.86865448	2.11877100	-0.3277457806E-03
20	0.86865448	6.81612260	0.4749778522E-03
21	2.79447630	0.17098674	-0.3460810077E-05
22	2.79447630	0.55006725	0.3075671947E-03
23	2.79447630	1.07956780	-0.6343122836E-03
24	2.79447630	2.11877100	0.6129185220E-03
25	2.79447630	6.81612260	-0.7981418030E-03

Bibliography

1. Donoghue, J. F., Golowich, E. & Holstein, B. R. *Dynamics of the standard model* (Cambridge university press, 2014).
2. Griffiths, D. *Introduction to elementary particles* (John Wiley & Sons, 2020).
3. Ramond, P. *Journeys beyond the standard model* (Perseus Books Cambridge, 1999).
4. Ter-Akopian, G. *et al.* Radioactive ion beam research made in Dubna. *Nuclear Physics A* **734**, 295–302 (2004).
5. Yano, Y. The RIKEN RI beam factory project: A status report. *Nuclear Instruments and Methods in Physics Research Section B: Beam Interactions with Materials and Atoms* **261**, 1009–1013 (2007).
6. Gade, A & Sherrill, B. NSCL and FRIB at Michigan State University: Nuclear science at the limits of stability. *Physica Scripta* **91**, 053003 (2016).
7. Hong, B. *et al.* Plan for nuclear symmetry energy experiments using the LAMPS system at the RIB facility RAON in Korea. *The European Physical Journal A* **50**, 49 (2014).
8. Fukuda, N *et al.* Identification and separation of radioactive isotope beams by the BigRIPS separator at the RIKEN RI Beam Factory. *Nuclear Instruments and Methods in Physics Research Section B: Beam Interactions with Materials and Atoms* **317**, 323–332 (2013).
9. Rutherford, E. VIII. Uranium radiation and the electrical conduction produced by it. *The London, Edinburgh, and Dublin Philosophical Magazine and Journal of Science* **47**, 109–163 (1899).

10. Stuewer, R. H. in *The kaleidoscope of science* 147–186 (Springer, 1986).
11. Poenaru, D., Gherghescu, R. & Greiner, W. Cluster decay of superheavy nuclei. *Physical Review C* **85**, 034615 (2012).
12. Descouvemont, P. & Baye, D. ^{12}Be molecular states in a microscopic cluster model. *Physics Letters B* **505**, 71–74 (2001).
13. Tohsaki, A., Horiuchi, H., Schuck, P. & Röpke, G. Alpha Cluster Condensation in $\text{C } 12$ and $\text{O } 16$. *Physical Review Letters* **87**, 192501 (2001).
14. Kanada-En'yo, Y., Horiuchi, H. & Ono, A. Structure of Li and Be isotopes studied with antisymmetrized molecular dynamics. *Physical Review C* **52**, 628 (1995).
15. Pudliner, B., Pandharipande, V., Carlson, J., Pieper, S. C. & Wiringa, R. B. Quantum Monte Carlo calculations of nuclei with $A < \sim 7$. *Physical Review C* **56**, 1720 (1997).
16. Zhukov, M. *et al.* Bound state properties of Borromean halo nuclei: ^6He and ^{11}Li . *Physics reports* **231**, 151–199 (1993).
17. Navrátil, P., Quaglioni, S., Stetcu, I. & Barrett, B. R. Recent developments in no-core shell-model calculations. *Journal of Physics G: Nuclear and Particle Physics* **36**, 083101 (2009).
18. Forssén, C., Navrátil, P., Ormand, W. & Caurier, E. Large basis ab initio shell model investigation of ^{9}Be and ^{11}Be . *Physical Review C* **71**, 044312 (2005).
19. Navratil, P. & Ormand, W. E. Ab initio shell model with a genuine three-nucleon force for the p-shell nuclei. *Physical Review C* **68**, 034305 (2003).
20. Navratil, P. & Ormand, W. E. Ab initio shell model calculations with three-body effective interactions for p-shell nuclei. *Physical review letters* **88**, 152502 (2002).
21. Tilley, D. *et al.* Energy levels of light nuclei $A = 8, 9, 10$. *Nuclear Physics A* **745**, 155–362 (2004).

22. Horiuchi, H. Generator coordinate treatment of composite particle reaction and molecule-like structures. *Progress of Theoretical Physics* **43**, 375–389 (1970).
23. Tang, Y.-C., LeMere, M. & Thompson, D. Resonating-group method for nuclear many-body problems. *Physics Reports* **47**, 167–223 (1978).
24. Wheeler, J. A. On the mathematical description of light nuclei by the method of resonating group structure. *Physical Review* **52**, 1107 (1937).
25. Nesterov, A., Arickx, F., Broeckhove, J. & Vasilevsky, V. Three-cluster description of properties of light neutron-and proton-rich nuclei in the framework of the algebraic version of the resonating group method. *Physics of Particles and Nuclei* **41**, 716–765 (2010).
26. Brink, D. & Bloch, C. *Proceedings of the International School of Physics “enrico fermi” Course XXXVI* 1966.
27. Descouvemont, P. & Baye, D. The R-matrix theory. *Reports on progress in physics* **73**, 036301 (2010).
28. Arai, K., Suzuki, Y. & Lovas, R. Structure of ${}^6\text{He}$ with an extended three-cluster model. *Physical Review C* **59**, 1432 (1999).
29. Descouvemont, P. Halo structure of ${}^{14}\text{Be}$ in a microscopic $\text{Be} \, {}^{12+} \text{n+n}$ cluster model. *Physical Review C* **52**, 704 (1995).
30. Kukulin, V. & Krasnopol’sky, V. A stochastic variational method for few-body systems. *Journal of Physics G: Nuclear Physics* **3**, 795 (1977).
31. Voronchev, V., Kukulin, V., Pomerantsev, V., Razikov, K. D. & Ryzhikh, G. Study of the Structure and Properties of Nuclei with $A = 9$ (${}^9\text{Be}$ - ${}^9\text{B}$) in Terms of Multicluster Dynamic Model $2\alpha + \text{N}$. *Yad. Fiz.* **57**, 1964–1980 (1994).
32. Kukulin, V., Krasnopol’Sky, V., Voronchev, V. & Sazonov, P. Detailed study of the cluster structure of light nuclei in a three-body model:(II). The spectrum of low-lying states of nuclei with $A = 6$. *Nuclear Physics A* **453**, 365–388 (1986).

33. Kukulin, V., Krasnopol'sky, V., Voronchev, V. & Sazonov, P. Detailed study of the cluster structure of light nuclei in a three-body model:(I). Ground state of ${}^6\text{Li}$. *Nuclear Physics A* **417**, 128–156 (1984).
34. Kukulin, V. & Pomerantsev, V. The orthogonal projection method in scattering theory. *Annals of Physics* **111**, 330–363 (1978).
35. Feshbach, H. The optical model and its justification. *Annual Review of Nuclear Science* **8**, 49–104 (1958).
36. Satchler, G. & Tobocman, W. Gamma Rays from Deuteron Stripping Reactions. *Physical Review* **118**, 1566 (1960).
37. Canto, L., Gomes, P., Donangelo, R & Hussein, M. Fusion and breakup of weakly bound nuclei. *Physics reports* **424**, 1–111 (2006).
38. Brown, T. A. D. *et al.* Decay studies for states in ${}^9\text{Be}$ up to 11 MeV: Insights into the $\text{n}+{}^8\text{Be}$ and $\alpha+{}^5\text{He}$ cluster structure. *Phys. Rev.* **C76**, 054605 (2007).
39. Papka, P. *et al.* Decay path measurements for the 2.429 MeV state in ${}^9\text{Be}$: Implications for the astrophysical $\alpha + \alpha + \text{n}$ reaction. *Phys. Rev.* **C75**, 045803 (2007).
40. Ter-Akopian, G. *et al.* Two-neutron exchange observed in the ${}^6\text{He} + {}^4\text{He}$ reaction. Search for the " di-neutron" configuration of ${}^6\text{He}$. *Physics Letters B* **426**, 251–256 (1998).
41. Oganessian, Y. T., Zagrebaev, V. & Vaagen, J. Dynamics of two-neutron transfer reactions with the Borromean nucleus ${}^6\text{He}$. *Physical Review C* **60**, 044605 (1999).
42. Khoa, D. T. & Von Oertzen, W. Di-neutron elastic transfer in the ${}^4\text{He}$ (${}^6\text{He}$, ${}^6\text{He}$) ${}^4\text{He}$ reaction. *Physics Letters B* **595**, 193–201 (2004).
43. Detraz, C., Duhm, H. H. & Hafner, H. The (${}^3\text{He}$, ${}^7\text{Be}$) Reaction on Light Nuclei. *Nucl. Phys.* **A147**, 488 (1970).
44. Detraz, C. *et al.* Selectivity in the ${}^{11}\text{B}({}^3\text{He}, {}^6\text{Li}){}^8\text{Be}$ Reaction. *Nucl. Phys.* **A228**, 39 (1974).

45. Golovkov, M., Kulikauskas, V., Voronchev, V., Krasnopol'skii, V. & Kukulin, V. Cross sections for low-energy deuteron reactions in ${}^6\text{Li}$. *Soviet Journal of Nuclear Physics* **34**, 480–481 (1981).
46. Glozman, L. Y., Kukulin, V. & Neudatchin, V. A study of the ${}^6\text{Li}$ (π^+ , pp) ${}^4\text{He}$ reaction within the three-body problem. *Nuclear Physics A* **430**, 589–604 (1984).
47. Zhusupov, M., Ibraeva, E., Kukulin, V. & Peresypkin, V. Elastic and inelastic scattering of protons and antiprotons by the ${}^6\text{Li}$ nucleus at intermediate energies. *Physics of Atomic Nuclei* **57**, 1937–1948 (1994).
48. Kukulin, V. I. & Voronchev, V. T. Pinch-based thermonuclear D^3He fusion driven by a femtosecond laser. *Phys. At. Nucl.* **73**, 1376 (2010).
49. Seksembayev, Z., Kukulin, V. & Sakhiev, S. Study of a dense hot plasma's burning in Z -pinch devices with inertial-magnetic confinement. *Phys. Scr.* **93**, 085602 (2018).
50. Kakenov, M., Kukulin, V., Pomerantsev, V. & Bayakhmetov, O. Properties of dibaryons in nuclear medium. *The European Physical Journal A* **56**, 1–18 (2020).
51. Blokhintsev, L., Kukulin, V., Sakharuk, A., Savin, D. & Kuznetsova, E. Determination of the α ${}^6\text{d}$ vertex constant (asymptotic coefficient) from the He ${}^4\text{d}$ phase-shift analysis. *Physical Review C* **48**, 2390 (1993).
52. Tursunov, E., Kadyrov, A., Turakulov, S. & Bray, I. Theoretical study of the $\alpha + \text{d} \rightarrow {}^6\text{Li} + \gamma$ astrophysical capture process in a three-body model. *Physical Review C* **94**, 015801 (2016).
53. Suzuki, Y., Suzuki, M. & Varga, K. *Stochastic variational approach to quantum-mechanical few-body problems* (Springer Science & Business Media, 1998).
54. Faddeev, L. & Merkuriev, S. Quantum Scattering Theory for Multi-particle Systems. *Mathematical Physics and Applied Mathematics* **11** (1985).

55. Kukulin, V., Voronchev, V. & Razikov, K. D. *Dynamic multicluster model of light nuclei. Main formalism* tech. rep. (Moskovskij Gosudarstvennyj Univ., 1990).
56. Satchler, G. R. & Love, W. G. Folding model potentials from realistic interactions for heavy-ion scattering. *Physics Reports* **55**, 183–254 (1979).
57. Satchler, G. *Direct Nuclear Reactions* ISBN: 9780198512691 (Clarendon Press, 1983).
58. Brown, A. *Lecture Notes in Nuclear Structure Physics* (Michigan State University, 2017).
59. De Shalit, A & Talmi, I. *Nuclear shell theory* 1963.
60. Luk'yanov, K. *Double folding model of nucleus-nucleus potential: Formulae, iteration method and computer code* tech. rep. (Laboratory of Information Technologies, 2008).
61. Anantaraman, N, Toki, H & Bertsch, G. An effective interaction for inelastic scattering derived from the Paris potential. *Nuclear Physics A* **398**, 269–278 (1983).
62. Day, B. Three-body correlations in nuclear matter. *Physical Review C* **24**, 1203 (1981).
63. Sack, S, Biedenharn, L. & Breit, G. The Elastic Scattering of Protons by Alpha Particles. *Physical Review* **93**, 321 (1954).
64. Buck, B, Friedrich, H & Wheatley, C. Local potential models for the scattering of complex nuclei. *Nuclear Physics A* **275**, 246–268 (1977).
65. Papadimitriou, G. *et al.* Charge radii and neutron correlations in helium halo nuclei. *Physical Review C* **84**, 051304 (2011).
66. Hussein, M., Descouvemont, P., Druet, T & Canto, L. F. Low-energy ${}^9\text{Be} + {}^{208}\text{Pb}$ scattering, breakup and fusion within a four-body model. *APS 2015*, T1–008 (2015).

67. Antonov, A. *et al.* Charge and matter distributions and form factors of light, medium, and heavy neutron-rich nuclei. *Physical Review C* **72**, 044307 (2005).
68. Hirai, M, Kumano, S, Saito, K. & Watanabe, T. Clustering aspects in nuclear structure functions. *Physical Review C* **83**, 035202 (2011).
69. Angeli, I. & Marinova, K. P. Table of experimental nuclear ground state charge radii: An update. *Atomic Data and Nuclear Data Tables* **99**, 69–95 (2013).
70. Bumiller, F., Buskirk, F., Dyer, J. & Monson, W. Elastic Electron Scattering from Li 6 and Li 7 at Low Momentum Transfer. *Physical Review C* **5**, 391 (1972).
71. Fey, G, Frank, H, Schütz, W & Theissen, H. Nuclear Rms charge radii from relative electron scattering measurements at low energies. *Zeitschrift für Physik* **265**, 401–403 (1973).
72. Tanihata, I *et al.* Measurements of interaction cross sections and nuclear radii in the light p-shell region. *Physical Review Letters* **55**, 2676 (1985).
73. Voronchev, V., Krasnopol'Sky, V. & Kukulin, V. A variational study of the ground and excited states of light nuclei in a three-body model on the complete basis. I. General formalism. *Journal of Physics G: Nuclear Physics* **8**, 649 (1982).
74. Thompson, I. J. Coupled reaction channels calculations in nuclear physics. *Comp. Phys. Rep.* **7**, 167 –212 (1988).
75. Avrigeanu, V, Hodgson, P. & Avrigeanu, M. Global optical potentials for emitted alpha particles. *Physical Review C* **49**, 2136 (1994).
76. Kunz, P. D. *Computer code DWUCK5* unpublished. <https://www.oecd-nea.org/tools/abstract/detail/nesc9872>.
77. Karpov, A. *et al.* NRV web knowledge base on low-energy nuclear physics. *Nucl. Instr. and Meth. Phys. Res.t* **A859**, 112 –124. <http://nrv.jinr.ru> (2017).

78. Lukyanov, S. *et al.* Study of internal structures of 9 , ${}^{10}\text{Be}$ and ${}^{10}\text{B}$ in scattering of ${}^4\text{He}$ from ${}^9\text{Be}$. *Journal of Physics G: Nuclear and Particle Physics* **41**, 035102 (2014).
79. Harakeh, M., Van Popta, J., Saha, A. & Siemssen, R. Strong coupled-channels effects in the ${}^9\text{Be}$ (α , t) ${}^{10}\text{B}$ reaction. *Nuclear Physics A* **344**, 15–40 (1980).
80. Szczurek, A. *et al.* Mechanism of Reactions Induced by 7 MeV Deuterons on ${}^9\text{Be}$ [(d, p), (d, d), (d, t), (d, ${}^4\text{He}$)]. *Z. Phys. A* **333**, 271 (1989).
81. Votava, H. J., Clegg, T. B., Ludwig, E. J. & Thompson, W. J. Proton Scattering from ${}^9\text{Be}$ between 6 and 30 MeV and the Structure of ${}^9\text{Be}$. *Nucl. Phys. A* **204**, 529 (1973).
82. Koning, A. J. & Delaroche, J. P. Local and global nucleon optical models from 1 keV to 200 MeV. *Nucl. Phys. A* **713**, 231 (2003).
83. Li, X., Liang, C. & Cai, C. Global triton optical model potential. *Nucl. Phys. A* **789**, 103 (2007).
84. Caurier, E., Martínez-Pinedo, G., Nowacki, F., Poves, A. & Zuker, A. P. The shell model as a unified view of nuclear structure. *Rev. Mod. Phys.* **77**, 427–488 (2005).
85. Cohen, S. & Kurath, D. Effective Interactions for the 1p Shell. *Nucl. Phys.* **73**, 1 (1965).
86. Volya, A. *Private communication*.
87. Kravvaris, K. & Volya, A. Study of Nuclear Clustering from an Ab Initio Perspective. *Phys. Rev. Lett.* **119**, 062501 (2017).
88. Della Rocca, V. & Iachello, F. Cluster shell model: I. Structure of ${}^9\text{Be}$, ${}^9\text{B}$. *Nucl. Phys. A* **973**, 1 (2018).
89. Galanina, L. I. & Zelenskaya, N. S. Mechanisms of sequential particle transfer and characteristics of light neutron-excess and oriented nuclei. *Phys. Part. Nucl.* **43**, 147 (2012).

90. Rudchik, A. T. *et al.* Elastic and inelastic scattering of ^{15}N ions by ^9Be at 84 MeV. *Nucl. Phys.* **A947**, 161 (2016).
91. Avrigeanu, V., Hodgson, P. E. & Avrigeanu, M. Global Optical Potentials for Emitted Alpha Particles. *Phys. Rev.* **C49**, 2136 (1994).
92. Cook, J. Global Optical-Model Potentials for the Elastic Scattering of $^{6,7}\text{Li}$ Projectiles. *Nucl. Phys.* **A388**, 153 (1982).
93. Kwasniewicz, E. & Jarczyk, L. Five-Nucleon Spectroscopic Amplitudes for 1p-Shell Nuclei. *Nucl. Phys.* **A441**, 77 (1985).
94. Tanaka, S. The $^9\text{Be}(\text{d}, \text{t})^8\text{Be}$ and $^9\text{Be}(\text{d}, \alpha)^7\text{Li}$ Reaction in the Energy Range from 12.17 MeV to 14.43 MeV. *J. Phys. Soc. Jpn.* **44**, 1405 (1978).
95. Jarczyk, L. *et al.* Five-Nucleon Simultaneous and Sequential Transfer in the $^{12}\text{C}(^{11}\text{B}, ^6\text{Li})^{17}\text{O}$ and $^{12}\text{C}(\text{d}, ^7\text{Li})^7\text{Be}$ Reactions. *Phys. Rev.* **C54**, 1302 (1996).